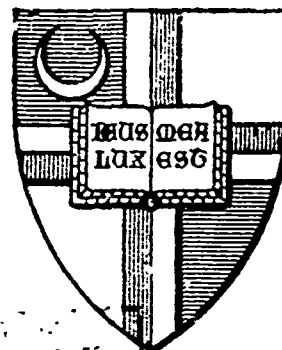
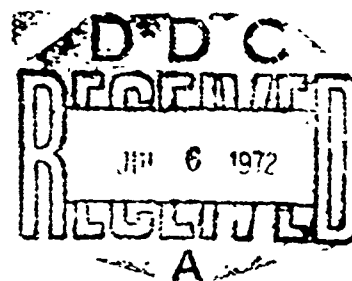
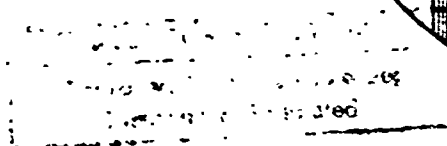


AD 744687

Institute of Ocean Science and Engineering  
School of Engineering and Architecture  
The Catholic University of America  
Washington, D.C. 20017



Kept in file  
NATIONAL TECHNICAL  
INFORMATION SERVICE  
U.S. Department of Commerce  
Washington, D.C. 20540



111

RELATIONSHIP BETWEEN INTERNAL DAMPING  
AND  
SUSCEPTIBILITY TO STRESS CORROSION CRACKING

by

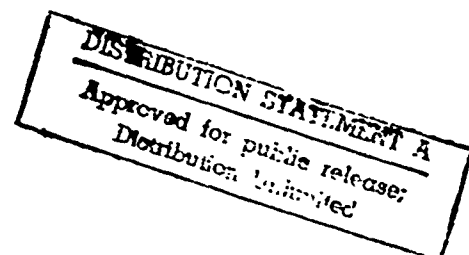
A. Hochrein, Jr. and A. Thiruvengadam

Details of illustrations in  
this document may be better  
studied on microfilm

June 1972

Department of Civil and Mechanical Engineering

N00014-67-A-0377-0003



## ABSTRACT

---

### RELATIONSHIP BETWEEN INTERNAL DAMPING AND SUSCEPTIBILITY TO STRESS CORROSION CRACKING

---

An experimental investigation of stress corrosion cracking in metals is reported for several alloy-corrodent systems. Internal damping measurements are made on the metals in the as-received condition and after they have been exposed to a corrosive environment.

This study is developed from the idea that metals which are susceptible to stress corrosion cracking exhibit changes in their damping properties after environmental exposure. From the obtained experimental evidence, susceptibility to stress corrosion cracking is associated with decreases in the peak amplitudes of the internal damping curves. For susceptible alloys the decrease in the amplitude is related to the exposure time or to the severity of environmental attack. The decrease occurs across either the thermal diffusion peak associated with the specimen thickness or with the grain size of the metal. Moreover, for alloys immune to stress corrosion cracking, it is shown that the peak amplitudes remain unchanged after environmental exposure and when compared to the same datum curve for the as-received material.

To explain the internal damping effects, a general theory of stress corrosion cracking is postulated. Based on the experimental data, stress corrosion cracking is caused by an increase in the dislocation density within the substructure. This increase in dislocation density is due to impurity atoms resulting from environmental exposure. In the presence of a stress field, dislocation concentration by impurity atoms in the interior of the grain or on the grain boundary produces strong local increases in internal strains which lead to the formation of stable microcracks.

# LIST OF SYMBOLS

A	cross section area	(in <sup>2</sup> )
a	differential parameter	(in <sup>2</sup> /sec)
B	damping force	(lb-sec/in <sup>2</sup> )
b	integer	
C	specific heat	(BTU/lb/°F)
c	concentration	
D	thermal diffusion coefficient	(in <sup>2</sup> /sec)
d	effective grain boundary thickness	(in)
E	modulus of elasticity	(lb/in <sup>2</sup> )
f	frequency	(Hz)
g	acceleration of gravity	(in/sec <sup>2</sup> )
H	activation energy	(BTU/mole)
h	specimen thickness	(in)
I	area moment of inertia	(in <sup>4</sup> )
K	thermal conductivity	(BTU/in <sup>2</sup> /in/°F/sec)
k	differential parameter	(1/in)
L	length	(in)
l	specimen length	(in)
M	attached mass	(lb-sec <sup>2</sup> /in)
m	grain size	(in)
N	atomic lengths	
n	grain density	(1/in <sup>2</sup> )
p	interatomic spacing	(in)
Q	reciprocal loss factor	

R	universal gas constant	(BTU/mole·°R)
s	density of disordered groups	
T	temperature	(°F)
t	time	(sec)
W	energy	(in-lb)
x,y	rectangular coordinates	(in)
$\alpha$	logarithmic decrement	
$\beta$	thermal expansion coefficient	(in/in/°F)
$\gamma$	weight per unit volume	(lb/in <sup>3</sup> )
$\delta$	displacement	(in)
$\eta$	viscosity	(lb-sec/in <sup>2</sup> )
$\mu$	frequency parameter	(rad/sec)
$\rho$	density	(lb-sec <sup>2</sup> /in <sup>4</sup> )
$\sigma$	amplitude time	(sec)
$\tau$	relaxation time	(sec)
$\omega$	angular frequency	(rad/sec)

## TABLE OF CONTENTS

ABSTRACT .....	ii
LIST OF SYMBOLS. ....	iii
LIST OF FIGURES.....	vii
LIST OF TABLES.....	ix
LIST OF EQUIPMENT. ....	x
Chapter	
I. INTRODUCTION . . . . .	1
II. THEORETICAL CONSIDERATIONS... ..	7
A. CALCULATION OF INTERNAL FRICTION .. ..	8
B. GRAIN BOUNDARY BEHAVIOR.... ..	10
C. INTERNAL FRICTION DUE TO DISLOCATIONS... ..	12
III. EXPERIMENTAL PROCEDURES. ....	15
A. OPERATING PRINCIPLES . . . . .	16
1. Description of Apparatus	
2. Operational Procedure	
B. EXPERIMENTAL VARIABLES . . . . .	20
1. Specimen Alignment	
2. Clamping Torque	
3. Stress Level	
C. ERROR ANALYSIS. ....	21
1. Determination of Decay Interval	
2. Specific Damping Capacity and Loss Factor	
3. Strain Hardening	
4. Amplification Factor Curve	
5. Temperature Effect	

6.	Air Drag and Internal Damping	
7.	Validity of Pure Aluminum	
D	LIMITATIONS OF THE APPARATUS . . . . .	26
1	Specimen Thickness	
2.	Geometric Factor	
E.	FIGURES. . . . .	28
IV.	EXPERIMENTAL DATA . . . . .	48
V.	DISCUSSION OF RESULTS . . . . .	72
A.	EXPERIMENTAL AND THEORETICAL CORRELATION OF DIFFUSION PEAKS. . . . .	73
B.	EXPERIMENTAL DETERMINATION OF RELAXATION TIMES. . . . .	74
C.	SUSCEPTIBLE SYSTEMS. . . . .	76
1	Aluminum	
2.	Stainless Steel	
D.	ENVIRONMENTAL MEASUREMENTS . . . . .	78
E.	NON-SUSCEPTIBLE SYSTEM EVALUATION. . . . .	79
F.	DESIGN PROCEDURE. . . . .	82
G.	MECHANISM OF FAILURE. . . . .	84
VI.	LIMITATIONS AND ASSUMPTIONS. . . . .	91
VII	CONCLUSIONS . . . . .	94
VIII	FUTURE WORK . . . . .	96

## REFERENCES

## LIST OF FIGURES

### Figure

- 1.1 Master Chart for Stress Corrosion Cracking
- 3.1 Experimental Apparatus
- 3.2 Schematic Diagram of Internal Damping Apparatus
- 3.3 Seating Device and Test Specimen
- 3.5 Specimen Alignment Calibration
- 3.6 Clamping Torque Calibration
- 3.7 Stress Level Calibration
- 3.10 Logarithmic Decrement versus Decay Interval
- 3.11 Data Photograph for Determining Decay Interval
- 3.13 Data for Loss Coefficient
- 3.14 Strain hardening Effect
- 3.15 Amplification Factor Curve
- 3.16 Effect of Temperature on Specific Damping Capacity
- 3.17 Internal Friction of Pure Aluminum
- 3.18 Determination of Specimen Thickness
- 3.19 Experimental Frequencies for Various Geometric Factors
- 4.1A Internal Damping Curve for 2024-T4 Aluminum Virgin Specimen  
(.1cm grain size)
- 4.1B Internal Damping Curve for 2024-T4 Aluminum - after 30 minutes  
immersion in mercury at 100°C and 30% yield strength (.1cm grain size)
- 4.1C Internal Damping Curve for 2024-T4 Aluminum - after one hour  
immersion in mercury at 100°C and 30% yield strength (.1cm grain size)
- 4.1D Internal Damping Curve for 2024-T4 Aluminum - after two hours  
immersion in mercury at 100°C and 30% yield strength (.1cm grain size)
- 4.1 Composite Diagram of Internal Damping Curves for 2024-T4 Aluminum  
(.1cm grain size)



- 4.2A Internal Damping Curve for 2024-T4 Aluminum - Virgin Specimen  
(.07cm grain size)
- 4.2B Internal Damping Curve for 2024-T4 Aluminum - after one hour  
immersion in mercury at 100°C and 30% yield strength (.07cm grain size)
- 4.2 Composite Diagram of Internal Damping Curves for 2024-T4 Aluminum  
(.07cm grain size)
- 4.3A Internal Damping Curve for 2024-T4 Aluminum - Virgin Specimen  
(.024cm grain size)
- 4.3B Internal Damping Curve for 2024-T4 Aluminum - after eight hours  
immersion in Potassium Dichromate at 80% yield strength (.024cm  
grain size)
- 4.3C Internal Damping Curve for 2024-T4 Aluminum - after five minutes  
immersion in mercury at 100°C and 50% yield strength (.024cm  
grain size)
- 4.3 Composite Diagram of Internal Damping Curves for 2024-T4 Aluminum  
(.024cm grain size)
- 4.4A Internal Damping Curve for 304 Stainless Steel - Virgin Specimen
- 4.4B Internal Damping Curve for 304 Stainless Steel - after one hour  
immersion in boiling magnesium chloride at 80% yield strength
- 4.4C Internal Damping Curve for 304 Stainless Steel - after two hours  
immersion in boiling magnesium chloride at 80% yield strength
- 4.4 Composite Diagram of Internal Damping Curves for 304 Stainless Steel
- 4.5 Variation in Specific Damping Capacity for Copper - immersed in sea  
water at 80% yield strength for cumulative exposure times
- 4.6 Variation in Specific Damping Capacity for Plain Carbon Steel -  
immersed in sea water at 80% yield strength for cumulative exposure  
times
- 4.7 Variation in Specific Damping Capacity for 70-30 Brass - immersed in  
ammonia vapors at 80% yield strength for cumulative exposure times
- 4.8 Composite Diagram of Internal Damping Curves for Copper - Virgin  
Specimen and sea water immersion

## LIST OF TABLES

### Chart

- 3.4 Correlation of frequency to Length as Calculated from Equation 3.7
- 3.8 Stress Computation for Cantilever Beam and Correlation of Maximum Deflection to Length
- 3.9 Specific Damping Capacity versus Length of Decay Interval
- 3.12 Specific Damping Capacity versus Interval Location on Decay Curve
- 3.20 Determination of Standard Deviation
- 4.9 Specific Damping Capacity versus Immersion Time
- 4.10 Specific Damping Capacity as a Function of Stress State

## LIST OF EQUIPMENT

1. Hewlett-Packard Model 5245L  
Electronic Counter with Time Interval Unit
2. Tektronix Oscilloscope Camera Model C-12
3. Tektronix Storage Oscilloscope Type 564  
with Type 3T77 Sampling Sweep
4. Bruel and Kjaer Frequency Analyzer Model 2107
5. Bruel and Kjaer Capacitance Transducer Model MM0002
6. Bruel and Kjaer Cathode Follower (0.5") Model 2615

Modern man, like his ancestors, is driven by an insatiable hunger for knowledge, and has struggled with the realization that the ocean is not his natural habitat. Through the eons of time, man has ascended this pit of darkness, and presently possesses a basic understanding of the ocean. By applying his experience and technology he now maintains the ability to mobilize and to operate for sustained periods of time within the sea. His interest in the ocean is not only stimulated by the thirst for acquiring knowledge, but also by the necessity for exploiting its vast resources. Consequently, an unprecedented tempo of activity has been created in studying the marine environment and with it a demand for structures which are functional and compatible with the ocean. The performance and service behavior for any structure depends greatly upon the ubiquitous environmental effects on the mechanical properties of the materials. This environmental interaction produces insidious phenomena in metallurgical engineering which is difficult to isolate and requires the special attention of the design engineer.

One of the more serious problems encountered in ocean engineering applications is stress corrosion cracking. The macrophenomenological definition constitutes a cracking process caused by the co-joint action of stress and exposure to certain corrosive environments - even for stress levels below yield strength. It is a truly insidious phenomena of metallurgical engineering because when failure occurs it is catastrophic. The firm entrenchment of steel as a construction material brought the problem of stress corrosion cracking to the forefront, and was found to occur in both ferritic and martensitic steels. (1)<sup>\*</sup> Its devastating effect was highlighted when a complete class of European submarines was scrapped because of cracking around the

---

\*Numbers in parenthesis designate References at the end of the report.

main hatch.(2) Later titanium alloys were hailed as the metallurgical cure for stress corrosion cracking, but recently a titanium alloy (Ti-6Al-4V) wire rope catastrophically failed when stressed to 80% of yield strength and exposed to sea water.(3) Such field failures combined with the future requirements of higher strengths and thinner sections confront the modern design engineer with the necessity of developing additional information. Presently the susceptibility of the high yield strength steels to stress corrosion cracking forbids their implementation as the construction material for modern ocean applications. As shown in figure 1.1, the design and material selection process draws information from basic research, material development, and screening tests. These tests combined with basic research have led to the successful design of ocean engineering structures manufactured with susceptible, high strength-to-weight ratio aluminum alloys.(4)

Originally, the phenomena of stress corrosion cracking was believed to be confined to a few alloy systems. However, it now appears to be very general and can be expected to occur in most alloy systems given the proper combination of alloy composition, heat treatment, and environment.(5) Therefore, screening tests were developed to perpetrate a more positive design approach. The tests initially devised for stress corrosion cracking constituted a variety of tensile loading specimen fixtures.(6) When loaded, the specimens were immersed either partially or completely in the corrosive environment with some alternate immersion testing also performed. These tests were basic in design and application, and the data was reported as the accumulative time to failure versus the applied stress level. A practical difficulty encountered in any stress corrosion cracking test is that the cracking takes place after a relatively long initiation period during which significant changes are difficult to observe as compared to the propagation period during which cracks

form and grow to critical size. Thus, it is time consuming to determine whether a given material is susceptible to a given environment. Sophistication in the testing technique was obtained when Brown (7) introduced his novel stress corrosion cracking test which detects crack propagation in precracked specimens. The major advantages of Brown's test are its simplicity and the relatively short time required to test prone materials. However, the test method purposely circumvents the crack initiation period and therefore does not address itself to the mechanism associated with the early phase of cracking.

Design engineers now realize that the phenomenon of stress corrosion cracking constitutes a limiting factor for any environmental design. Thus it is of paramount importance that detection tests be developed to ascertain susceptibility before crack propagation occurs and that the mechanism of susceptibility be fully understood. This understanding of why materials fail below their yield strength in certain environments would significantly aid the efforts of the design engineer in recognizing the magnitude of the problem and affording him alternate design procedures. An elegant approach to detecting the proneness of susceptible systems in the crack-initiation phase has been introduced by Thiruvengadam.(8) By examining the individual damping characteristics of materials exposed to susceptible environments, changes were detected in the material damping properties long before any microscopic evidence of cracking became noticeable.

Naturally, the initial technique required additional testing to insure reproducibility and to validate the reliability that susceptible materials undergo changes in their internal damping characteristics. It was this motivation which prompted the present investigation. Among the great variety of testing techniques, detecting changes in the internal damping characteristics of susceptible materials is the most important of all approaches. This concept utilizes the specific damping capacity of virgin specimens (i.e., unexposed to

corrosive environments) in evaluating changes resulting from environmental exposure. As a result, prone materials are determined before crack propagation begins, and the mechanism of stress corrosion cracking can for the first time be evaluated from changes in a specific property of the material. It is therefore the objective of this investigation to develop a reliable detection technique and to establish a design criterion to detect susceptible systems.

In chapter II, the theoretical considerations of internal friction are presented. This presentation includes a discussion of internal friction as a thermal relaxation process, and an application of thermal diffusion as a relaxation process to study the mechanical behavior of grain boundaries. Moreover, the phenomenon of internal damping is considered from the motion of dislocations which are "pinned-down" by impurities.

Chapter III is introduced with a description of the apparatus which includes a discussion of the operational procedure. It is concerned with the experimental variables involved and an analysis of the data.

The experimental data is presented in chapter IV.

A discussion of the experimental data is presented in chapter V, which includes a comparison of the experimental and theoretical values of the diffusion peaks. Moreover, internal damping curves are presented for susceptible alloys as a function of exposure time and for different corrosive environments. Non-susceptible alloys are evaluated and a design procedure is presented for the various aluminum systems. A general theory of stress corrosion cracking is postulated as approached from the concept of increased dislocation density and measurements of the material's specific damping capacity.

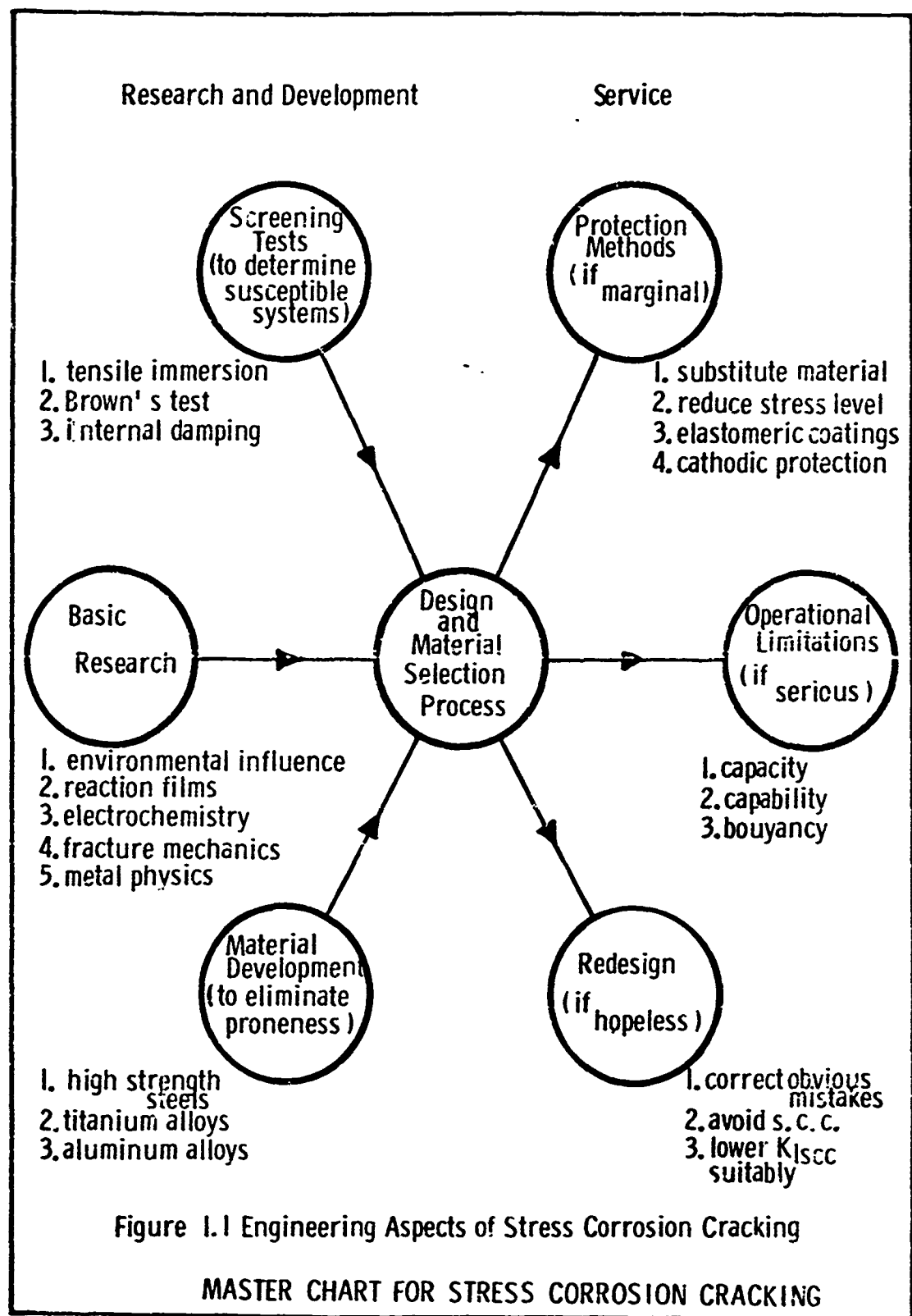
In chapter VI, a discussion is presented of the limitations and assumptions which are made in this report. It is recognized that this study is the beginning

step towards an important goal of establishing relationships between changes in the damping properties of a material and the material's reaction to its environment.

The conclusions reached are discussed in chapter VII.

The report is concluded with a discussion of the future work that should be performed. This future work is presented in chapter VIII and considers the effect of specimen thickness and the previous stress history. The engineering applications of this investigation are also presented.





A. CALCULATION OF INTERNAL FRICTION

From the theory of elasticity based on Hooke's Law, a body is considered in equilibrium under the action of applied forces and the elastic deformations take on static values. In this case, the equations of motion of the solid are obtained by equating the products of the masses and accelerations to the elastic forces - wherein it is assumed that no other forces are involved. This treatment is sufficiently accurate for solids in which the time between the application of the force and the resulting effective equilibrium is short as compared to the time during which the observation is made. Many solids do not depart seriously from this perfectly elastic behavior for small deformations and the obtained results agree well with the predictions from the elastic theory. Within the realm of Hooke's Law the only differences between individual solids results from differences in their elastic constants and their densities. However, when solids are subjected to forces which are rapidly changing, the response to these forces must be considered in terms of the dynamic elastic properties of the material (9)

Real solids are never perfectly elastic, so when they are set in vibration some of the mechanical energy is always converted to heat. Thus during vibration, the free oscillations of the specimen decay even if it is environmentally isolated. The various mechanisms by which this occurs are collectively termed as internal friction. The vibrational amplitude of a specimen should, in the absence of internal friction, increase indefinitely when vibrating at its resonant frequency; but in practice this amplitude always assumes a finite value. Moreover, real solids exhibit a hysteresis loop whereby the stress-strain curve for decreasing stresses does not exactly retrace its

upward path. Even though the magnitude of the hysteresis loop is negligible for static loading, it is an important factor in the materials dynamic response. In addition to hysteresis, engineering materials exhibit mechanical relaxation by an asymptotic increase in strain resulting from the sudden application of a fixed stress, and conversely by an asymptotic relaxation in stress whenever they are suddenly strained. This mechanical relaxation has an associated relaxation time, the direct result of which is the severe attenuation of vibrations whenever the frequency of vibration has a period that approximates the relaxation time.

The most direct method for defining internal friction is the ratio  $\Delta W/W$  where  $\Delta W$  is the energy dissipated in one cycle and  $W$  is the total elastic energy of the cycle. This ratio is called the specific damping capacity and can be measured for a given cycle without any assumptions being made about the nature of internal friction. However, the obtained value generally depends upon the specimens' stress level and the frequency of vibration.

For polycrystalline metals, it was shown by Zener (10) that thermal losses are the contributing factor for internal friction and therefore, the mechanism of internal friction is described herein as a thermal relaxation process. Changes in the volume of a solid are accompanied by changes in its temperature. When a solid is compressed its temperature rises and when it is under tensile load its temperature drops. In considering the case of a reed vibrating in transverse oscillation, each time the reed flexes, the inner side is heated while the outer side is cooled. Thus there is a continual flow of heat across the reed as it undergoes transverse vibrations. If the motion is slow, the heat has no time to flow across the reed, adiabatic conditions occur and again there is not heat loss. For transverse vibrations whose frequencies are comparable with the time required for heat to flow across the reed, there is an

irreversible conversion of mechanical energy into heat which appears as internal friction. Zener (11) has solved this heat transfer problem and shows that for a vibrating reed the specific damping capacity is given by

$$\frac{\Delta W}{W} = \frac{1}{2\pi} \left( \frac{TE\beta^2}{C} \right) \frac{\omega\mu}{\omega^2 + \mu^2} \quad (2.1)$$

where  $\mu = (\pi/h)^2 D$  and  $\beta$  is the thermal diffusion coefficient. The thickness of the reed (h) is in the plane of vibration. The frequency (fo) at which the specific damping capacity is a maximum for a rectangular cross-section reed is obtained from equation 2.1 as

$$f_0 = \frac{\pi}{2} \frac{D}{h^2} \quad (2.2)$$

Internal friction resulting from thermal diffusion occurs whether or not the solid is homogeneous. Within any polycrystalline material, neighboring grains may have different crystallographic directions with respect to the direction of strain and are thus stressed by different amounts when the specimen is deformed. This produces temperature differences between grains and minute thermal currents flow across the grain boundaries. Randall, Rose and Zener (12) have measured the internal friction in brass specimens of various grain sizes and found that, at the frequencies used, the maximum damping occurred when the size of the grain had a value close to that predicted by equation 2.2. However, care must be exercised in determining the grain size (m) which is defined (13) in centimeters as

$$\text{grain size} = \frac{1}{n^{1/2}} \quad (2.3)$$

Here  $(n)$  is represented as the mean number of grains per square millimeter. The important physical interpretation of this theoretical work is that thermal diffusion is a relaxation process. This process is governed by a characteristic time which corresponds to the peak frequency and is referred to as the relaxation time.

#### B. GRAIN BOUNDARY BEHAVIOR

We used the ideas of internal damping as a thermal diffusion and relaxation process in order to study the mechanical behavior of grain boundaries for polycrystalline materials. (14) By conducting experiments on the damping characteristics of pure aluminum, the corresponding internal friction being produced by grain boundary slip was investigated. Moreover, it was shown that the internal friction could be accounted for by assuming that the grain boundaries behave as a viscous material, and an elementary model for viscous slip along the grain boundary was constructed. The result of the model relates the viscosity  $(\eta)$  of polycrystalline metals to their relaxation time  $(\tau)$  as follows:

$$\tau = \frac{d}{m} E \tau \quad (2.4)$$

where  $(d)$  is the effective grain boundary thickness,  $(E)$  is the Young's Modulus and  $(m)$  is the grain size. The viscosity for pure aluminum was computed from equation 2.4 by determining the elastic modulus as a function of temperature from the natural frequency of vibration, and by determining the relaxation time from internal damping measurements. The calculated value for the coefficient of viscosity for aluminum as obtained from equation 2.4 was found to be within experimental error as measured by conventional means.

Another approach to the mechanism of viscous slip along the grain boundary was presented by Orowan (15) who considered disordered arrangements of atoms which are referenced as "disordered groups" or dislocations. By determining the stress distribution around the two critical atoms in the "disordered group", and by determining the shear process by which they can pass over one another, an expression was obtained for the coefficient of viscosity of intercrystalline slip as:

$$\eta = \frac{T}{s} e^{H/RT} \quad (2.5)$$

where the activation energy (H) is that which is required to pass the two critical atoms over each other, and (s) is the density of "disordered group". Equation 2.5 concurs with the observed fact that the temperature variation of grain boundary viscosity follows an exponential law. By observing the viscous behavior of grain boundaries under small shearing stresses; King, Cahn and Chalmers (16) showed that the mechanism of grain boundary slip in terms of "disordered groups" experimentally satisfied the mechanical behavior of grain boundaries.

Prior to Orowan's work, Ke (17) had considered the temperature dependence of internal friction and of the modulus of elasticity for aluminum as a function of frequency and grain size of the specimen. Employing torsional vibrations, it was demonstrated that the manifestations of internal damping can be expressed as a function of the parameter ( $m \cdot f e^{H/RT}$ ) and a relationship was experimentally obtained for the specific damping capacity of aluminum as follows:

$$\frac{\Delta W}{W} = (m f e^{H/RT}) \quad (2.6)$$

where  $(H)$  is the activation energy associated with the stress relaxation across the grain boundary, arising from the viscous behavior of the grain boundaries. Internal friction measurements were experimentally observed for two different grain sizes of aluminum and for two different frequencies of vibration. The data was then plotted against the above parameter. This data formed a smooth curve showing that the generalized statement given in equation 2.6 is valid within the range of grain size studies.

The considerations described above hold only when the grain size is smaller than the linear dimensions of the specimen. For vibrating reeds, this means that the grain size must be smaller than the thickness of the specimen. When the grain is extended completely across the specimen, its grain boundaries can no longer be considered as isolated viscous regions surrounded by an elastic matrix. The locking action of the grain edges and corners may not exist and the stress relaxation may be unlimited.

### C. INTERNAL FRICTION DUE TO DISLOCATIONS

It is well known that the phenomena of internal damping results from the motion of dislocations which are "pinned down" by impurities, by precipitates and by other dislocations. Internal damping for metal crystals is sensitively dependent on the amount of previous cold work and on the purity of the metal. (18) By performing internal damping measurements made over several orders in magnitude range, Koehler (19) considered the effect of impurities on the logarithmic decrement. Copper specimens were subjected to external shearing stresses for a large range of frequencies and it was assumed that since diffusion is an extremely slow process at room temperature, the impurity atoms are completely unable to follow the alternating stress. The dislocations are therefore anchored to the impurity atoms and

it is assumed that the portion of the line dislocation between two impurity atoms oscillates on its slip plane like a stretched string. Thus, the fewer the impurities the longer is the string length. Moreover, interactions of dislocations between one another is assumed negligible. Koehler solved the governing differential equation relating the applied shearing stress tending to move the dislocation along its slip plane to the equation of motion of the pinned-down dislocation loop.

It should be noted that impurity atoms tie down only edge-type dislocations. The splitting of a whole dislocation into partial dislocations occurs in the body and face centered cubic metals in such a way that it is impossible to obtain a screw-type dislocation in such crystals. (20) If this were not the case, the influence of impurities on the mechanical behavior of the cubic crystals would be much less marked.

Koehler obtained expressions for the average displacement of a dislocation of a given length, and for the shearing strain produced by this single loop in a cube of material of edge (L). Furthermore by considering a random distribution of solute atoms along the dislocation line, an expression was obtained for the probability of finding two impurities separated by solvent atoms. The probability is directly proportional to the concentration of impurities (c) along the dislocation line. Finally, the logarithmic decrement was calculated from equation 3.11 by obtaining expressions for the energy loss per cycle and for the total vibrational energy in the cube. The decrement was found to vary with concentration of impurities as follows:

$$\gamma = \frac{NB_0 p^3 (1 - \nu)^2 (1 + \nu)}{c^4 L^3 E} \quad (2.7)$$

where (p) is the interatomic spacing, and (N) is the number of atomic lengths



of dislocation line and (B) is the damping force acting on the dislocation. Experimental verification of equation 2.7 is found in the fact that internal damping measurements conducted on copper after forty hours exposure at  $1000^{\circ}\text{C}$  in vacuum showed that the logarithmic decrement was an order of magnitude greater when compared to the logarithmic decrement of copper after twenty hours exposure at  $1000^{\circ}\text{C}$  in hydrogen at atmospheric pressure. Dislocation concentration was further increased when a small percent by weight of iron was added to the copper during melting and exposed to the above vacuum anneal. The logarithmic decrement for the copper-iron alloy decreased two orders of magnitude as compared to initial copper measurements.

Further verification to the theory regarding a decrease in internal friction by the pinning of free lengths of dislocation lines by impurity atoms is presented by Thompson and Holmes. (21) Internal friction measurements were made on copper specimens subject to neutron bombardment. The investigators shown that the neutron damage adds to the effective impurity pinning already present through interstitial and vacancy atoms. The work is empirical in the fact that the logarithmic decrement decreases for increased neutron bombardment. However, it is impossible to obtain dependable values for the dislocation line density or the original pinning point density from the data because of the uncertainty in the effective number of pinning points produced per neutron collision and because of the uncertainty in the magnitude of the contribution from a given free length of dislocation line to internal friction.

The development of an experimental procedure for detecting changes in the internal damping capacity of engineering materials is one of the highlights of the present investigation. Testing is performed on cantilever specimens of constant rectangular cross-section which are clamped at one end and set into natural vibration by manually exciting the free end. From the resulting decay envelope, the frequency of oscillation and the specific damping capacity of the test materials are easily calculated. (22,23,24)

Within the framework of developing a testing procedure, it is imperative that the experimental variables be isolated initially and then standardized. Whenever the cumulative magnitude of these variables exceeds engineering reproducibility, their individual effects on the specific damping capacity must be evaluated. In this fashion, the debilitating effects of variable parameters remain dormant during successive phases of the experiment, and engineering reproducibility of results can be achieved. Moreover, before an experimental procedure can be validated, it is necessary to consider an error analysis of the data. Only after those variables which affect the engineering reproducibility of data have been contained, is an error analysis of the data possible.

This chapter is introduced with a description of the apparatus which includes a discussion of the operational procedure, and subsequently addresses itself to the experimental variables involved, and to an analysis of the engineering data. The chapter is concluded with a discussion of the physical limitations of the apparatus. In the subheadings that follow, by definition, experimental variables constitutes standardized parameters necessary for data reproducibility, whereas error analysis includes those factors effecting the validity of the result.

## A. OPERATING PRINCIPLES

### 1. DESCRIPTION OF APPARATUS

The apparatus used for this experiment is shown pictorially and schematically in figures 3.1 and 3.2 respectively and consists of a commercially available capacitive transducer and cathode follower, frequency analyzer and oscilloscope with camera attachment. In order to determine accurately the frequency of vibration, an electric counter was added.

The core of the apparatus constitutes a test fixture which clamps the specimen and houses the capacitive transducer. This test fixture is adjustable for variable specimen thicknesses and lengths. Secondary vibrations including ground-loops are completely negated by design. Moreover, a small seating device insures identical boundary conditions at the clamped end every time the specimen is removed from the test fixture. This device is shown in figure 3.3 with a test specimen. Furthermore, the energy dissipated between the vibrating specimen and the clamps is minimized by employing ground and hardened steel jaws. Thus the data is based on longitudinal stress distribution and needs no consideration of stress concentrations at the fixed end.

### 2. OPERATIONAL PROCEDURE

Standard ASTM sample preparation procedures for conducting stress corrosion cracking tests on aluminum alloys dictates that the specimens be cleaned in 5% sodium hydroxide solution at 80°C for one minute and then desmutted in cold concentrated nitric acid for thirty seconds and finally rinsed with hot tap water. (25)

Once sample preparation is completed, it is necessary to position the specimen properly in the test fixture. Attention is given to the specimen positioning since specimen alignment and clamping torque are two of the

variable parameters found to exist in the experimental apparatus. Therefore, proper positioning must insure that the face of the specimen is aligned parallel to the capacitive transducer, and that the clamping torque is adjusted to its predetermined level. By utilizing a set of calipers, the maximum skewed deviation between the specimen and transducer is .002 inches. Better parallelism could be obtained with more sophisticated instrumentation, but the excellent reproductibility of results and the precise validity of the specific damping capacity does not warrant the more expensive equipment.

When the positioning of the specimen in the test fixture is completed, the actual testing of the material is initiated. The design of the experimental procedure evolves from the fact that the specific damping capacity measurements are made over an order of magnitude in frequency. By knowing the material properties of the test specimen, the natural frequency of vibration can be obtained from the solution of the governing differential equation for the free lateral vibration of prismatic bars. (21) Assuming that the flexural rigidity ( $EI$ ) remains constant along the length of the bar, the general equation for the lateral vibration is:

$$\frac{\partial^2 y}{\partial t^2} + a^2 \frac{\partial^4 y}{\partial x^4} = 0 \quad (3.1)$$

where  $a^2 = (EIg/A\gamma)$ , and ( $\gamma$ ) is the weight of material per unit volume.

The solution of equation (3.1) can be represented as follows:

$$y = X(A \cos \omega t + B \sin \omega t) \quad (3.2)$$

Substitution of equation 3.2 into equation 3.1 gives:

$$\frac{d^4 X}{dx^4} = \frac{\omega^2 X}{a^2} \quad (3.3)$$

The general solution of equation 3.3 is written in the form:

$$X = C_1 (\cos kx + \cosh kx) + C_2 (\cos kx - \cosh kx) + C_3 (\sin kx + \sinh kx) + C_4 (\sin kx - \sinh kx) \quad (3.4)$$

where  $k^4 = (\omega^2/a^2)$ . The boundary conditions for the clamped-free beam are as follows:

1)	$X$	$= 0$	2)	$X'$	$= 0$
	$x = 0$			$x = 0$	
3)	$X''$	$= 0$	4)	$X'''$	$= 0$
	$x = l$			$x = l$	

Apply the first two boundary conditions to equation 3.4 and making full use of the symmetry of the problem,  $C_1 = C_3 = 0$  in the general solution. The two remaining boundary conditions give two equations for the remaining unknown coefficients. Since the expression for these coefficients is superfluous, and since they may not simultaneously and identically vanish, it is required that the determinant of the coefficients for the two equations must vanish. The aforesaid gives the following transcendental equation:

$$\cos kl \cosh kl = -1 \quad (3.5)$$

for which the first root is  $k_1 \ell = 1.875$ . The frequency of vibration of any mode is:

$$f_i = \frac{\omega_i}{2\pi} \quad (3.6)$$

Thus the first modal frequency is:

$$f_1 = \frac{3.515}{2\pi} \left[ \frac{EIg}{A\gamma\ell^4} \right]^{1/2} \quad (3.7)$$

Representative theoretical and experimental values for equation 3.7 are given in figure 3.4. The relevancy of this exercise is found in the fact that the frequency variation is obtained by shortening the specimen length. Thus prior frequency to length correlation is beneficial. Initially, weights were added to a smaller specimen length in order to obtain the lower frequency boundary condition (4) is no longer valid when the attached mass becomes "appreciable" (27). For this situation the boundary at  $x = \ell$  is free, but is rigidly connected to a body of negligible dimensions and appreciable mass (M). Thus, the moment is zero, but the shear force causes an acceleration of the body (M) which equals the acceleration of the boundary section to which the body is attached. Whenever the mass becomes appreciable, boundary condition (4) is replaced by:

$$EI \frac{\partial^3 y}{\partial x^3} = -M \frac{\partial^2 y}{\partial t^2}$$

Employing this condition, a complex form of the transcendental equation is obtained.

## B. EXPERIMENTAL VARIABLES

### 1. SPECIMEN ALIGNMENT

As previously mentioned, specimen alignment is one of the experimental variables found to exist in the experimental apparatus. The deleterious effect of specimen mis-alignment on the specific damping capacity of 2024-T4 aluminum is shown in figure 3.5. This curve is obtained by varying the alignment between the specimen face and the capacitive transducer as shown in the inset. Only when the specimen is parallel to the face of the transducer is reproducibility obtainable. The specimen alignment is made with a set of calipers and is valid within a total variation of .002 inches. Moreover, the aligned specimen, although indicating engineering reproducibility, appears to be dependent on the specimen clamping torque.

### 2. CLAMPING TORQUE

Because of the aforesaid indicated dependency of the specific damping capacity on the specimen clamp torque, figure 3.6 was obtained to ascertain the magnitude of this experimental variable. As shown, the damping capacity variation is non-existent for large clamping torques.

### 3. STRESS LEVEL

It is a well known fact that the specific damping capacity of pure aluminum varies as a function of the stress level. (28) Therefore, experimental data was obtained for various stress levels of 2024-T4 aluminum, and the stress level effect is evaluated as shown in figure 3.7. Data reproducibility becomes extremely accurate with the foregoing experimental apparatus providing the above mentioned variables are evaluated and standardized within the experimental procedure. Standardization of the experimental variables established for 2024-T4 aluminum requires proper specimen alignment, a clamping torque of 140 inch pounds and a specimen stress level of 1000 psi.

Experimentally, the maximum stress level of the specimen is obtained by deflecting the free edge a distance  $\delta_{max}$ , as shown in the inset of figure 3.8. Because the specimen is shortened continually during the experiment, it is necessary to correlate the maximum deflection corresponding to variable specimen lengths for a given applied stress level. This is accomplished by use of the beam equation, and representative computations are shown in figure 3.8.

### C. ERROR ANALYSIS

#### 1. DETERMINATION OF DECAY INTERVAL

Before the experimental procedure can be validated, it is necessary to consider an error analysis of the data. A representative data decay envelope contains approximately 120 cycles. The problem regarding the determination of the decay interval is two-fold in scope. The first part of the problem is to determine what percentage of the total cycles should be considered for the decay interval, and secondly where within the decay interval should these cycles initiate and terminate. Figure 3.9 shows the variation in the specific damping capacity of 2024-T4 aluminum with respect to the length of the decay interval. The mean specific damping value from the data is .0338 as represented by a decay interval of 70 cycles. Also by varying the abscissa, the linearity of the associated logarithmic decrements is found in figure 3.10. The associated standard deviation for the decay intervals varying from 56 to 112 cycles is  $1.2 \times 10^{-4}$ . The above data is obtained from the photograph in figure 3.11, and from the accompanying charts in figures 3.9 and 3.20.

Experimentally, the amplitudes are measured with a Gerber scale every ten cycles and then the  $A_0/A_n$  ratios are plotted on semi-logarithm graph paper through which a straight line is drawn. The logarithm of the intercept is



recorded and the logarithmic decrement is obtained by dividing the intercept by the appropriate number of cycles. The specific damping capacity is obtained from the logarithmic decrement.

Because of the linearity of the logarithmic decrements and the associated standard deviation, a frequency data interval of 70 cycles is chosen. It is now necessary to determine where the data interval should be located along the complete decay curve. Figure 3.12 shows the variation in specific damping capacity as a function of interval location along the decay envelope. For example,  $\alpha_A$  is the logarithmic decrement associated with the specific damping capacity for cycles  $A_0 - A_{70}$ ; whereas  $\alpha_B$  is the decrement associated with the damping capacity for cycles  $A_{14} - A_{84}$ , etcetera. The maximum error found in the variation of the specific damping capacity is 1.2%. Because of the obtained specific damping values the data interval reference is chosen at  $A_{14}$  and terminates at  $A_{84}$ .

## 2. SPECIFIC DAMPING CAPACITY AND LOSS FACTOR

The question arises concerning the exact form of data presentation. Many investigators (29,30) present their data in the form of the loss coefficient defined as:

$$Q^{-1} = \frac{\ln b}{\pi \sigma_b f}$$

where (b) is an integer (usually 2) and ( $\sigma_b$ ) is the time required for the amplitude to decrease 1/b of its original value. From the photograph shown in figure 3.13,  $\sigma_b$  is measured as .6 seconds and for  $b = 2$  and at a frequency of 72 Hertz the loss coefficient is:

$$Q^{-1} = \frac{\ln 2}{\pi \times .6 \times 72} = .00510$$

By an alternate definition, the loss coefficient can also be calculated from the logarithmic decrement (31)  $\alpha$  as:

$$\begin{aligned} Q^{-1} &= \frac{\alpha}{\pi} \\ &= \frac{1}{\pi} \left( \frac{1}{70} \ln 3.05 \right) = .00507 \end{aligned} \quad (3.9)$$

Employing the same data, the specific damping capacity (32) is calculated as:

$$\begin{aligned} \frac{\Delta W}{W} &= 1 - e^{-2\alpha} \\ &= .03185 \end{aligned} \quad (3.10)$$

where  $\Delta W$  is the energy dissipated on one cycle, and  $W$  is the total energy of the cycle. Expanding equation 3.10 the following approximation is obtained:

$$\begin{aligned} \frac{\Delta W}{W} &\approx 2\alpha \\ &\approx .03186 \end{aligned} \quad (3.11)$$

Thus, there exists the following approximate relationship between the specific damping capacity and the loss coefficient (33):

$$\frac{1}{2\pi} \frac{\Delta W}{W} = .00504 \approx Q^{-1} \quad (3.12)$$

The first definition of the loss coefficient, equation 3.8, is discarded because of the uncertainty in determining the relaxation time  $\tau_b$ . Moreover, the loss coefficient as defined by equation 3.9, is normally associated with steady state vibration, and not natural decay. Thus, the specific damping capacity, although a slightly more tedious calculation, is used as the measurement of internal damping.

### 3. STRAIN HARDENING

The decay curve is obtained by deflecting the free end of the cantilever specimen, a distance  $x_{max}$  and then releasing the specimen. Since the specific damping capacity is measured for a range of frequencies, it is advantageous to determine any detrimental strain hardening effects on the material damping properties. Thus the specific damping capacity of 2024-T4 aluminum must be evaluated against a number of times the specimen is deflected and then released. As shown in figure 3.14 the material damping capacity remains unchanged even after the specimen has experienced 1000 vibrational decays.

### 4. AMPLIFICATION FACTOR CURVE

An original controversy regarding the internal damping curves constituted the age old argument that the testing apparatus measures an amplification factor and not the material response. The only amplification existing in the testing apparatus is the distance between the capacitive transducer and the specimen. Therefore, an amplification factor curve was obtained to determine what effect, if any, this distance has on the damping capacity. As shown in figure 3.15, the amplification proved negative. Furthermore, the presented results are in agreement with damping values as indicated in reference 34. This agreement with other investigators is noteworthy.

### 5. TEMPERATURE EFFECT

Internal damping is described as a thermal relaxation process, and therefore the damping response is temperature dependent. For aluminum alloys the thermal relaxation peak occurs at approximately  $300^{\circ}\text{C}$  and the specific damping capacity is temperature independent to  $150^{\circ}\text{C}$ . Because of the fluctuations in room temperature, the damping capacity of 2024-T4 aluminum was evaluated for representative temperatures, and as shown in figure 3.16, the temperature effect on the specific damping capacity is non-existent.

## 6. AIR DRAG AND INTERNAL DAMPING

When a thin beam vibrates transversely in air, the various dissipative forces cause the vibrations to decay. These forces develop from the internal characteristics of the beam material or from the various external effects such as air drag and energy dissipation to the beam support. Baker, Woolam, and Young (35) present the results of an analytical and experimental investigation into several of the effects which damp vibrations of thin beams. The specific effect studied is air drag on internal damping. All other possible sources of damping were neglected in the analysis and minimized in the experiments. These investigators report measurements of internal damping for cantilever beams in air at standard and reduced atmospheric pressure. The independence of the drag forces on beam dimensions and frequency of vibration is fully investigated. From this investigation, it is concluded that one need not consider drag forces. Thus, no attempt is made to standardize the atmospheric pressure.

## 7. VALIDITY OF PURE ALUMINUM

After those factors which control the reproducibility of the natural frequency and the corresponding error in the measurement have been evaluated, the validity of the experimental procedure is determined by comparing a known frequency curve with data obtained from the present procedure. A frequency curve is defined herein as the variation in internal friction as a function of frequency. Bennewitz and Rotger (36) present the frequency curve for pure aluminum as measured with a torsional pendulum. This curve is reproduced in figure 3.17 along with data points obtained by the present experimental procedure. The comparison between the frequency curve presented by Rotger and the obtained experimental data points is, for all intents and purposes, identical. Thus, the experimental procedure is proven both reproducible and reliable.

Specifically, for this experiment, the internal damping curve for the virgin specimen of 2024-T4 aluminum was reproduced. Thereafter, the internal damping values for each frequency were determined from a single set of datum.

#### D. LIMITATIONS OF THE APPARATUS

##### 1. SPECIMEN THICKNESS

With the collection of experimental data, it is imperative that the limitations of the apparatus be realized. Within the confines of this experiment, we concern ourselves with specimen thickness and geometric factor as related to the maximum specimen frequency.

The limitations on the specimen thickness contain both upper and lower bounds. Very thin specimens may not obtain the magnitude in frequency that is required to transverse the internal friction peaks associated with thermal diffusion across the grain diameter or specimen thickness. On the other hand, very thick specimens cannot be set into natural vibration by manually exciting the free end. The specimen thicknesses for aluminum alloy 2024-T4 that are evaluated in this experiment range from .030 inches to .120 inches. As shown in figure 3.18 the frequency reaches a maximum of 750 Hertz for a specimen thickness of .044 inches. The maximum frequencies associated with the various thicknesses results from shortening the specimen to its minimum obtainable length and still maintaining a representative decay curve on the oscilloscope.

##### 2. GEOMETRIC FACTOR

The natural frequency of vibration as obtained from the exact solution of the governing differential equation is given by equation 3.7 as:

$$f_1 = \frac{3.515}{2\pi} \left( \frac{EI}{\Delta x^4} \right)^{1/2}$$

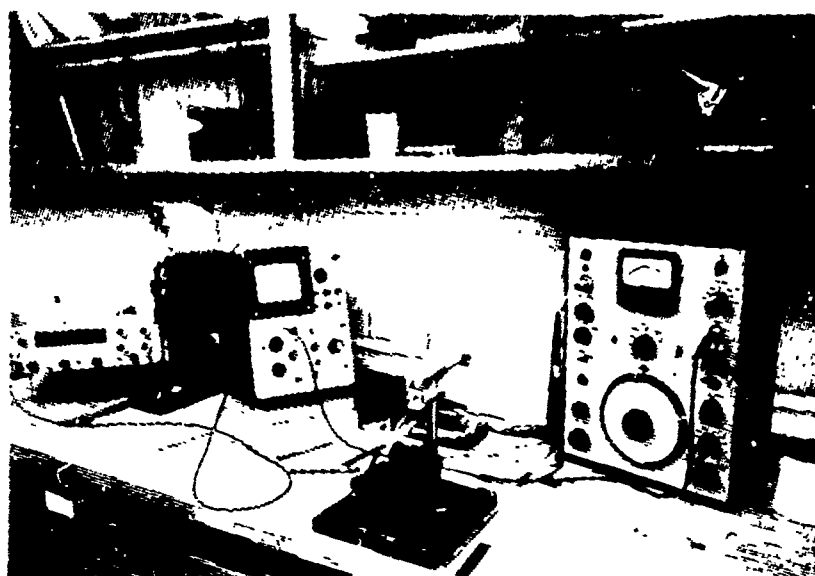
For specimens of rectangular cross-section, equation 3.7 can be reduced to:

$$f_1 = \frac{5.515}{2} \left( \frac{Eg}{12} \right)^{1/2} \left( \frac{h}{l^2} \right) \quad (3.13)$$

= constant  $(h/l^2)$

where  $(h/l^2)$  is defined as the specimen geometric factor. Thus one can determine experimentally the minimum length associated with each specimen thickness and obtain the corresponding geometric factor. The experimental frequencies are compared with the theoretical values in figure 3.19.

The geometric factors associated with a frequency greater than 500 Hertz are below the theoretical values. Thus, the apparatus does not permit a representative decay curve to be obtained for the theoretically calculated minimum length. Even though the specimen lengths could be reduced, the observed decay curves were not representative. These limitations placed on the maximum frequency by the apparatus, also place a limitation on the internal damping peak associated with the grain diameter. For extremely small grains, the apparatus does not have the capability to determine the corresponding internal damping peak, because peaks associated with very small grain diameter specimens would be above the maximum obtainable frequency. The limitation placed on the grain size of 2024-T4 aluminum is .024cm.



Reproduced from  
best available copy. 

Figure 3.1 Experimental Apparatus

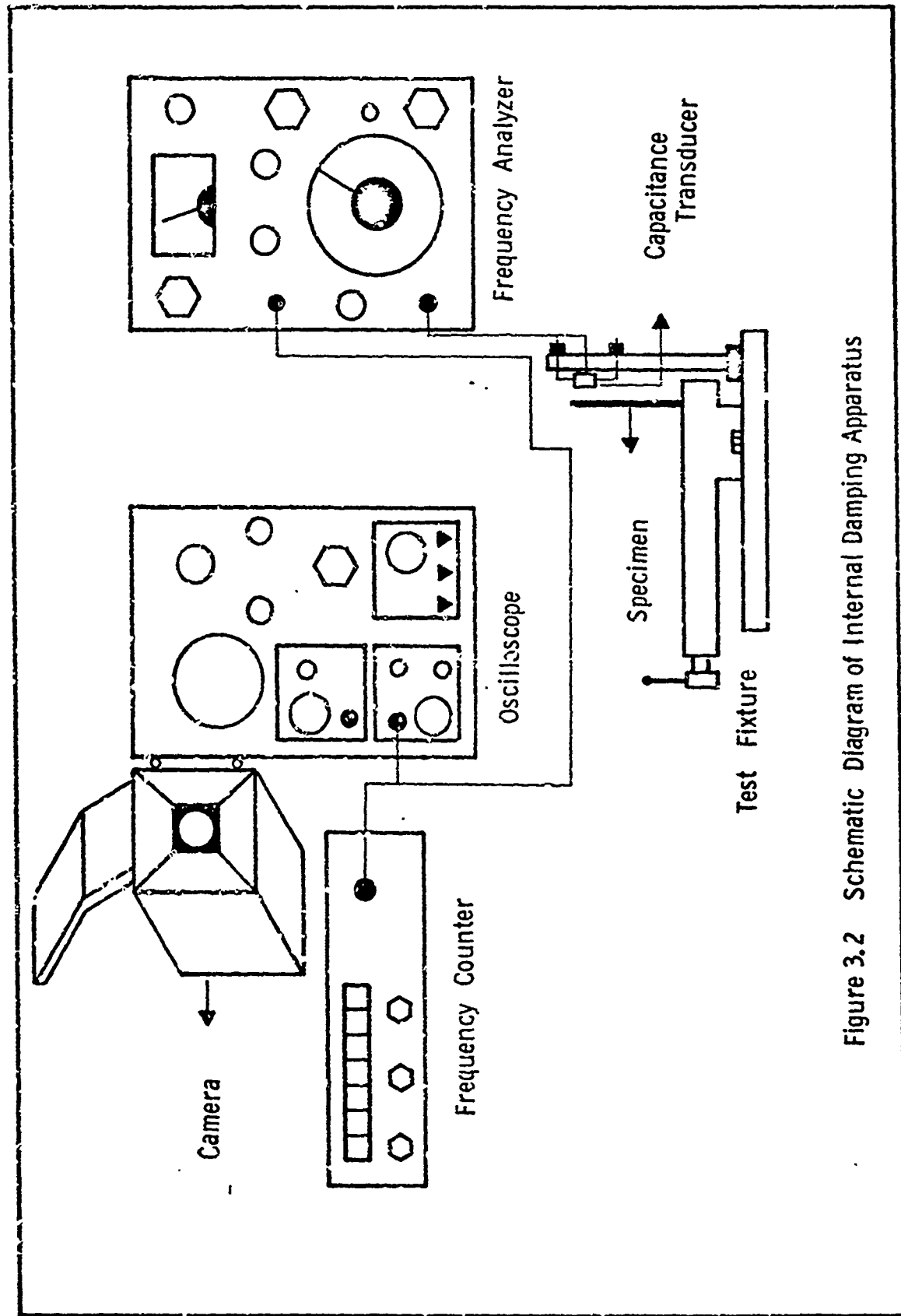
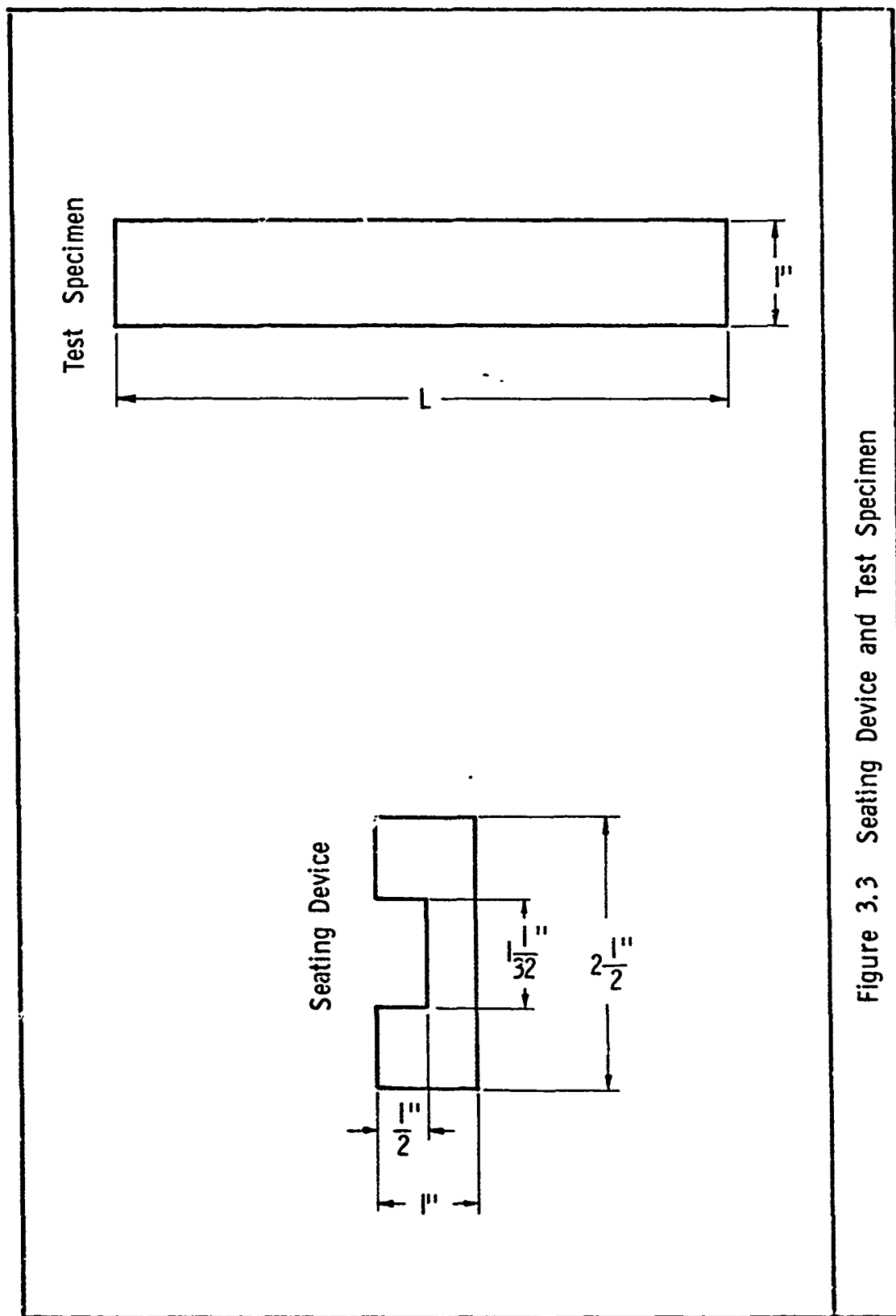


Figure 3.2 Schematic Diagram of Internal Damping Apparatus





Specimen Length	Specimen Frequency ( Hertz )			Calculation From Equation 7 $\gamma = .1 \text{ lbs/in}^3$ $b = 1''$ $h = .060''$
	Oscilloscope	Counter	Calculation	
10"	19.8	19.9	19.6	
8"	30.1	30.8	30.7	
6"	53.9	54.2	54.0	
4"	120.0	122.0	122.5	
2"	482.0	488.0	489.0	

Figure 3.4 Correlation of Frequency to Length

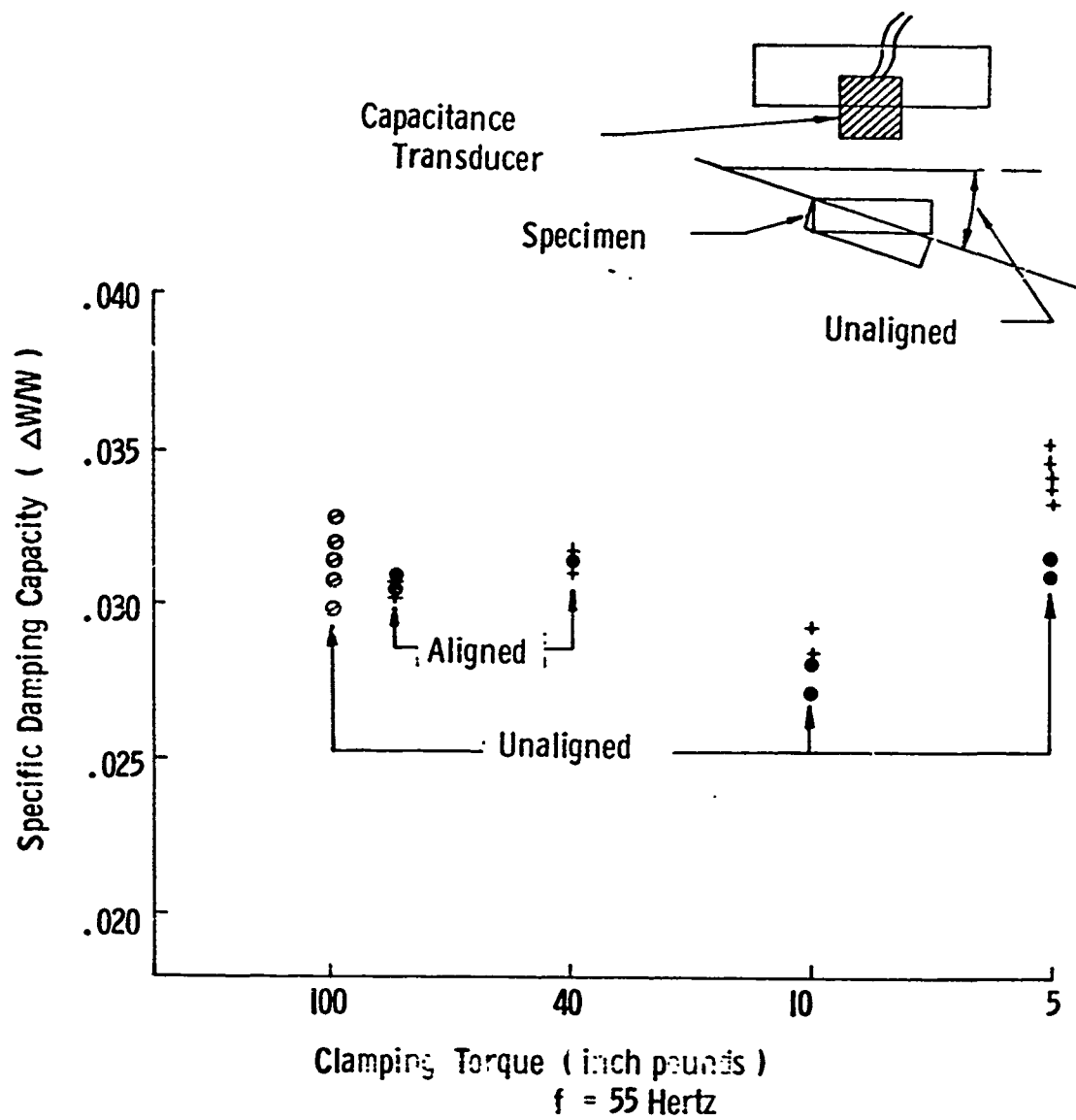


Figure 3.5 Specimen Alignment Calibration

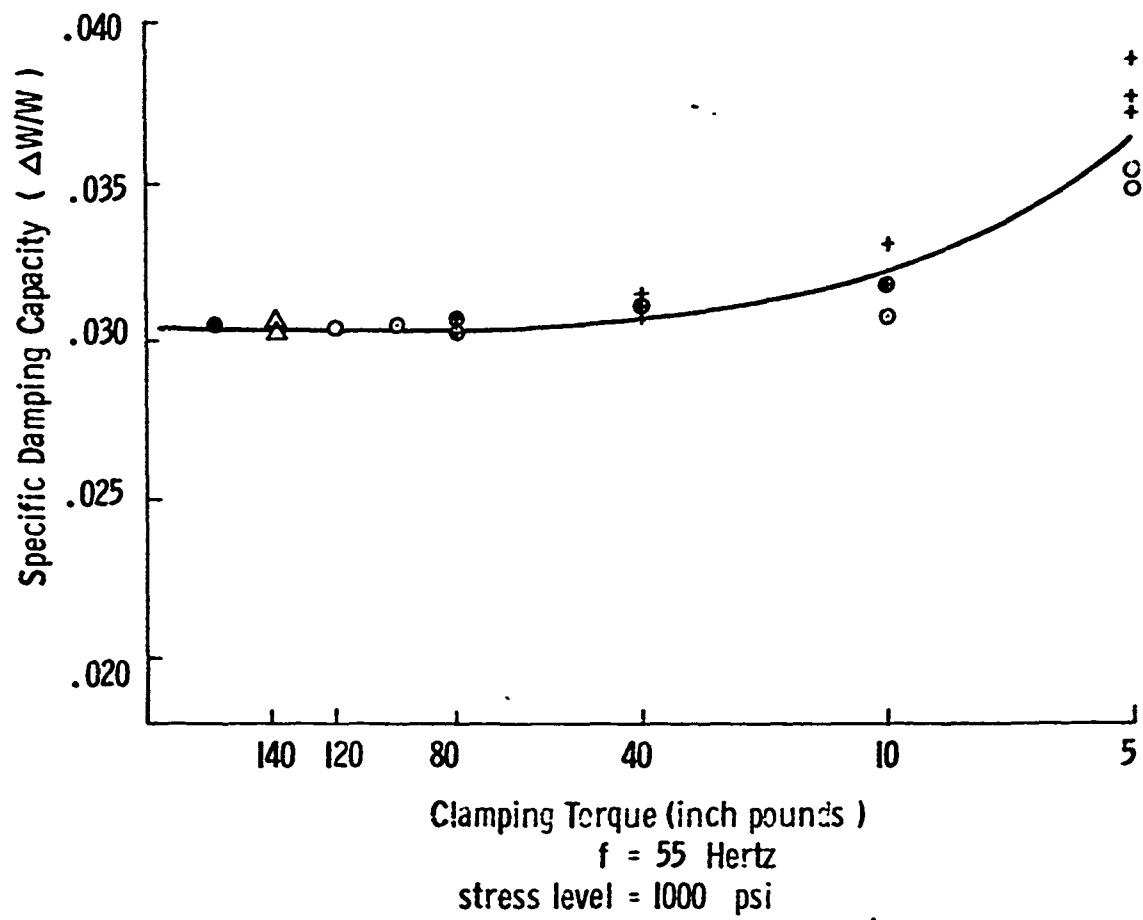


Figure 3.6 Clamping Torque Calibration

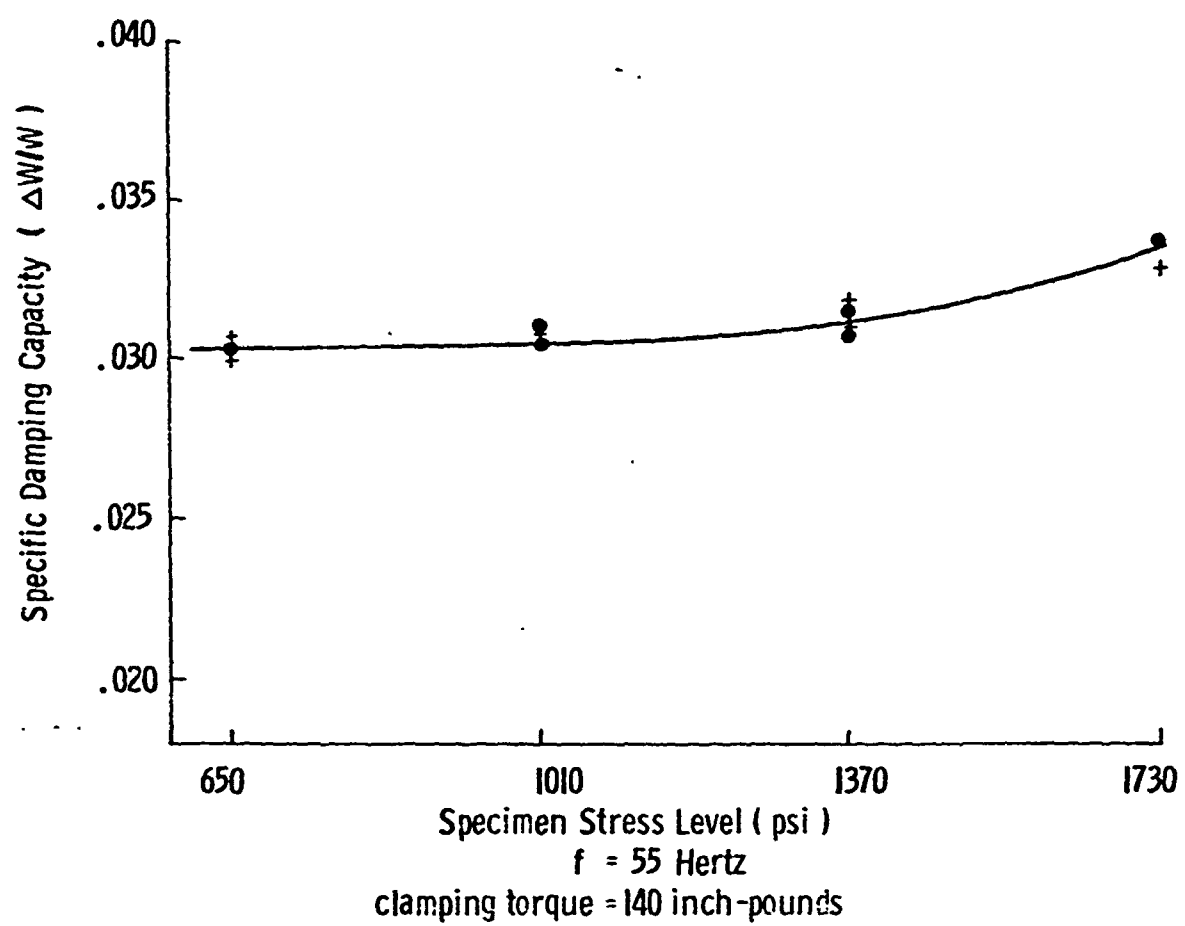


Figure 3.7 Stress Level Calibration

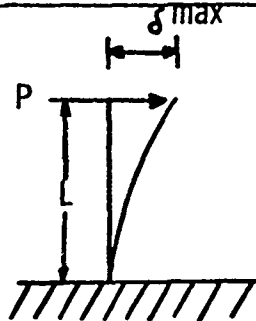
Specimen Length ( inches )	Actual Experimental Values $\delta_{\max}$	 $P = \frac{3 E I \delta_{\max}}{L^3}$ <p>where: <math>\sigma = \frac{M c}{I} = \frac{M \cdot h/2}{I}</math></p> $M = P \cdot L$ $\sigma = \frac{P L h}{2 I} ; P = \frac{2 I \sigma}{h L}$ $\frac{3 E I \delta_{\max}}{L^3} = \frac{2 I \sigma}{h L}$ <p>or <math>\sigma = \frac{3 E h \delta_{\max}}{2 L^2}</math></p>
5.0	.034	
4.5	.028	
4.0	.022	
3.5	.017	
3.0	.012	
2.5	.0085	
2.0	.0055	

Figure 3.8 Stress Computation for Cantilever Beam  
and  
Correlation of Maximum Deflection to Length

Amplitude	$A_0/A_n$	$\alpha = (1/N) \ln(A_0/A_n)$	$\Delta W/W = 1 - e^{-2\alpha}$
$A_0 = 6.0$	1.00		
$A_{14} = 4.70$	1.28	.01764	.0346
$A_{28} = 3.70$	1.62	.01724	.0339
$A_{42} = 2.90$	2.07	.01733	.0341
$A_{56} = 2.30$	2.61	.01714	.0336
$A_{70} = 1.85$	3.33	.01719	.0338
$A_{84} = 1.40$	4.28	.01724	.0339
$A_{98} = 1.13$	5.32	.01713	.0336
$A_{112} = 0.88$	6.82	.01714	.0336

Figure 3.9      Specific Damping Capacity vs  
Length of Decay Interval

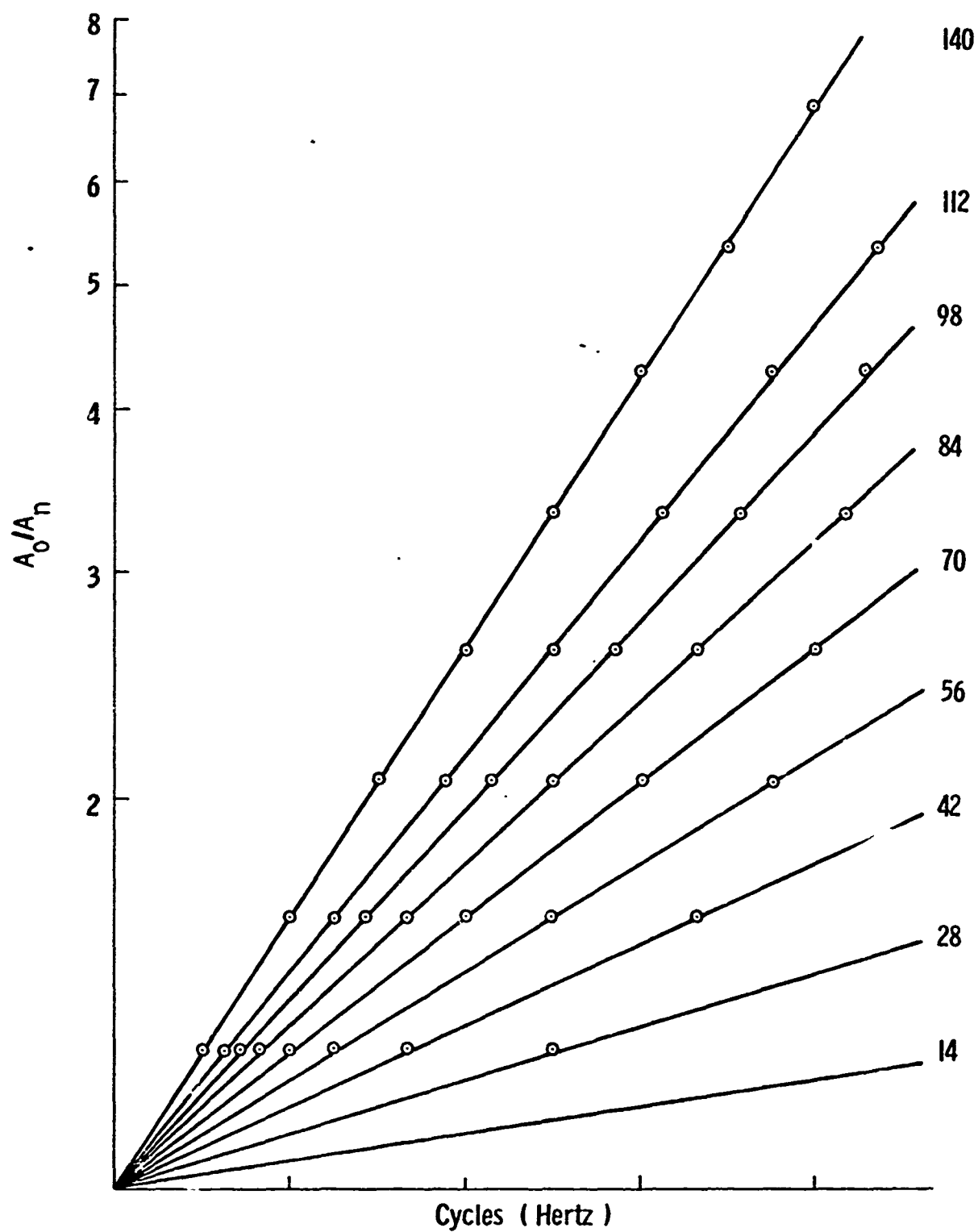
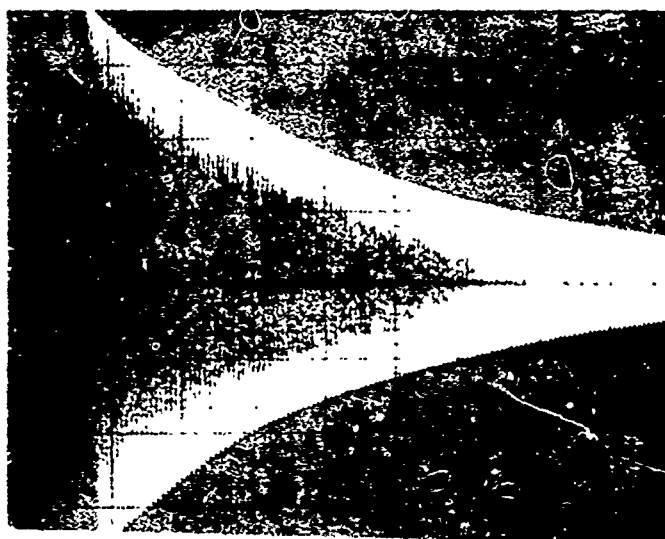


Figure 3.10 Logarithmic Decrement vs Decay Interval






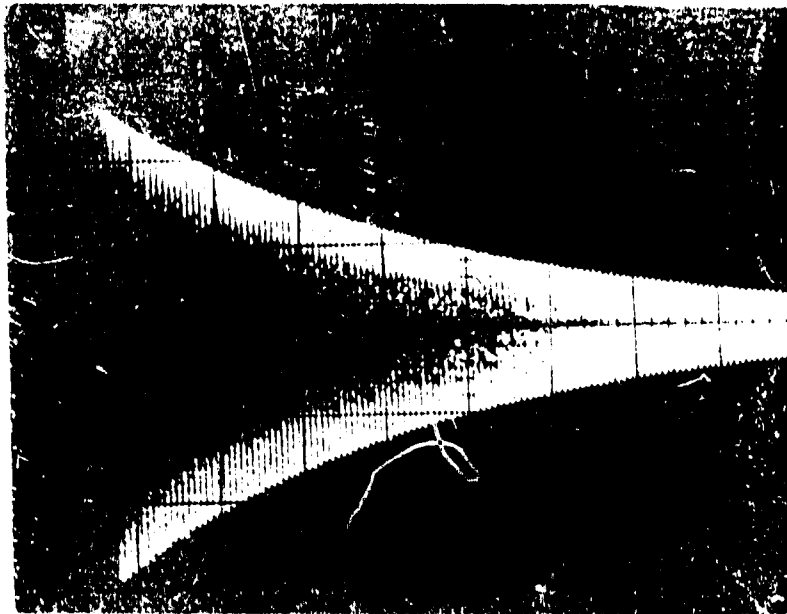
Reproduced from  
best available copy. 

Figure 3.11 Data Photograph for Determining  
Decay Interval

Amplitude	$A_0/A_n$	$\alpha = (1/70) \ln(A_0/A_n)$			$\Delta W/W = 1 - e^{-2\alpha}$
$A_0 = 6.0$	1.00	$\alpha_A = (1/70) \ln 3.30$			0.0335
$A_{14} = 4.7$	1.28	1.00	$\alpha_B = (1/70) \ln 3.25$		0.0331
$A_{28} = 3.7$	1.62	1.27	1.00	$\alpha_C = (1/70) \ln 3.25$	0.0331
$A_{42} = 2.9$	2.07	1.62	1.28	1.00 $\alpha_D = (1/70) \ln 3.27$	0.0334
$A_{56} = 2.3$	2.61	2.04	1.61	1.26	
$A_{70} = 1.85$	3.33	2.54	2.00	1.57	
$A_{84} = 1.40$		3.36	2.64	2.07	
$A_{98} = 1.13$			3.27	2.57	
$A_{112} = .88$				3.30	
<p>Figure 3.12      Specific Damping Capacity vs Interval Location on Decay Curve</p>					




Reproduced from  
best available copy. 

Figure 3.13 Data For Loss Coefficient

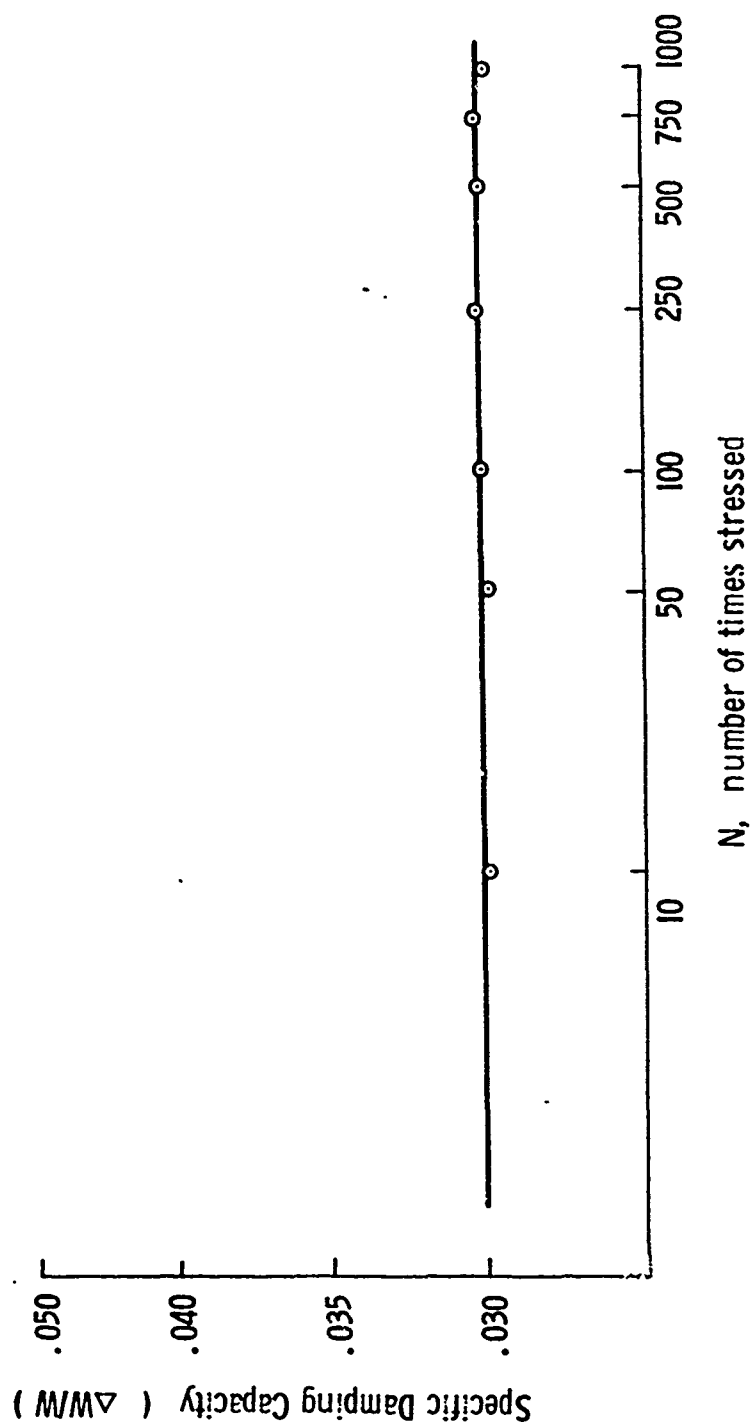


Figure 3.14 Strain Hardening Effect ( 2024-T4 Al )

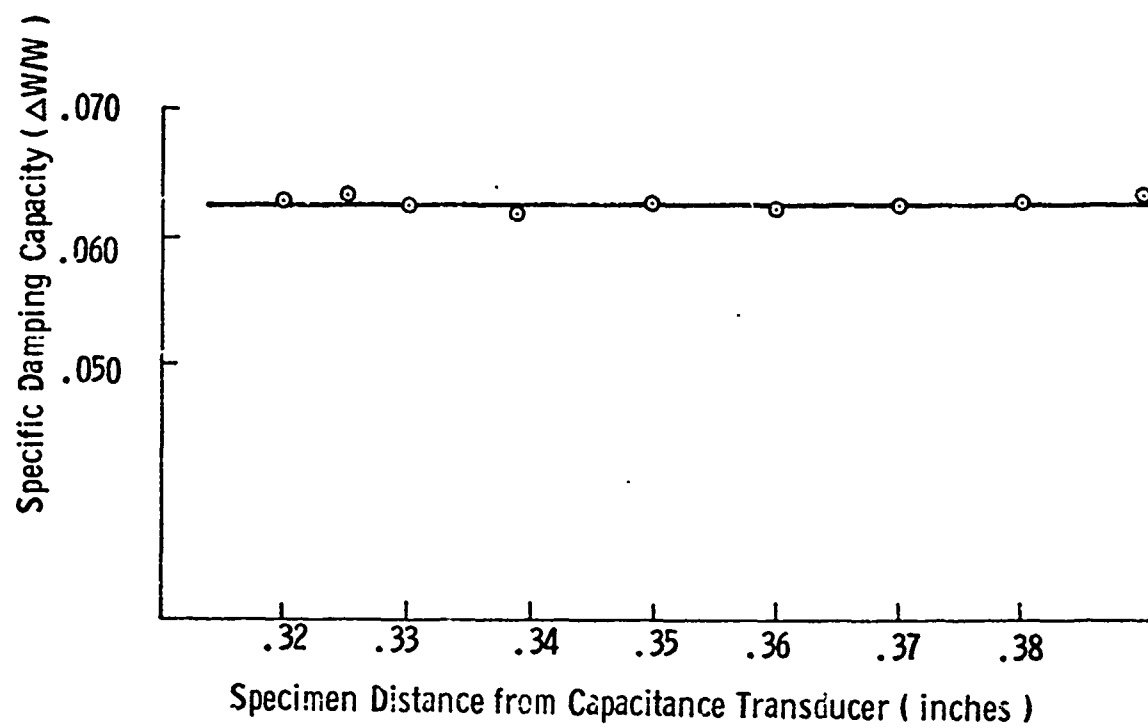


Figure 3.15 Amplification Factor Curve

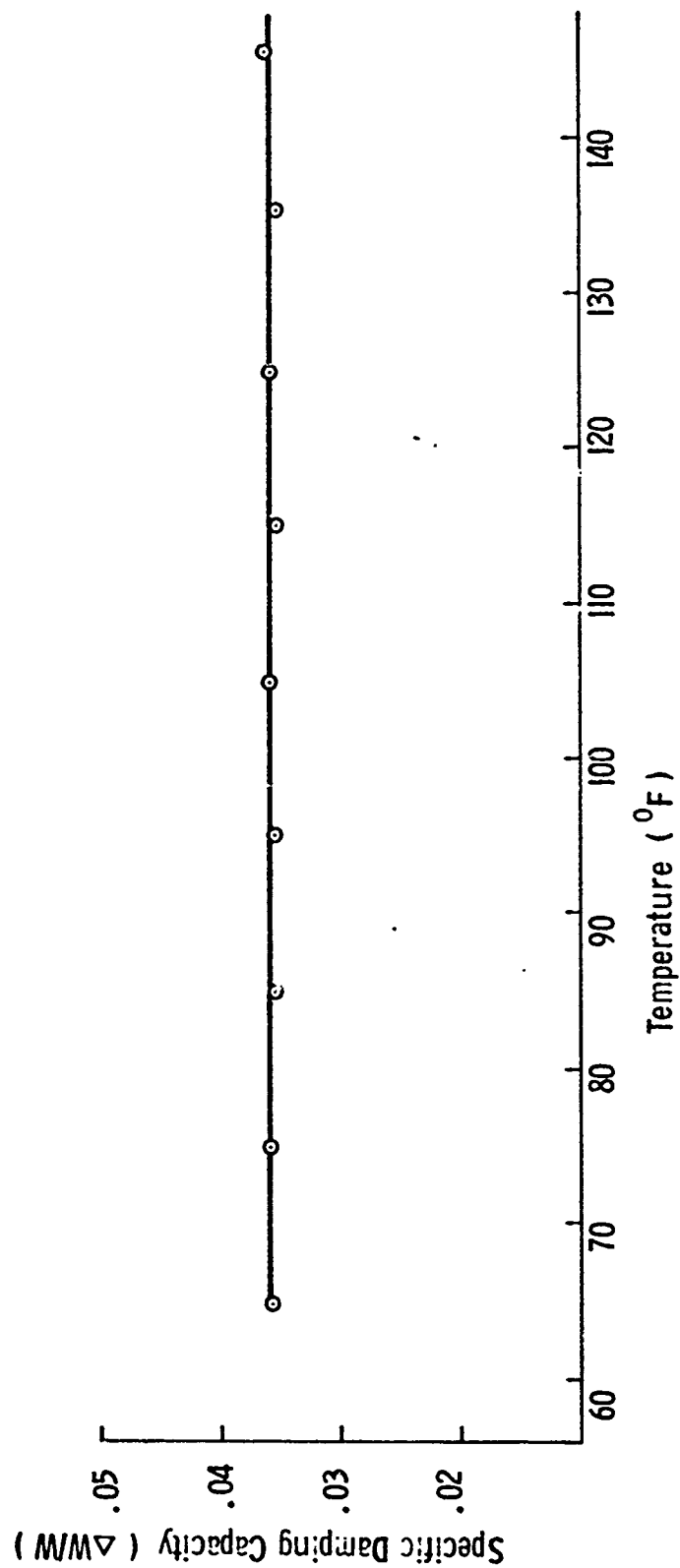


Figure 3.16 Effect of Temperature on Specific Damping Capacity ( 2024-T4 Al )

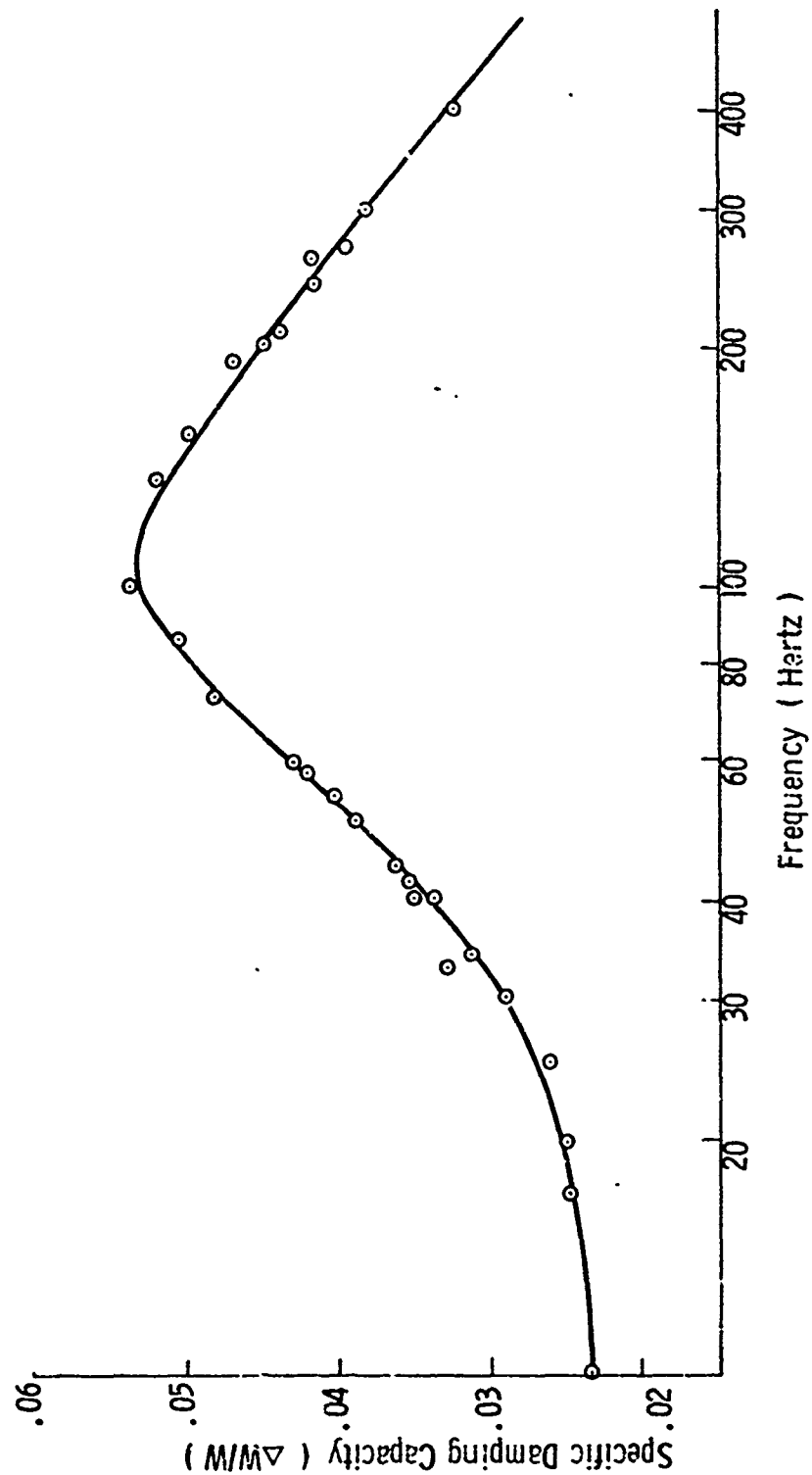


Figure 3.17 Internal Friction of Pure Aluminum

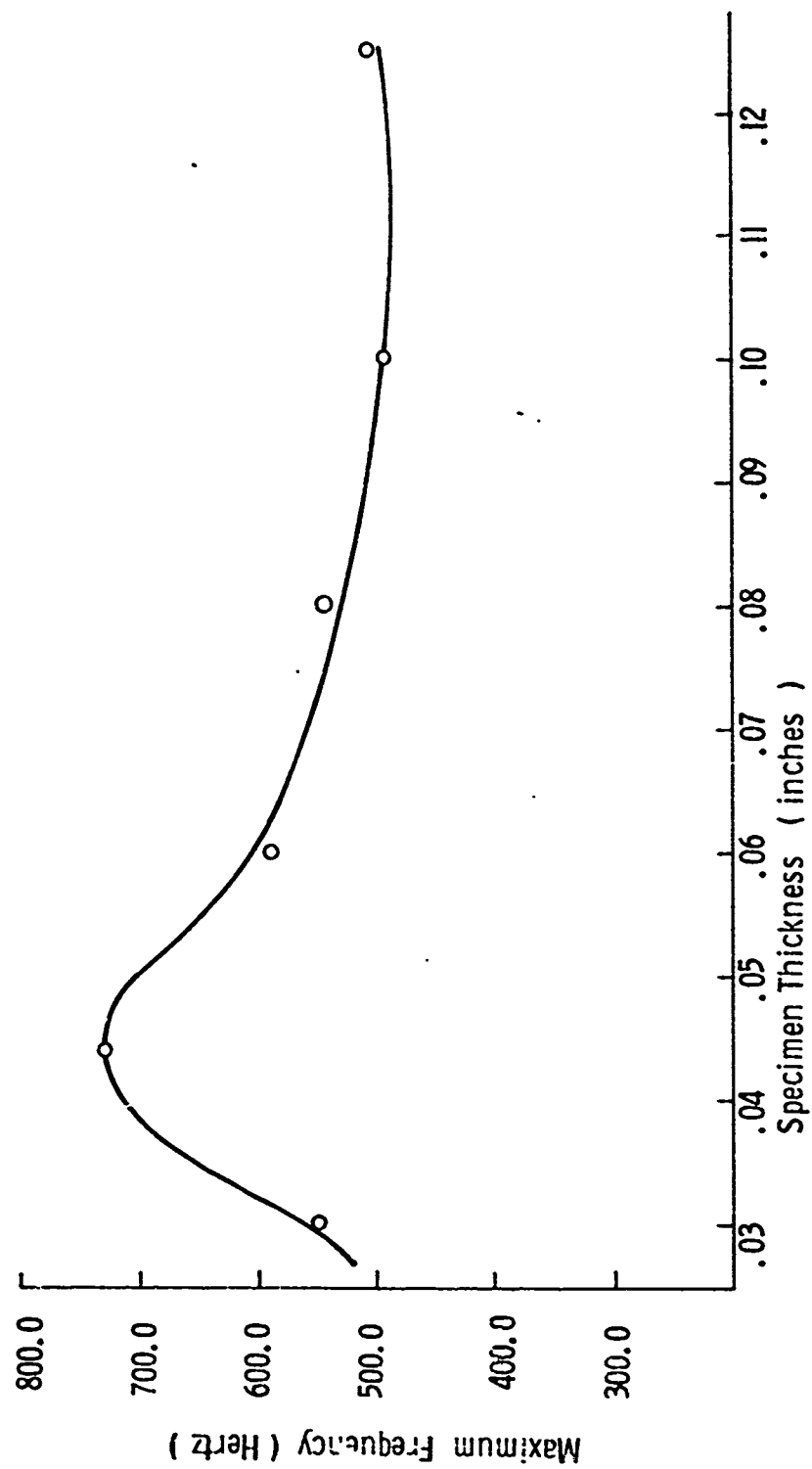


Figure 3.18 Determination of Specimen Thickness



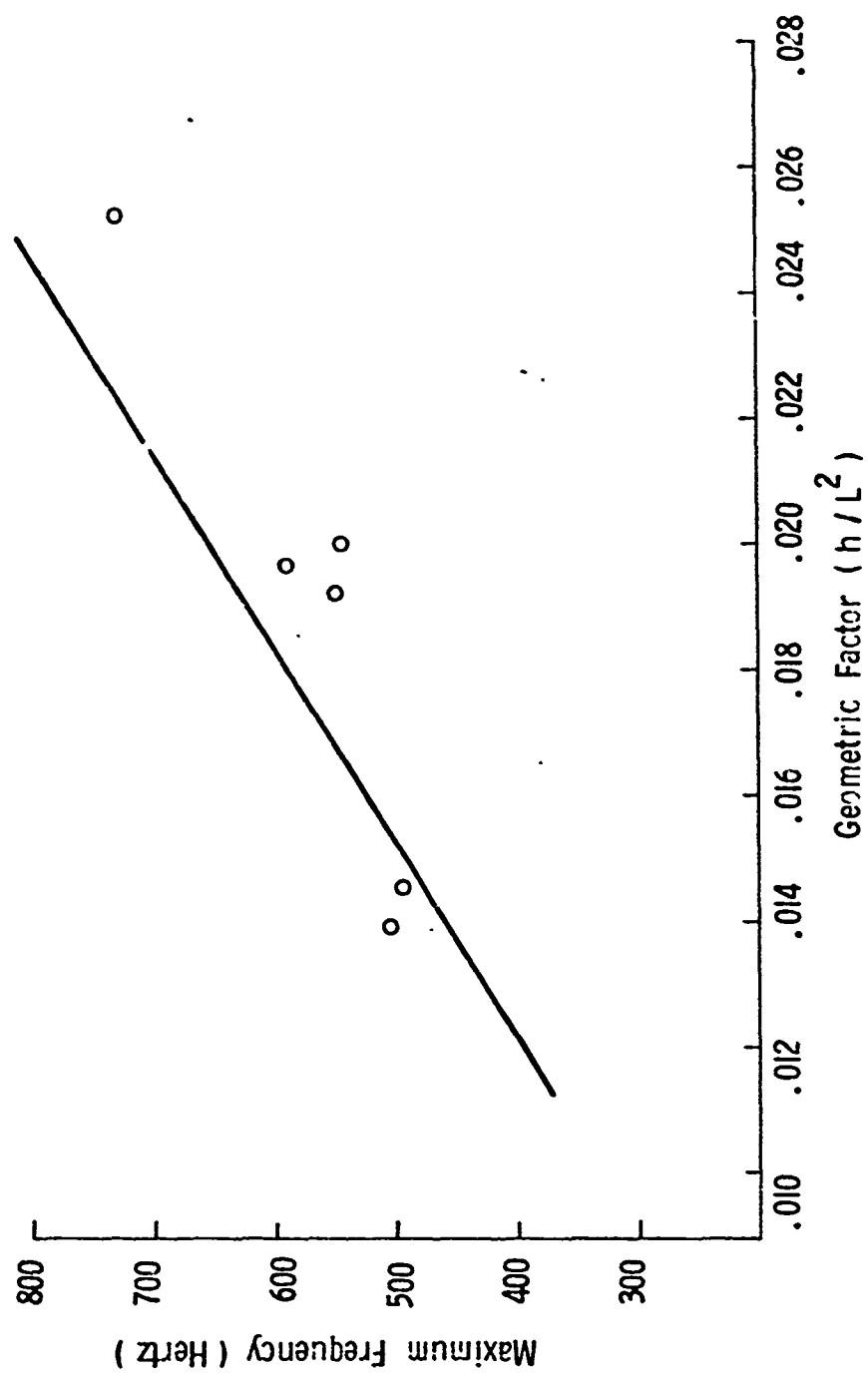


Figure 3.19 Experimental Frequencies for Various Geometric Factors

SAMPLE	DATA $X_i$	MEAN DEVIATION $X_i - \bar{X}$	$(X_i - \bar{X})^2$
1	.0336	-.0001	$1 \times 10^{-8}$
2	.0338	+.0001	$1 \times 10^{-8}$
3	.0339	+.0002	$4 \times 10^{-8}$
4	.0336	-.0001	$1 \times 10^{-8}$
5	.0336	-.0001	$1 \times 10^{-8}$
$X_i = .1685$ $\bar{X} = .0337$ $\sum  X_i - \bar{X}  = .0006$ $\sum (X_i - \bar{X})^2 = 8 \times 10^{-8}$ $\sigma = \left( \frac{1}{5} \times 8 \times 10^{-8} \right)^{\frac{1}{2}}$ $\sigma = \text{standard deviation} = 1.26 \times 10^{-4}$			
Figure 3.20 Determination of Standard Deviation			

The internal damping curves and supporting charts presented herein constitutes data from a series of experiments conducted on known systems - either susceptible or non-susceptible to stress corrosion cracking. Figures 4.1 - 4.1D and 4.2 - 4.2B represent internal damping curves for aluminum alloy 2024-T4 and includes specimens of .1cm and .07cm in grain size respectively. Supporting data is found in the charts of figures 4.9 and 4.10.

The results of experiments conducted on aluminum alloy 2024-T4 after exposure to different corrosive environments are found in figures 4.3 to 4.3C. In contrast to these, a time controlled experiment was performed on type 304 stainless steel in boiling magnesium chloride with the representative curves found in figures 4.4 to 4.4C. Variation in the specific damping capacity as a function of time is presented in figures 4.5 to 4.7 for both susceptible and non-susceptible systems, i.e. copper in sea water, steel in sea water, and brass in ammonia respectively. Figure 4.8 shows the resulting change in the specific damping capacity of a non-susceptible system before and after exposure to a corrosive environment.

In utilizing the method for measuring the dynamic elastic properties of the materials presented herein, the internal friction could not be calculated from the experimental measurements unless certain assumptions were made about the linearity of the system. The assumption made was that the type of mechanical behavior was independent of the amplitude of the deformation within the range of stress as employed in the experiments. It should be emphasized that since the elastic properties are independent of amplitude

(as discussed in Chapter III), the mechanical properties of the materials under investigation are linear. Therefore, at a given frequency, the period and the logarithmic decrement for free vibrations define the mechanical behavior of the material. Thus, Boltzmann's (37) superposition principle is assumed valid, and the internal damping curves can be obtained from a series of measurements made over a range of frequencies.

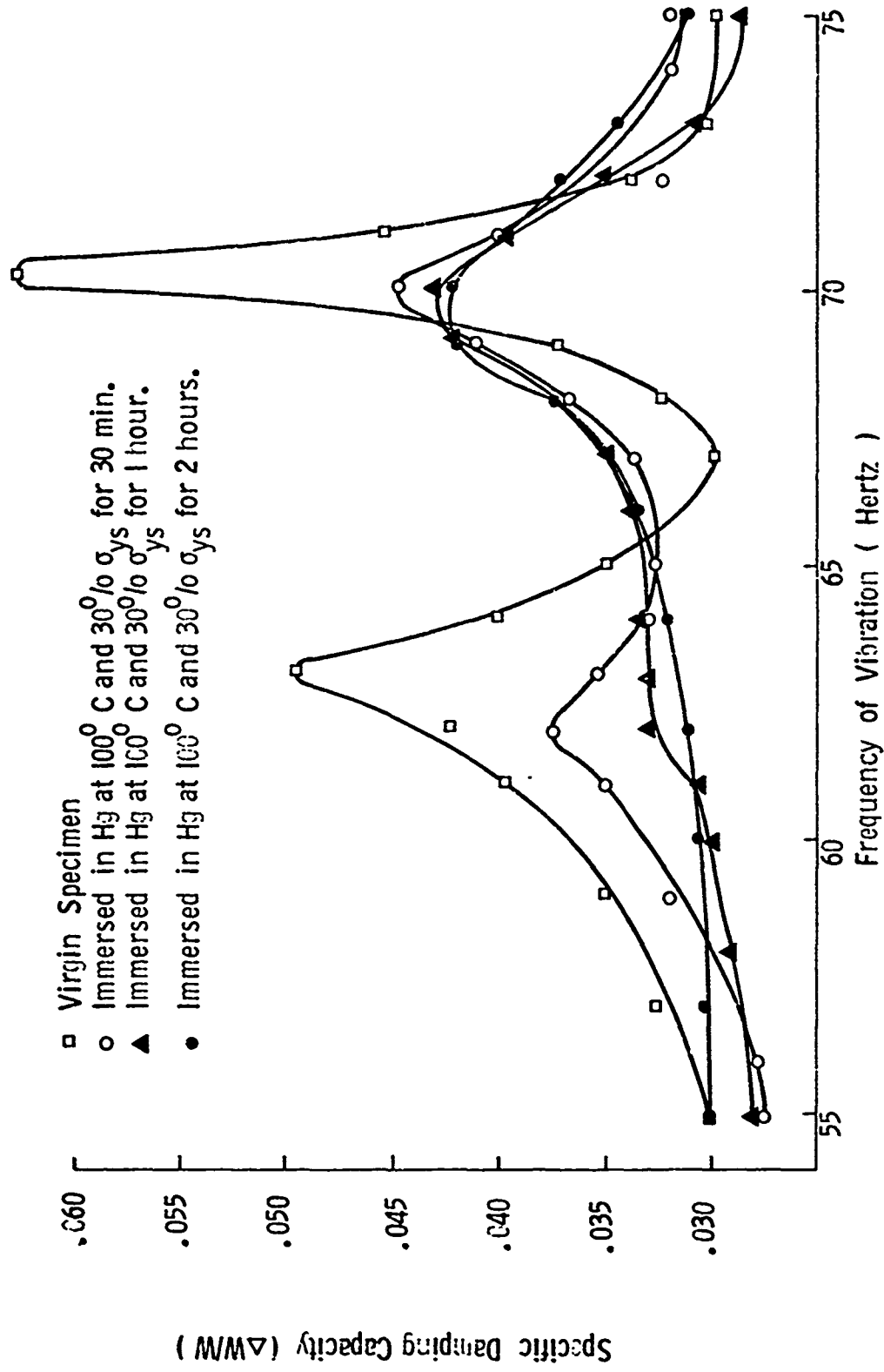


Figure 4.1 Internal Damping Curve for 2024-T4 Al ( 0.1 cm grain size )

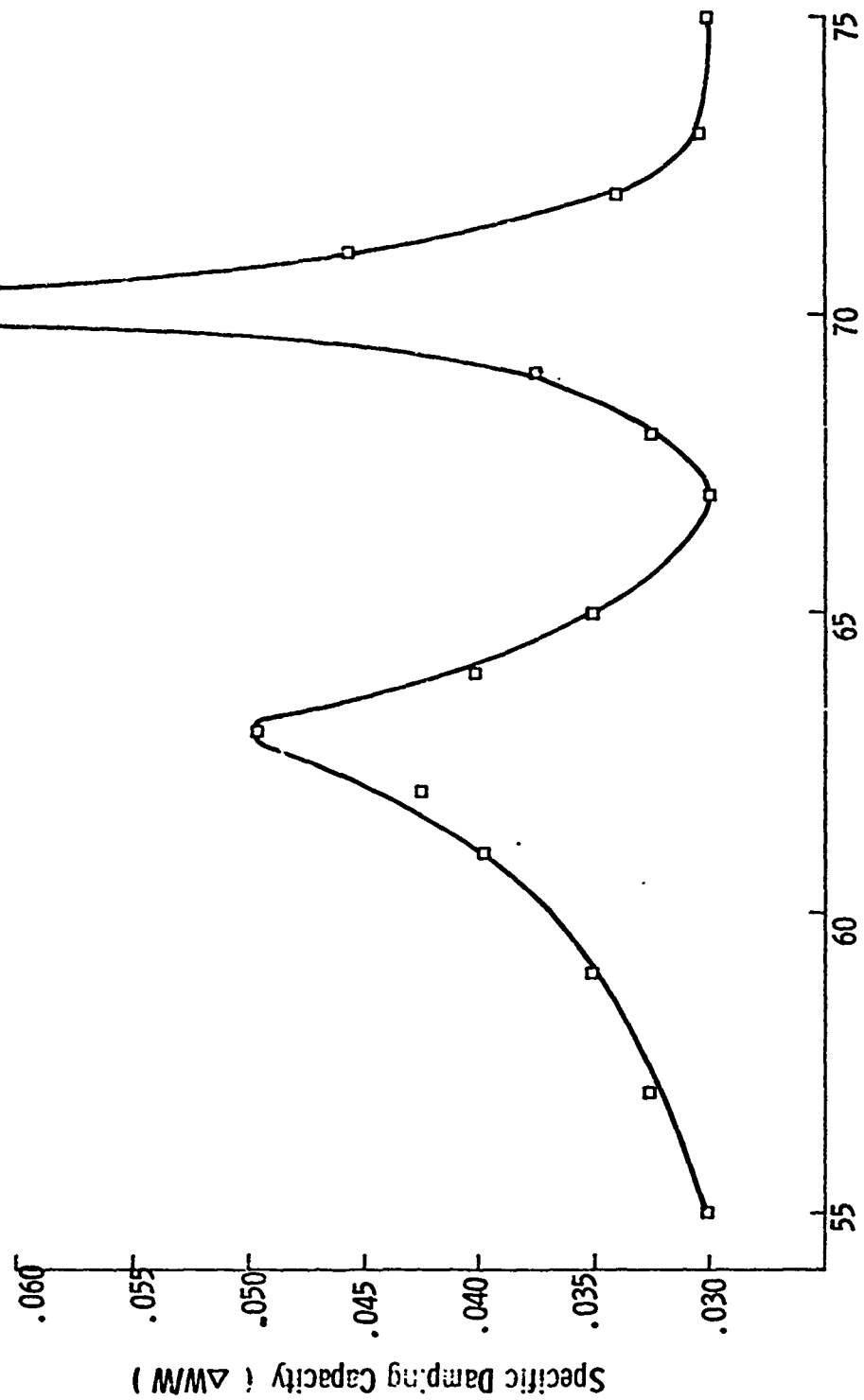


Figure 4.1A Internal Damping Curve for 2024-T4 Al ( 0.1 cm grain size )  
Virgin Specimen



Figure 4.1B Internal Damping Curve for 2024-T4 Al ( 0.1 cm grain size )  
Immersed in Hg at 100°C and 30% to  $\sigma_{ys}$  for 30 minutes

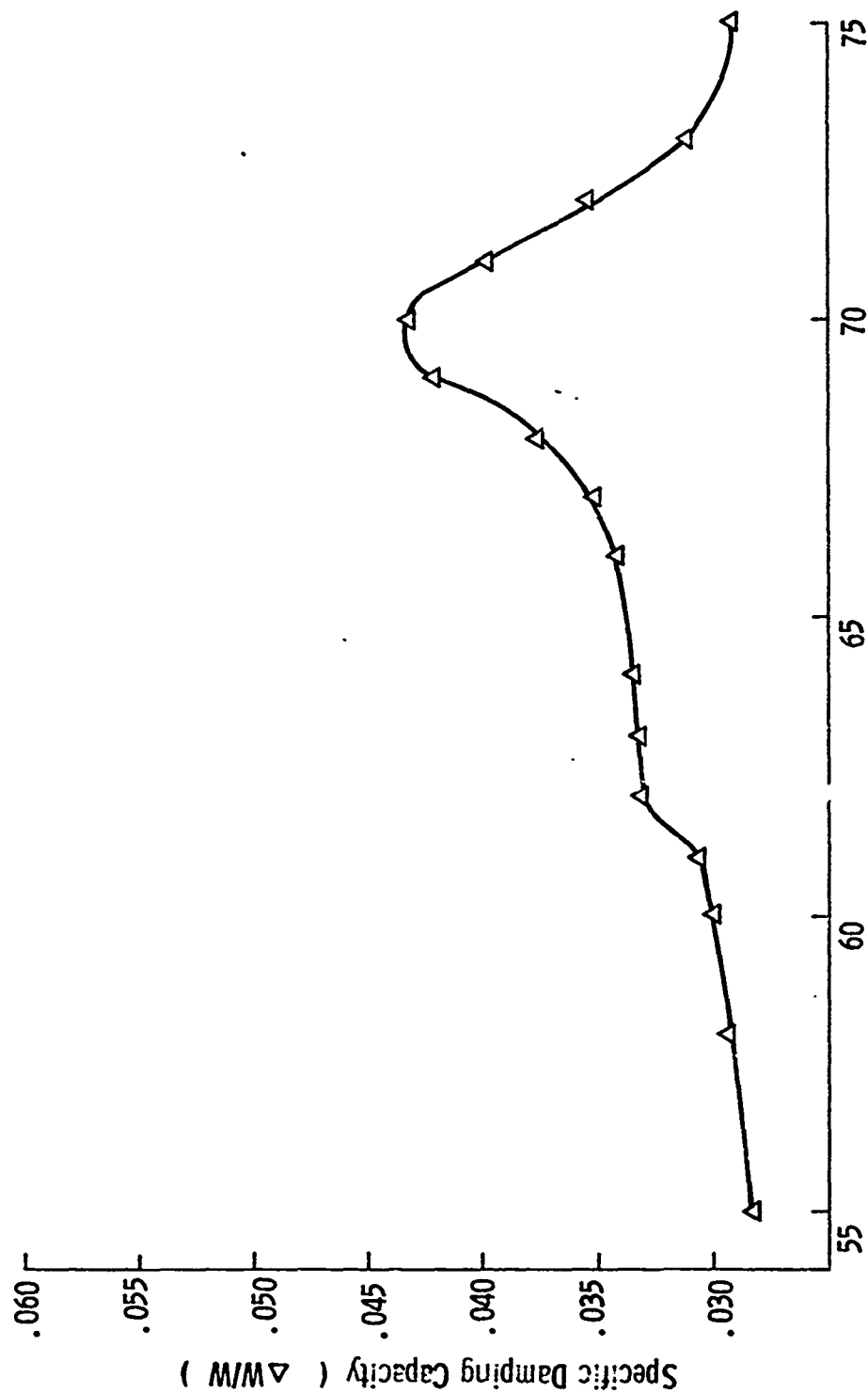


Figure 4.1C Internal Damping Curve for 2024-T4 Al ( 0.1 cm grain size )  
Immersed in Hg at 100°C and 30°/o  $\sigma_{ys}$  for 1 hour



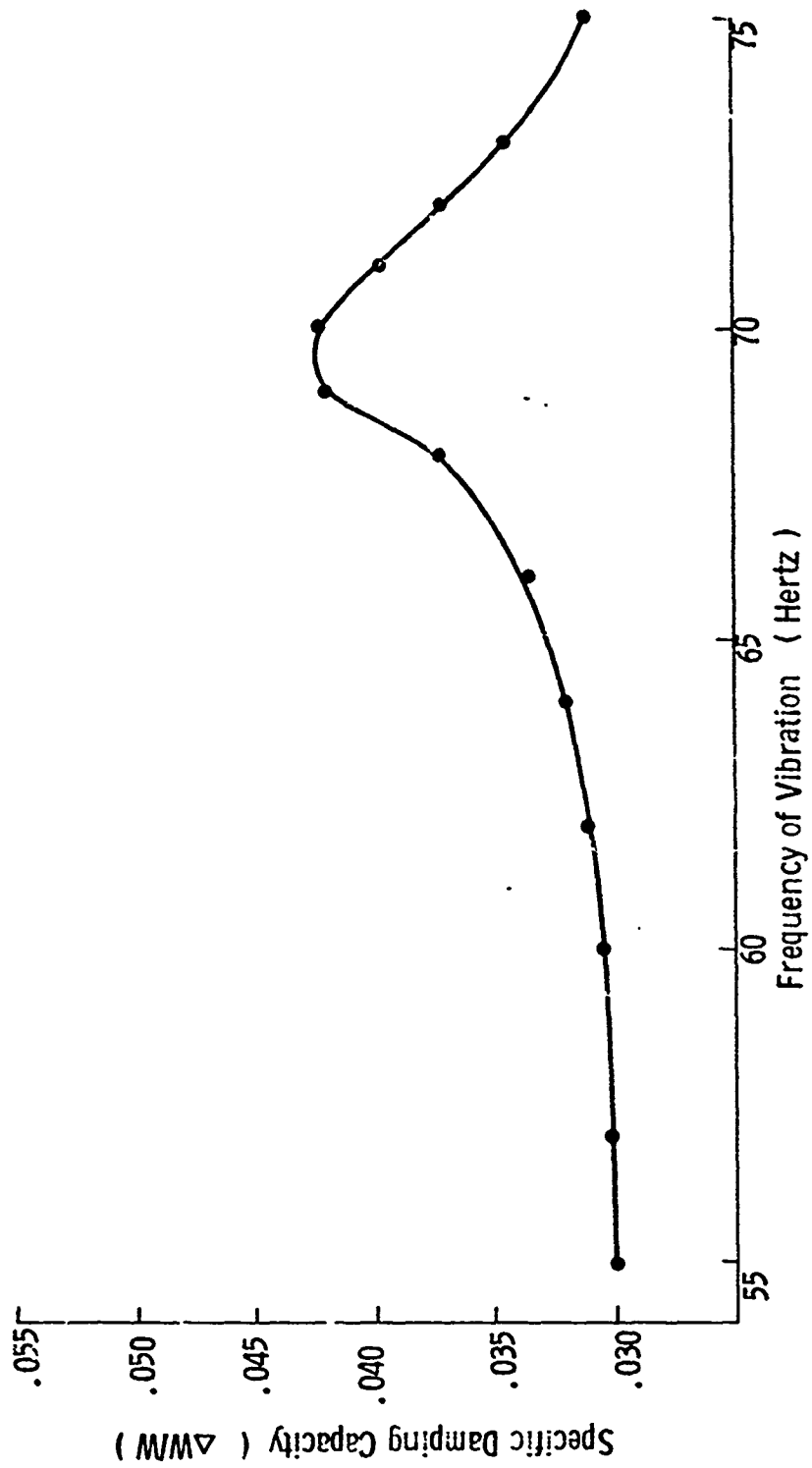


Figure 4.1D Internal Damping Curve for 2024-T4 Al ( 0.1 cm grain size )  
Immersed in Hg at 100°C and 30%  $\sigma_{ys}$  for 2 hours

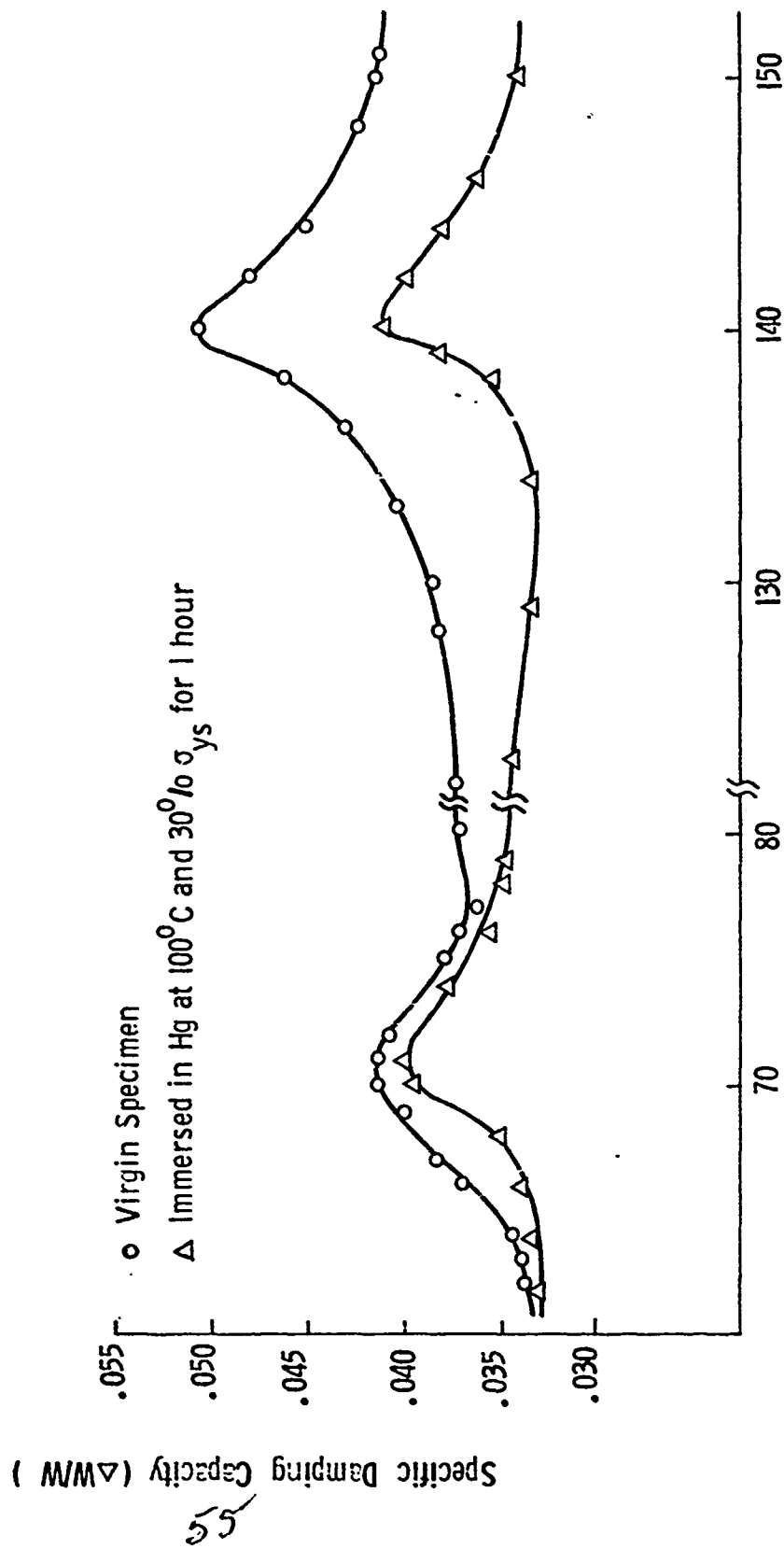


Figure 4.2 Internal Damping Curve for 2024-T4 Al (0.07 cm grain size)

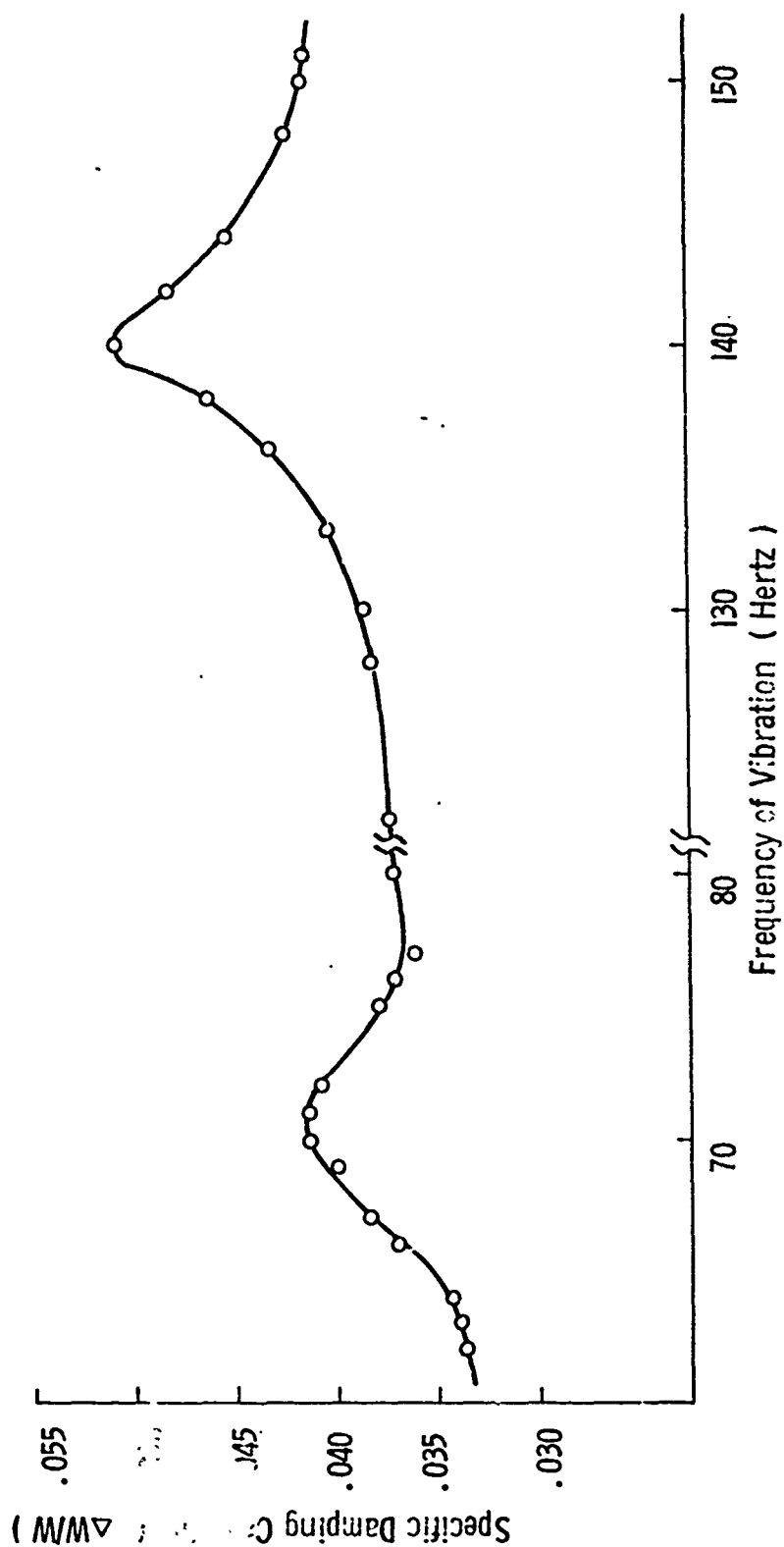


Figure 4.2 A Internal Damping Curve for 2024-T4 Al ( 0.07 cm grain size )  
Virgin Specimen

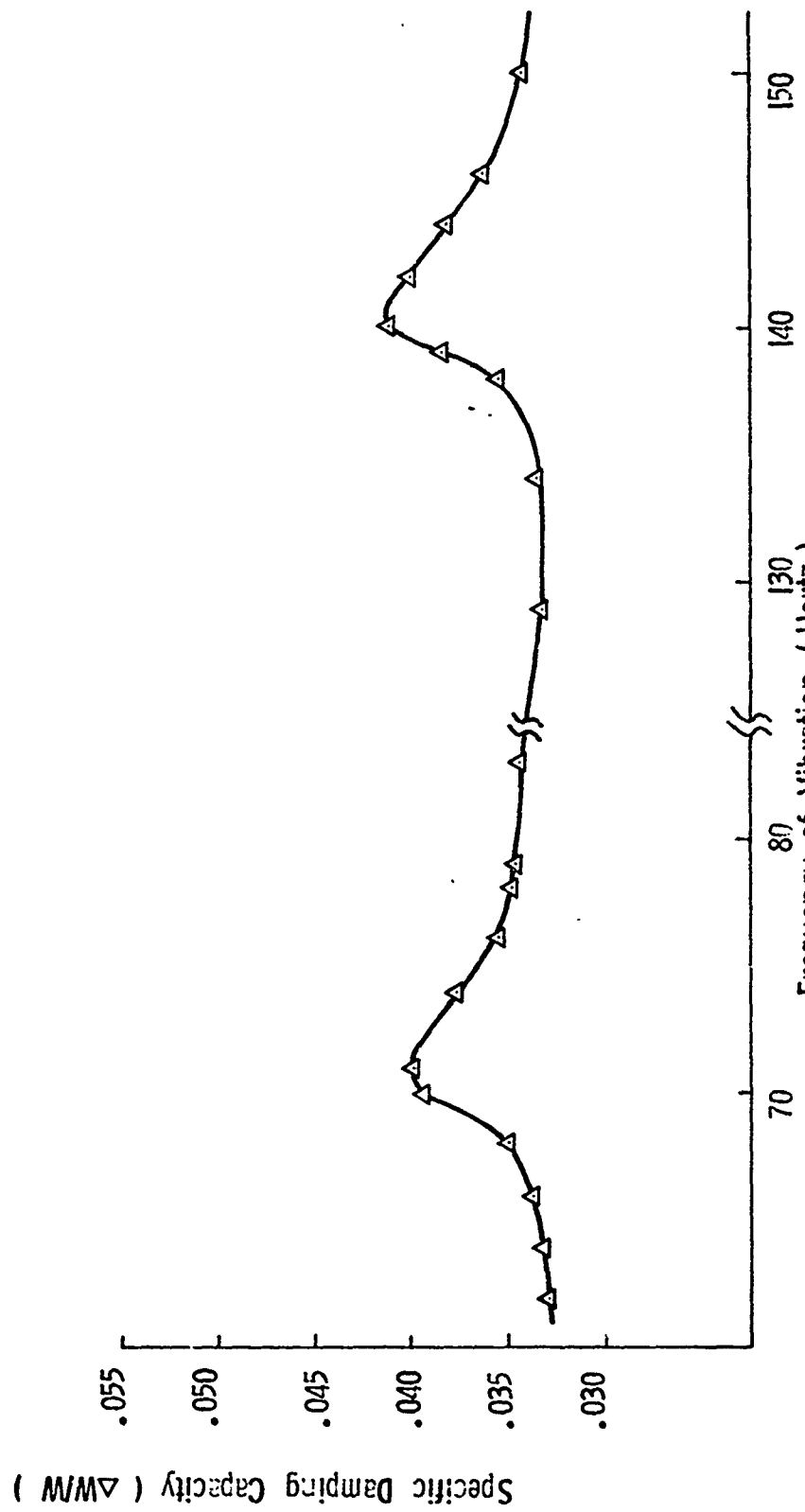


Figure 4.2B Internal Damping Curve for 2024-T4 Al (0.07 cm grain size )  
Immersed in Hg at 100°C and 30%  $\sigma_{ys}$  for 1 hour

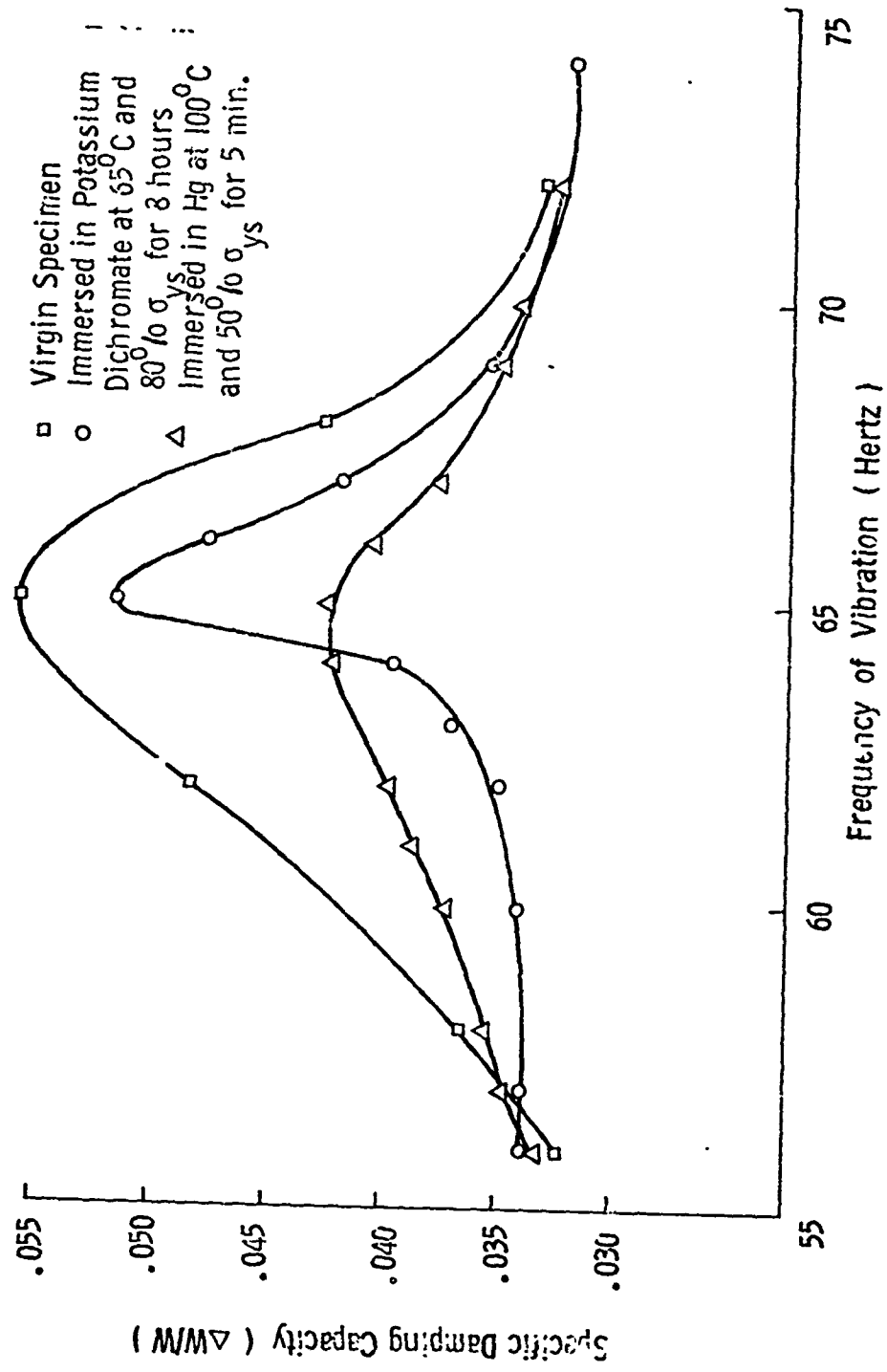


Figure 4.3 Internal Damping Curves for 2024-T4 Al ( 0.024 cm grain size )

58

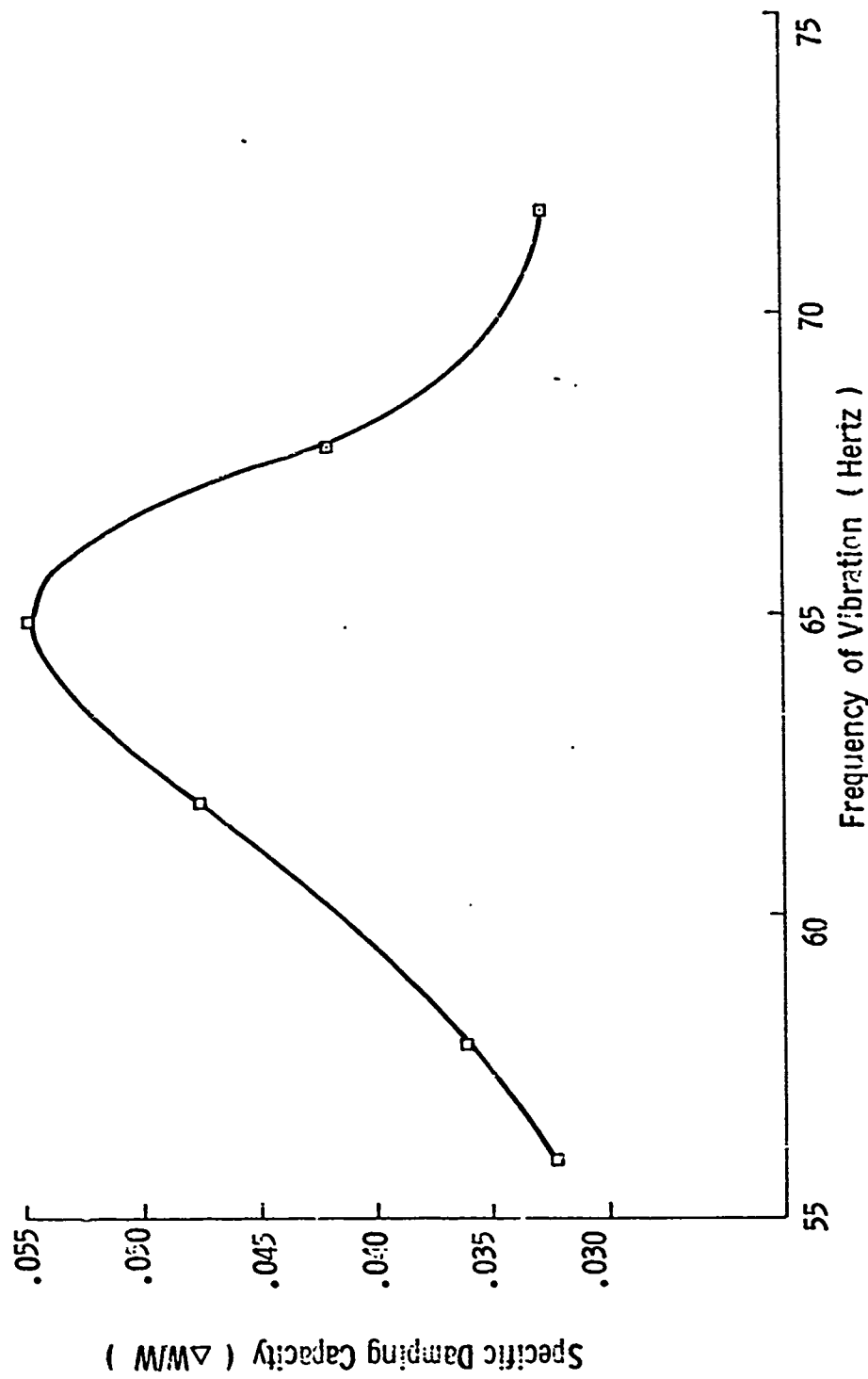


Figure 4.3A Internal Damping Curve for 2024-T4 Al (0.024 cm grain size )  
Virgin Specimen

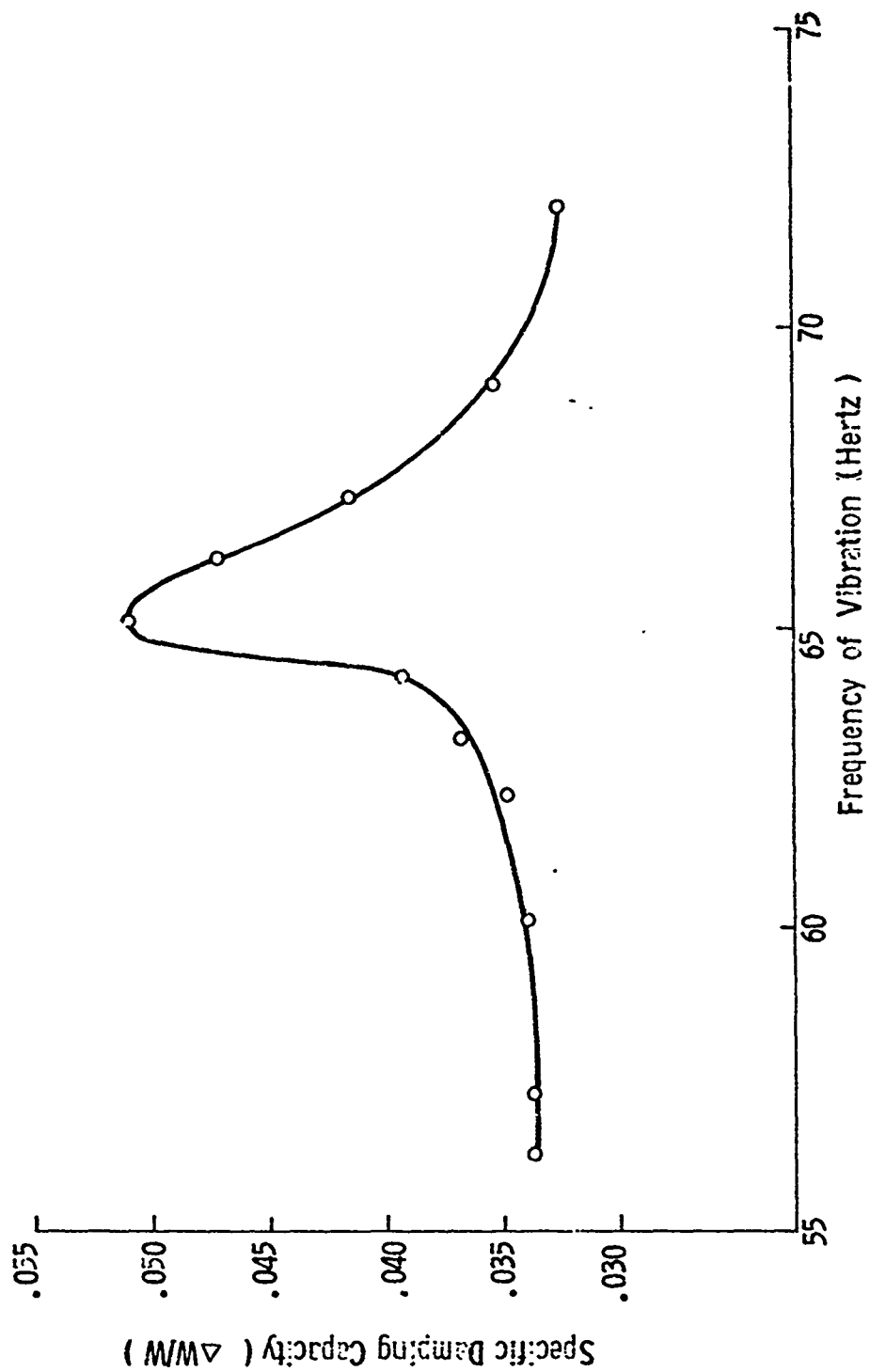


Figure 4.3B Internal Damping Curve for 2024-T4 Al (0.024 cm grain size )  
Immersed in Potassium Dichromate at 65°C and 80%  $\sigma_{ys}$  for 8 hours

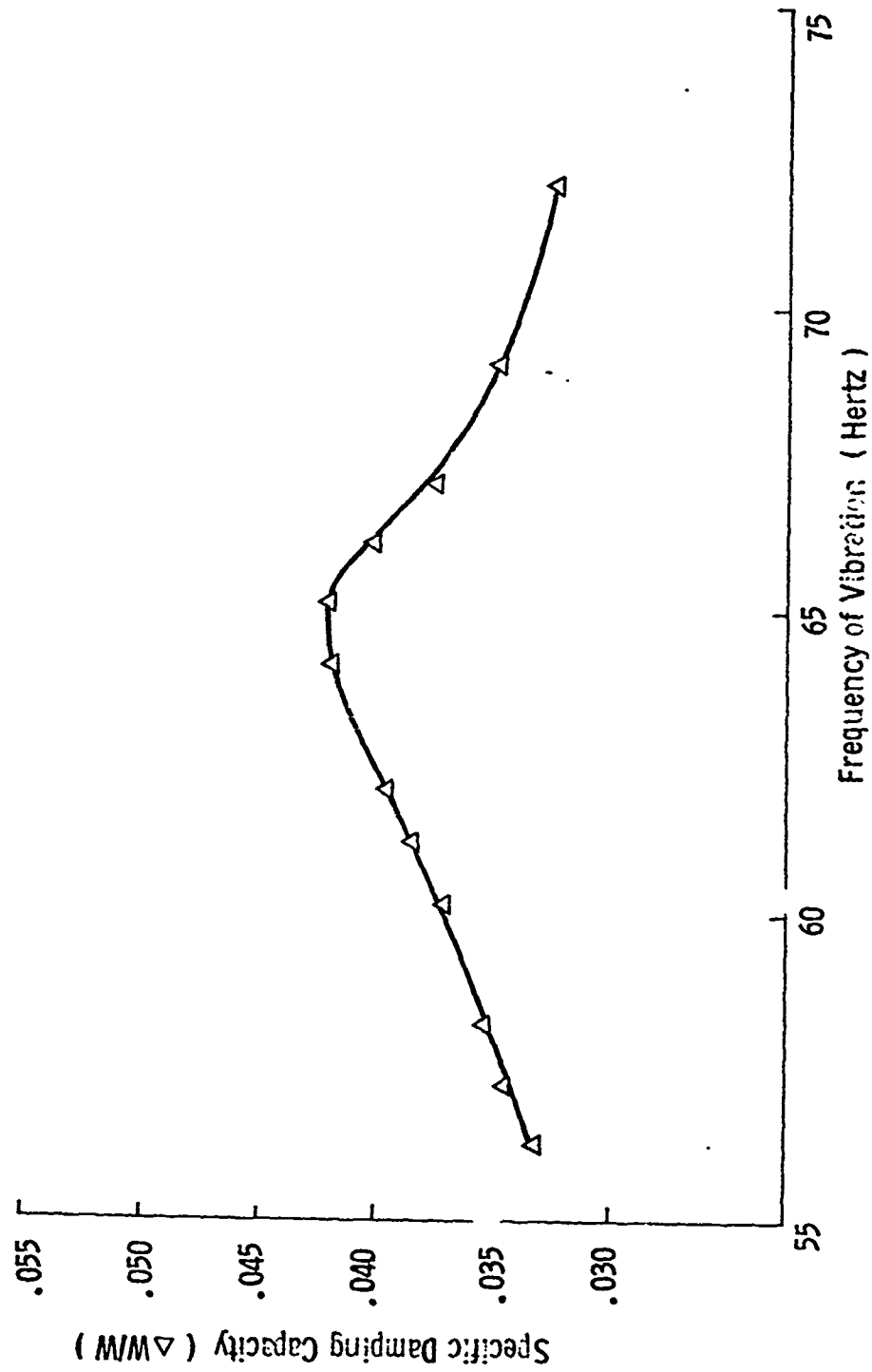


Figure 4.3C Internal Damping Curve for 2024-T4 Al (0.024 cm grain size )  
Immersed in Hg at 100°C and 50%  $\sigma_{ys}$  for 5 minutes



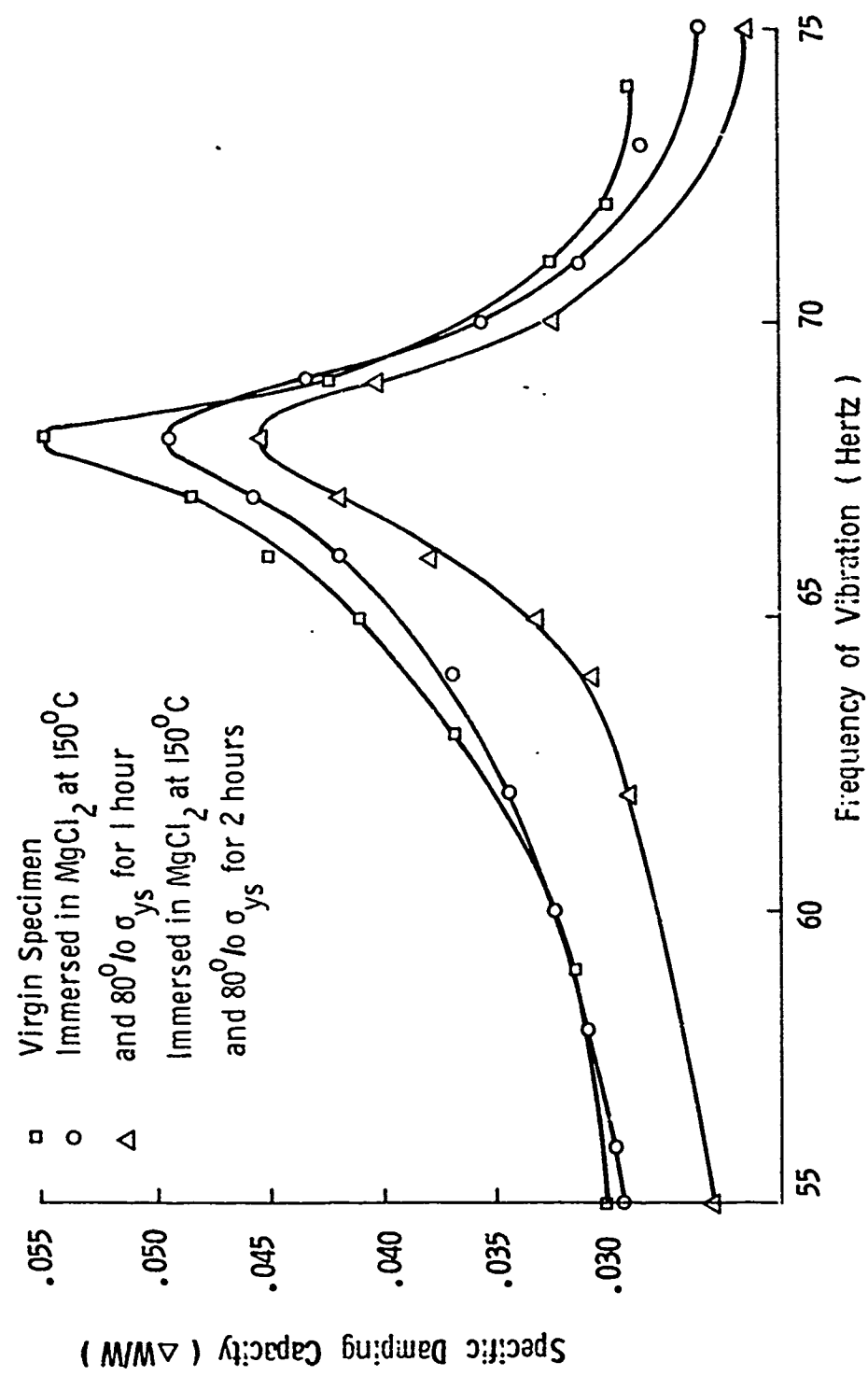


Fig. e 4.4 Internal Damping Curves for 304 Stainless Steel

62

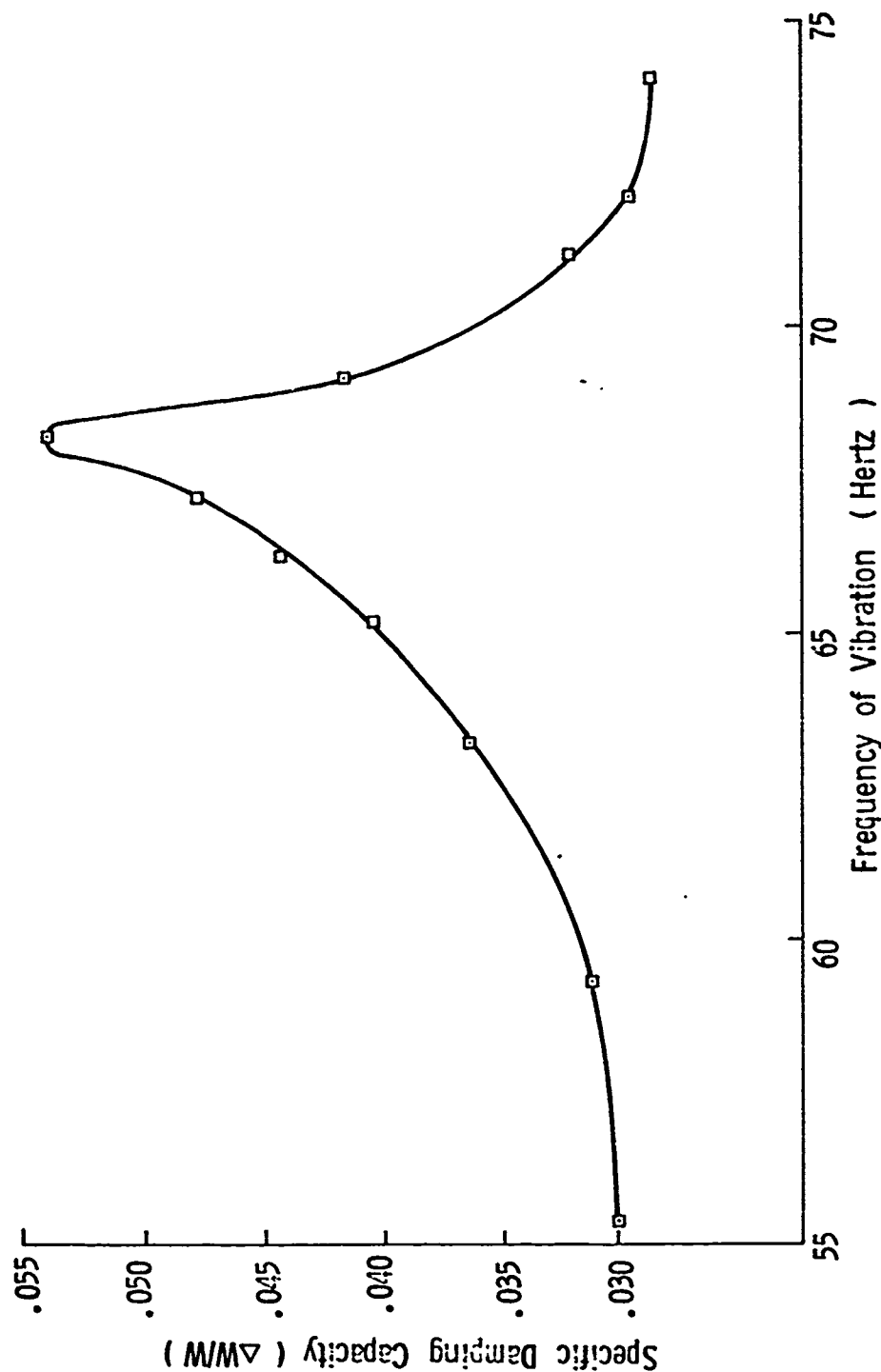


Figure 4.4A Internal Damping Curve for 304 Stainless Steel  
Virgin Specimen

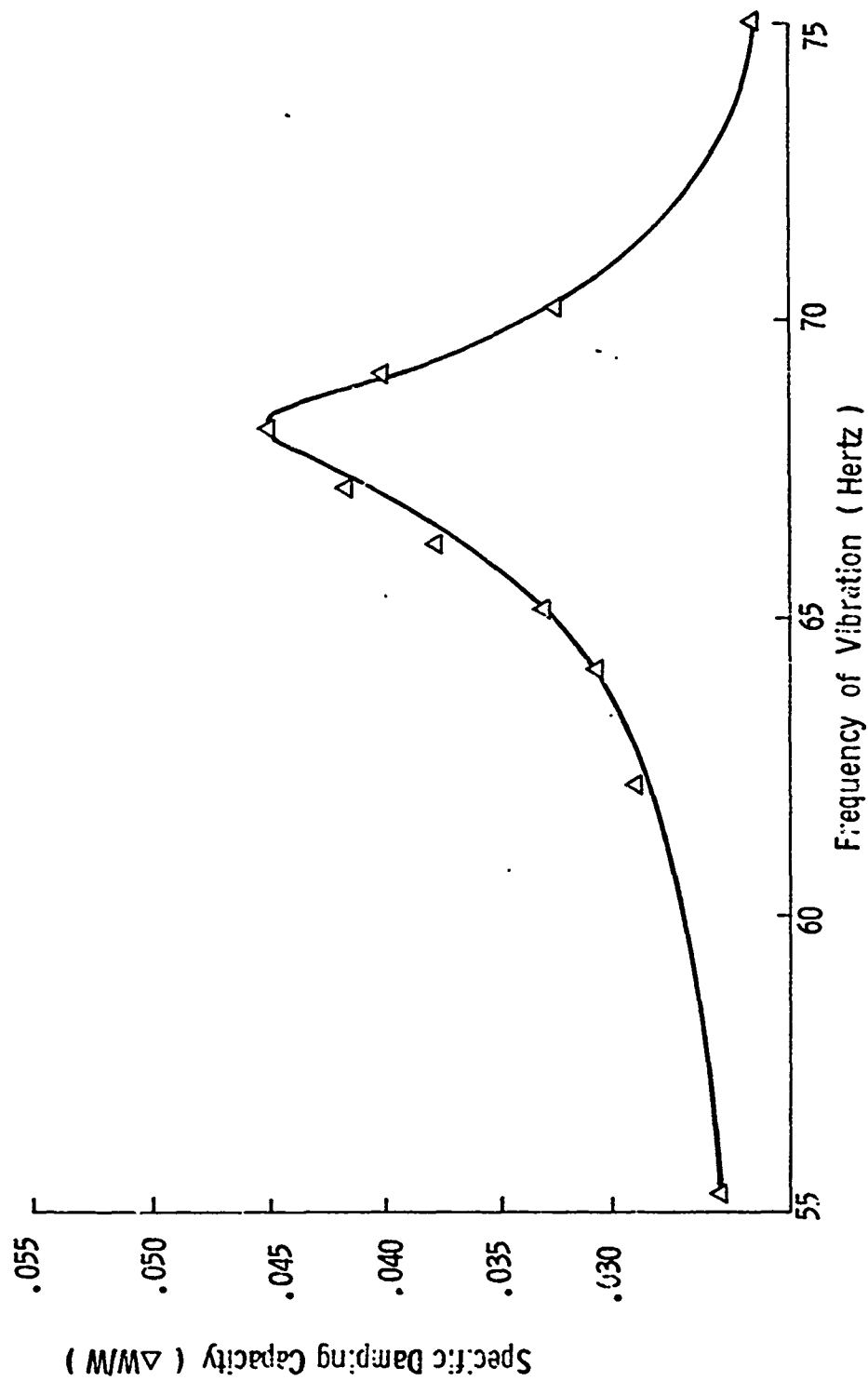


Figure 4.48 Internal Damping Curve for 304 Stainless Steel  
Immersed in  $MgCl_2$  at  $150^\circ C$  and  $80\% \sigma_{ys}$  for 1 hour

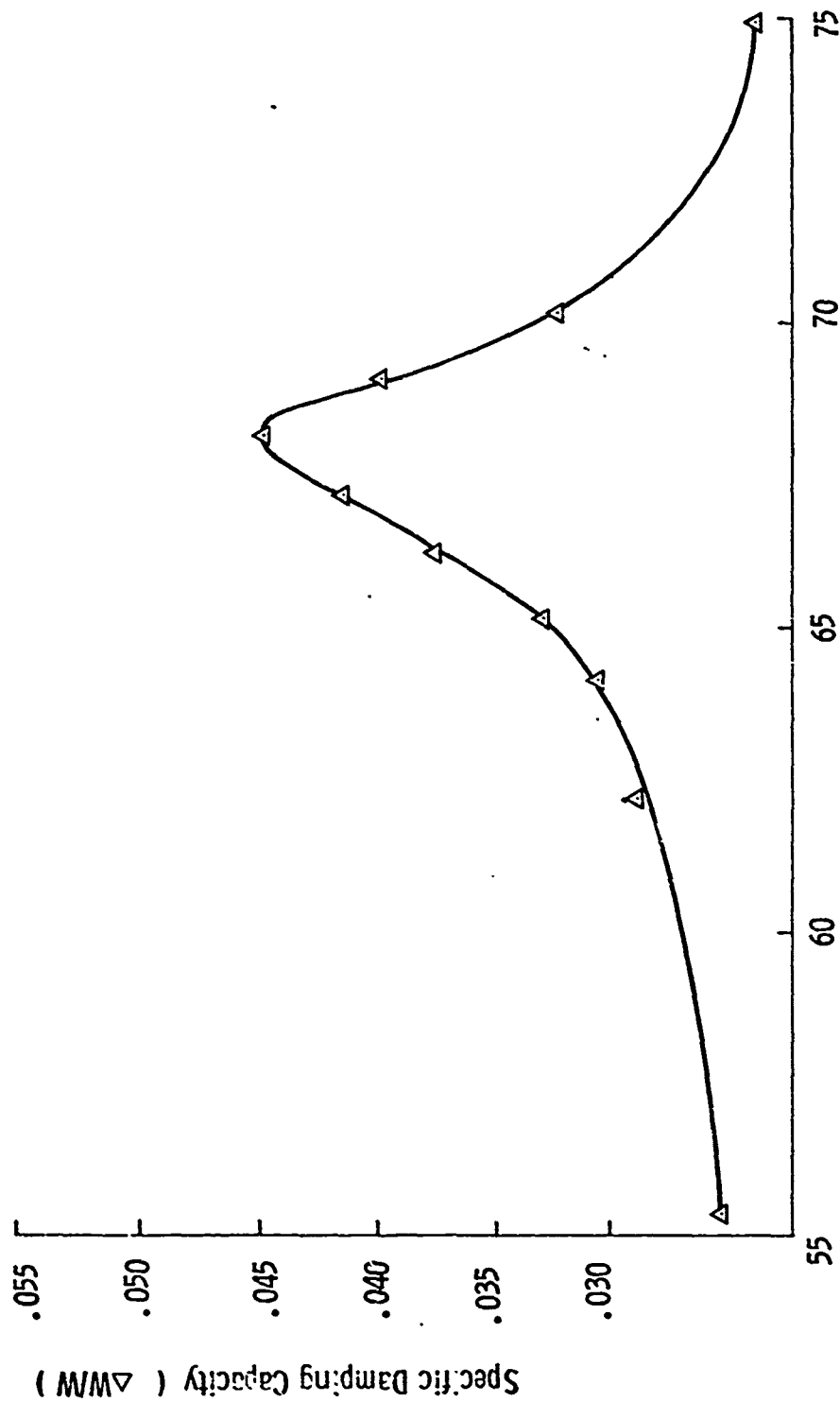


Figure 4.4C  
 Internal Damping Curve for 304 Stainless Steel  
 Immersed in  $MgCl_2$  at  $150^\circ C$  and  $80^\circ / \sigma_{ys}$  for 2 hours

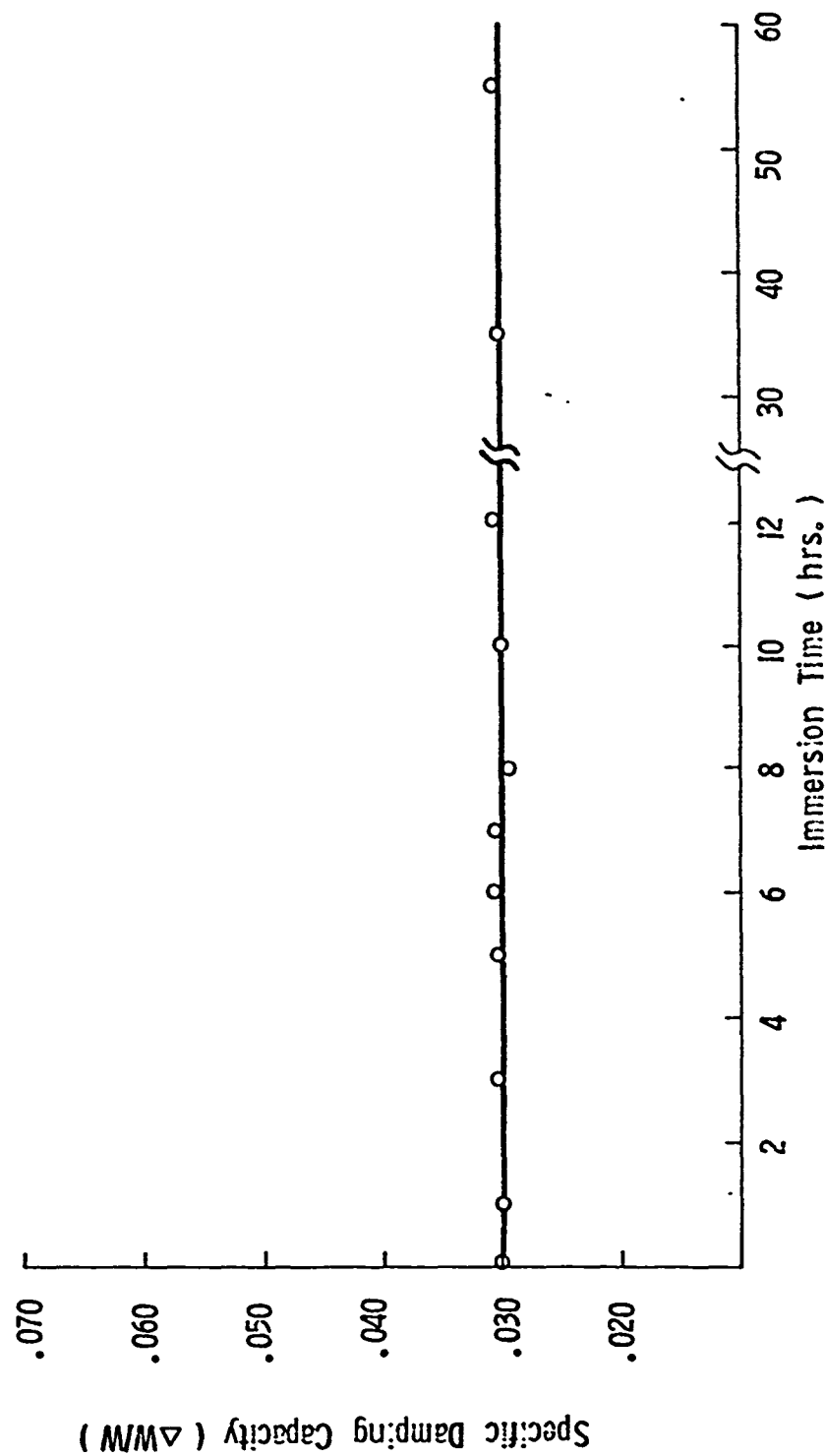


Figure 4.5 Internal Damping Curve for Copper  
Immersed in Sea Water at Room Temperature and  $80^\circ/\sigma_{ys}$

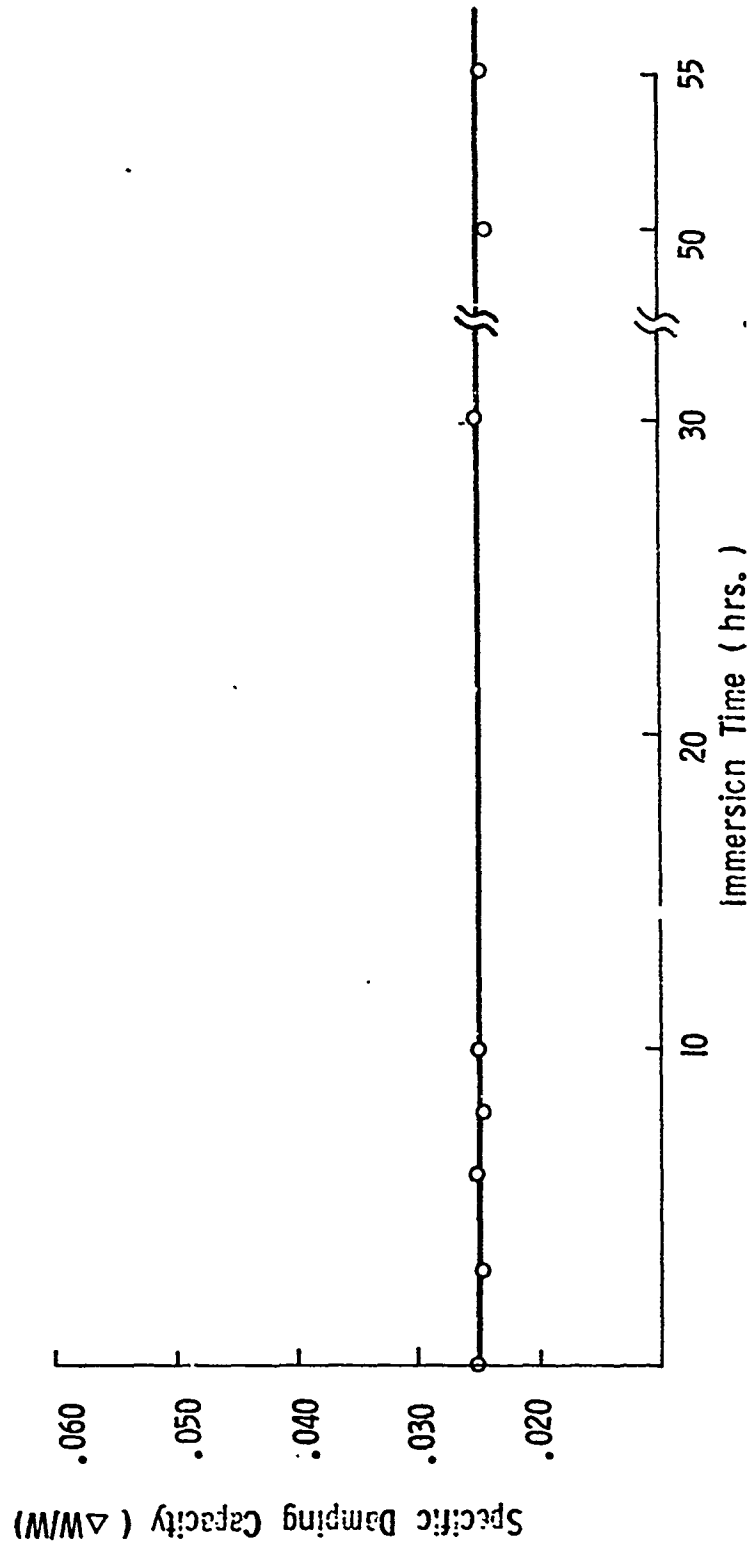


Figure 4.6 Internal Damping Curve for 1020 Steel  
Immersed in Sea Water at Room Temperature and 80%  $\sigma_{ys}$

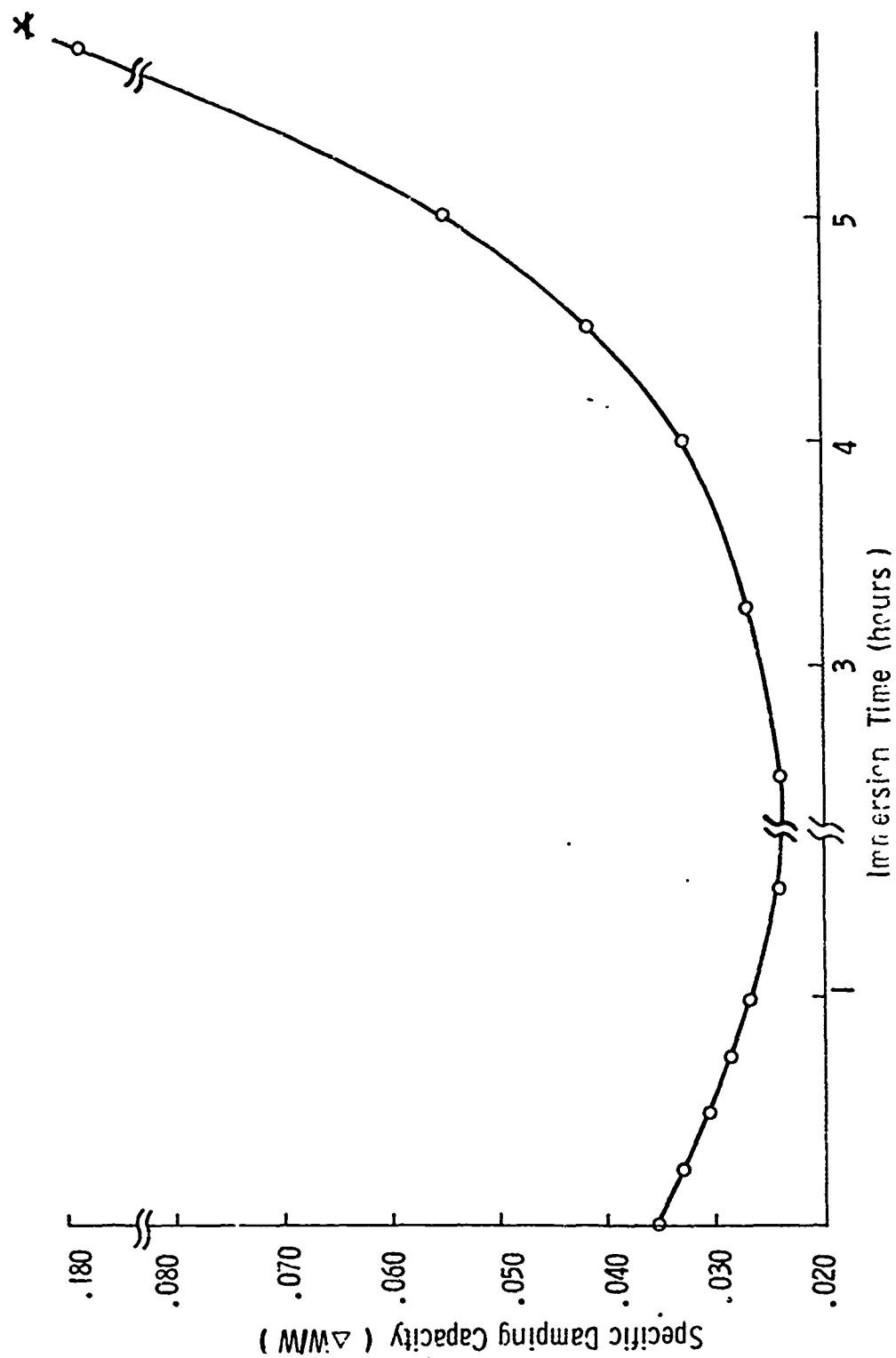


Figure 4.7 Internal Damping Curve for 70-30 Brass  
Immersed in Ammonia Vapors at Room Temperature and 80%  $\sigma_{ys}$

//

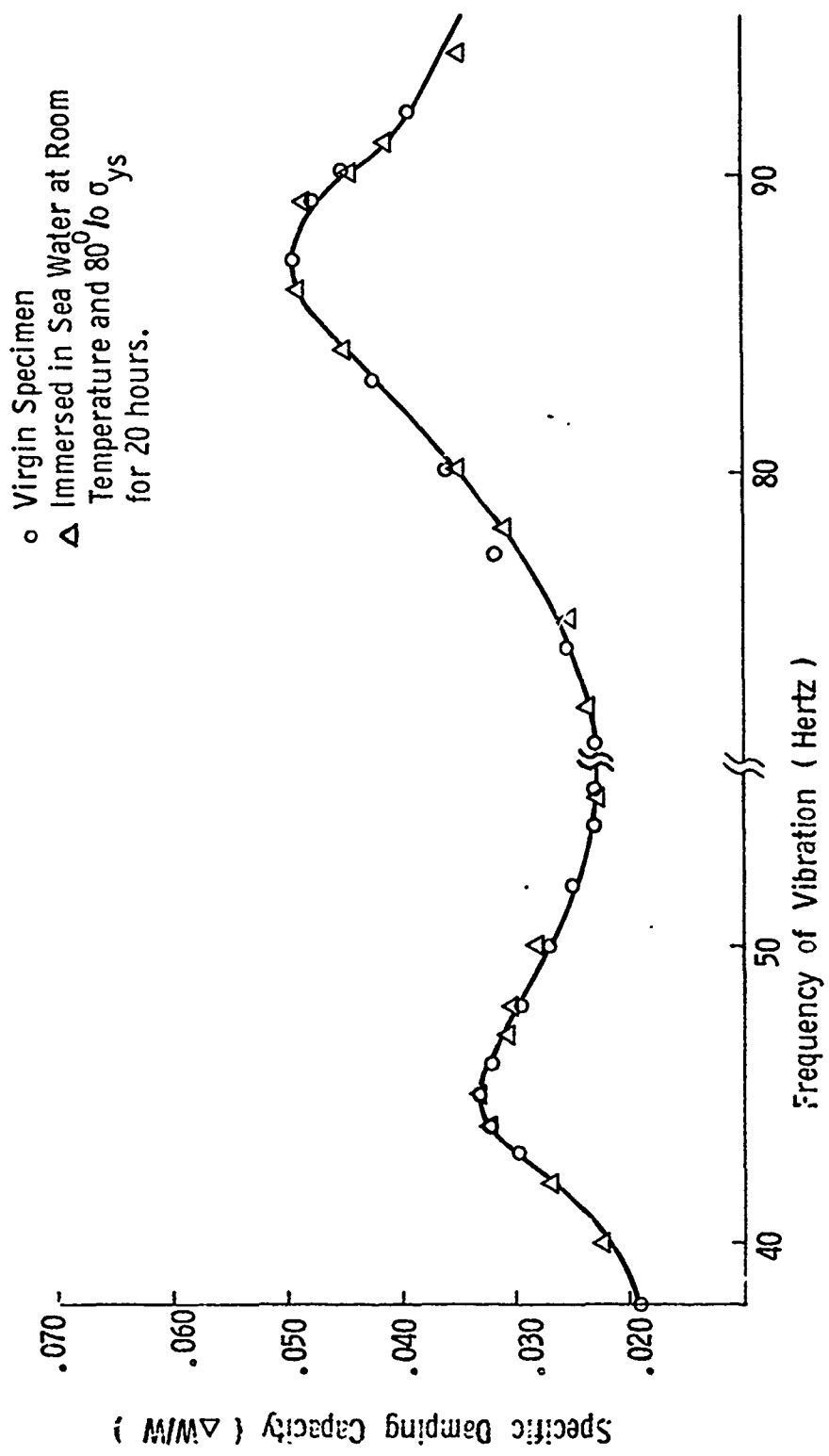


Figure 4.8 Internal Damping Curve for Copper



Exposure Time	Virgin Specimen	5 minutes	20 minutes	30 minutes
Specimen Stressed at $30\% \sigma_{ys}$ in $H_f$ at $100^\circ C$  ( frequency )	.03265  ( 55 )	.03335  ( 55 )	.03745  ( 55 )	.03950  ( 55 )

Figure 4.9 Specific Damping Capacity and Frequency for Different Immersion Times

Total Time	Virgin Specimen	after 5 min.	after 10 min.	after 15 min.	after 20 min.	after 25 min.	after 30 min.
No Stress in Air ( frequency )	.03265 ( 55 )	.03265 ( 55 )					.03265 ( 55 )
30% $\sigma_{ys}$ in Air ( frequency )	.03350 ( 56 )	.03310 ( 56 )		.03310 ( 56 )			.03310 ( 56 )
No Stress in Hg ( frequency )	.03265 ( 55 )		.03265 ( 55 )	.03220 ( 55 )			.03265 ( 55 )
30% $\sigma_{ys}$ in Hg ( frequency )	.03265 ( 55 )	.03265 ( 55 )	.03410 ( 55 )	.03630 ( 55 )	.03665 ( 55 )	.03885 ( 55 )	.04330 ( 55 )
Figure 4.10 Specific Damping Capacity as a Function of Stress State							

### A. EXPERIMENTAL AND THEORETICAL CORRELATION OF DIFFUSION PEAKS

This dissertation is developed from the idea that materials which are susceptible to stress corrosion cracking exhibit changes in their specific damping capacity after exposure to a corrosive environment as compared to the specific damping capacity of the virgin specimen. Earlier attempts to relate metallurgical phenomena with changes in internal damping consists of a set of interesting experiments conducted by Bastien and Azou (38) regarding the effect of hydrogen on the damping characteristics of mild steel. Their investigation found that cold working did not produce any appreciable changes in the specific damping capacity at small strain amplitudes; however, charging the mild steel with hydrogen produced a significant increase in the damping characteristics. Mina and Hori (39) studied the stress corrosion cracking of austenitic stainless steels by measuring room temperature internal friction after exposure to 42% boiling magnesium chloride solution. It was found that the change in internal friction varied with the progress of the stress corrosion cracking. The above experiments confirmed the findings of Thiruvengadam (40) that active environments which cause metal embrittlement do affect the damping characteristics of the material. Furthermore, it was found that the specific damping capacity of 2024-T4 aluminum both increased and decreased after environmental exposure in mercury. Indeed, the present investigation verifies the fact that the specific damping capacity associated with the initial specimen length of 2024-T4 aluminum both increases and decreases as a function of environmental exposure.

Since the change in the specific damping capacity associated with the original specimen length varied positively and negatively as a function of

environmental exposure, the question is raised regarding the experimental determination of a susceptible system. The above results being inconsistent, it was therefore necessary to peruse the damping characteristics of metal specimens in order to obtain consistency of results. As discussed in Chapter II, Zener's theory predicts the peak frequencies for the thermal diffusion associated with the specimen thickness and grain diameter. Because stress corrosion cracking in susceptible alloys is invariably intergranular (41), consideration was given to the specific damping capacity resulting from the peak frequencies which are associated with the grain diameter and the specimen thickness.

In order to obtain experimental location of the peak frequencies, internal damping measurements were made as a function of frequency. The theoretical values for the peak frequencies associated with both the specimen thickness and the grain diameter were calculated from equation 2.2. Close correlation between the experimental and theoretical results was obtained. Referring to figure 4.1A, the specimen thickness measured .042 inches, and  $D = .455 \text{ cm}^2 / \text{sec}$  which calculates a theoretical peak frequency due to specimen thickness of 62.3 Hertz as compared to the experimental value of 63 Hertz. When the grain diameter is substituted for the specimen thickness, as in the case of the 0.1 cm grain size, the theoretical peak frequency resulting from thermal diffusion across the grain is 71.5 Hertz as compared to the experimental value of 70 Hertz. When the smaller grain size (.07 cm) is substituted into equation 2.2, the theoretical peak frequency is 146 Hertz. Experimentally, the diffusion peak occurred at 140 Hertz. The resulting discrepancies are attributed to a grain diameter distribution that results from any grain growing process. The latter values are found in figure 4.6. The important physical interpretation of these curves is that the energy dissipation

is a maximum when the thermal diffusion length in the material is of the order of the specimen thickness or grain diameter.

#### B. EXPERIMENTAL DETERMINATION OF RELAXATION TIMES

The hypothesis previously employed to explain changes in the specific damping capacity as a function of environmental exposure was based on a shift in the internal damping curves. That is, the peak frequencies, or associated relaxation times for thermal diffusion, were assumed to shift as a function of exposure to a corrosive environment. This hypothesis utilized Ke's theory of viscous slip in the grain boundaries which related the viscosity to the product of the modulus and the relaxation time. (See equation 2.4). Moreover, investigative evidence was presented that inferred the modulus remained unchanged and thus it was assumed that changes in internal friction resulted from changes in the relaxation time. To evaluate this hypothesis, tests were conducted on 2024 T4 aluminum immersed in mercury for various exposure times. As shown in figures 4.1A to 4.1D, the peak frequencies associated with both the specimen thickness and the grain diameter remain unchanged. Thus, environmental exposure does not change the relaxation time of the material. Further testing was conducted on smaller grain size aluminum specimens with similar results. The experimental data for the internal damping curves of the virgin specimen and the exposed specimen is found in figures 4.2A and 4.2B with a composite curve being given in figure 4.2. The previous results are again verified by the fact that the peak frequencies associated with both the specimen thickness and the grain diameter remain unchanged.

Subjectively, it can be argued that the absence of a peak shift is expected when the thermal diffusion across the specimen thickness is evaluated. For this case, only a variation in the specimen thickness could produce a

peak shift. Since the metal surface is not etched away by the corrosive media, the specimen thickness remains unchanged during the experiment, and the associated peak frequency should not indicate a shift. Moreover, the experimental results indicate that the thermal diffusion coefficient does not vary as a function of environmental exposure.

A similar argument can be presented for the relaxation times associated with the grain diameter, however due to the grain boundary interaction a quantitative argument will be made from the equations as given in Chapter II. By eliminating the viscosity term from equation 2.4 and 2.5, the following expression is obtained:

$$\frac{d}{dt} E \tau = \frac{T}{S} e^{H/RT} \quad (5.1)$$

Substituting the exponential term into equation 2.6 gives:

$$\frac{\Delta W}{W} \propto f \cdot dE \cdot \frac{S}{T} \quad (5.2)$$

Consideration is given at the peak frequencies where

$$\cdot = \frac{1}{f_0}$$

and

$$f \approx f_0$$

Therefore:

$$\cdot f \approx 1$$

for frequencies in the vicinity of the peak frequency. Thus equation 5.2 becomes:

$$\frac{\Delta W}{W} \propto (dE \cdot \frac{S}{T}) \quad (5.3)$$

This shows that the specific damping capacity associated with the peak frequencies is not dependent upon the relaxation time of the material. Thus by considering the grain boundary models and internal damping parameters, it is shown that the relaxation time does not change for the associated peak frequencies resulting from environmental exposure.

### C. SUSCEPTIBLE SYSTEMS

#### 1. ALUMINUM

We now return to the original question posed earlier in this chapter - namely how does one determine a susceptible system. It has been shown that the peak frequencies - and thus the relaxation times - associated with the specimen thickness and with the grain diameter remain unchanged during environmental exposure. Presented in figures 4.1A to 4.1D are the internal damping curves for the virgin specimen and for specimens experiencing immersion times up to two hours respectively. A composite of these four curves is given in figure 4.1.

As can be seen from the composite diagram, the amplitude of the specific damping capacity for the peaks decreases as the immersion time increases. This decrease in the specific damping capacity occurs for the peak associated with the specimen thickness as well as for the peak associated with the grain size. In both cases, the amplitude of the peak decreases for increased environmental exposure times. Attention is focused on the internal damping peaks because of the overlapping of the damping curves in the regions removed from the peaks. Thus, before internal damping measurements can be correlated to susceptibility, it is imperative that the location of these damping measurements on the specimens' damping curve be known.

Once the peak frequencies are determined for the virgin specimens, specific damping capacity measurements can be made for an exposed specimen in the vicinity of the peak frequencies. Susceptibility is then determined by any decrease in the amplitude of the specific damping capacity associated with either the specimen thickness or grain size. For the experiment conducted on the large grain size aluminum specimens, the thermal diffusion peaks associated with the specimen thickness decreases in amplitude to the point that it is completely negated after two hours of environmental exposure. In this case the heat flow is solely transgranular.

Similar internal damping curves were obtained for the smaller grain size aluminum specimen. The damping curve of the virgin specimen is found in figure 4.2A and that of the exposed specimen is in figure 4.2B with the composite diagram given in figure 4.2. Again, the relaxation times associated with the specimen thickness or the grain size remain unchanged for environmental exposure. Moreover, consistency of results is obtained in the fact that the amplitude of the specific damping capacity decreases for environmental exposure. It is the decrease in the amplitude associated with the peak frequencies that is indicative of a susceptible system to stress corrosion cracking and not changes in damping associated with any given specimen frequency.

## 2. STAINLESS STEEL

The validity of the above conclusion was tested for another susceptible system - namely 304 stainless steel in boiling magnesium chloride. Material specimens were subjected for different exposure times and internal damping curves were obtained for the diffusion across the specimen thickness. Various individual curves are presented in figures 4.4A to 4.4C with the composite diagram found in figure 4.4. As shown in the composite diagram, the magnitude of



the specific damping capacity peak for thermal diffusion across the specimen thickness decreases as the material is "boiled" in the solution for longer time intervals. These results are in agreement with the findings made in the aluminum system.

#### D. ENVIRONMENTAL MEASUREMENTS

The paramount experimental findings presented herein show that the relaxation times remain unchanged resulting from environmental exposure, and by scanning the peak frequencies associated with the specimen thickness and the grain diameter, the amplitude of these peaks decreased for increased exposure times. Since susceptibility implies a decrease in peak amplitude, similar results should be obtained for material exposure to different corroding environments. By scanning the peak frequency for thermal diffusion across the specimen thickness, quantitative internal damping measurements were made on small grain (.024cm grain size) aluminum specimens in two different stress corrosion cracking environments - namely mercury and potassium dichromate ( $K_2Cr_2O_7$ ) solution. The results are recorded in figures 4.3A to 4.3C, with the composite diagram given in figure 4.3. The small grain size was employed to insure that thermal diffusion associated with the grain diameter would not occur. Thus the presented specific damping capacity peak is a direct result of thermal diffusion associated with the specimen thickness. The peak amplitude for each specimen occurred at 65 Hertz and with identical specimen thickness of .041 inches, excellent correlation resulted between the experimental and theoretical values for the peak frequency.

The potassium dichromate solution is a weak corrosive environment for aluminum (42), which is indicated by the respective graphs. The peak amplitude decreases as the material passes from the virgin state through the potassium

dichromate solution to the mercury environment. These results confirm the previous findings that the magnitude of the associated peak decreases as the system becomes more susceptible to stress corrosion cracking. Again, the necessity of knowing where on the internal damping curve the measurements are to be made is demonstrated by the fact that the curves cross each other at the lower frequency levels.

#### E NON-SUSCEPTIBLE SYSTEM EVALUATION

From the established experimental evidence of this investigation, susceptibility to stress corrosion cracking is directly associated with decreases in the peak amplitudes of the internal friction curves. This decrease in amplitude is shown to be proportional to the exposure time or to the severity of environmental attack. Furthermore, the decrease results across either the thermal diffusion peak associated with the specimen thickness or with the grain size. It follows that the above findings should be negated in evaluating non-susceptible systems, i.e. systems which are not prone to stress corrosion cracking. Moreover, materials exposed to non-susceptible environments should not experience changes in their damping capacity as a function of immersion time. In order to validate these surmises, the variation in the specific damping capacity as a function of exposure time was determined for two non-susceptible systems, namely copper in sea water and plain carbon steel in sea water. These time exposure measurements are then compared with the results obtained from a susceptible system, brass in ammonia vapor. The results of these investigations are found in figures 4.5 to 4.7.

The variation in the specific damping capacity for copper resulting from cumulative immersion times in sea water is shown in figure 4.5. The specific damping capacity is close to the peak amplitude for thermal diffusion across

the specimen thickness. The damping capacity shows no change resulting from increased exposure times to stress conditions in sea water. Moreover, the frequency of vibration remains unchanged and the specimen length is held constant throughout the experiment.

Confirming experimental results are obtained for plain carbon steel in sea water as shown in figure 4.6. The experimental procedure is similar to that employed in obtaining the data in figure 4.5. Again for a non-susceptible system, the material experiences no changes in its specific damping capacity resulting from cumulative immersion times. From these two systems, it is concluded that materials which are exposed to non-susceptible environments do not exhibit changes in their specific damping capacity as compared to the virgin specimen.

As previously mentioned, aluminum alloy 2024-T4 experiences changes in its specific damping capacity when subjected to cumulative exposure times in mercury as shown in charts 4.9 and 4.10. In addition to the aluminum-mercury system, the susceptibility of brass to stress corrosion cracking in ammonia vapors is evaluated. Figure 4.7 shows that when brass is exposed to ammonia vapors at 80% of yield strength, it fails in approximately six hours. The resulting changes in the materials specific damping capacity is also shown in the same figure. It should be noted that contrary to material behavior in non-susceptible systems, the brass experiences both increases and decreases in its specific damping capacity after ammonia exposure and as compared to the damping characteristics of its virgin specimen. These results complement the behavior of aluminum after exposure to mercury.

Of the three susceptible systems considered in this investigation, i.e. aluminum-mercury, stainless steel-boiling magnesium chloride, and brass-ammonia vapors, and each material experiences changes in its specific damping capacity

as compared to the damping characteristics of its virgin specimen. These changes are both positive and negative in the fact that they increased or decreased when compared to the specific damping capacity of the virgin specimen. However, the conclusion reached in this dissertation is that such material damping changes are not sufficient to indicate susceptibility to stress corrosion cracking. Materials experiencing metallurgical phenomena other than stress corrosion cracking can exhibit changes in their damping properties. For example, measurements made on steel subjected to corrosion fatigue indicated increases in its specific damping capacity as compared to its virgin value. Moreover, materials subjected to extensive cold working also experience changes in their damping properties. The investigative evidence in this dissertation finds that it is not the specific changes in the materials damping properties that is indicative of the susceptibility to stress corrosion cracking, but rather the decreasing amplitudes of the internal friction peaks which are associated with thermal diffusion across the specimen thickness or grain diameter. Assuming correct logic, it then follows that for systems immune to stress corrosion cracking, the materials should experience no decrease in the peak amplitude of the internal friction curves. That is, the material should exhibit identical peak amplitudes after exposure as compared to the internal friction curves of the virgin specimen. From the data presented in figures 4.5 and 4.6, it has already been shown that for immune systems, there are no initial changes in the materials' damping characteristics.

An immune copper alloy was tested in sea water in order to evaluate the effect of environmental exposure on the amplitude of the diffusion peaks for the internal damping curve. As shown by figure 4.8, the exposure has no effect on the peak amplitudes associated with thermal diffusion across the

specimen thickness or across the grain diameter. From this non-susceptible system it is concluded that the peak amplitudes remain unchanged after environmental exposure and when compared to the same data curve for the virgin specimen. This finding validates the negative approach to determine a non-susceptible system. Thus it is concluded that materials which are susceptible to stress corrosion cracking exhibit decreases in their peak amplitudes and that materials which are immune to stress corrosion cracking experience no changes in their peak amplitudes.

#### F. DESIGN PROCEDURE

The design procedure presented herein is based on experimental consideration given to various aluminum systems. It is suggested that the same procedure be followed for the steel and titanium alloy systems. Moreover, the values for the clamping torque, stress level and other experimental variables are indicative of aluminum alloys and should not be considered as constant experimental parameters for evaluating other alloy systems.

1. Determine the thermal diffusion coefficient for each specific test alloy.
2. Calculate the peak frequencies from equation 2.2 (assuming a rectangular cross-section reed) for internal friction resulting from thermal diffusion across the specimen thickness ( $a$  = specimen thickness), and across the grain diameter ( $a$  = grain size). The grain size value is calculated from equation 2.3.
3. Determine the specimen lengths that are associated with the frequency peaks. These lengths are obtained by substituting the frequency values as found in step two into equation 3.7.
4. Align the specimen correctly in its fixture and determine the

necessary clamping torque and specimen stress level. The original specimen length should be such that its associated frequency is removed from either of the internal damping peaks. It is suggested that the initial frequency be in the frequency plateau that precedes the thermal diffusion peak associated with the specimen thickness. This suggestion assumes that the specimen thickness is larger than the specimen grain diameter.

5. Correlate the maximum deflection for reduced specimen lengths by use of the beam equation. The original specimen stress level and the accompanying specimen length have been predetermined in step four.
6. Specify a decay interval associated with the logarithmic decrement and the location of the decay interval within the decay curve. This can be accomplished by comparing the linearity of the logarithmic decrement as a function of the decay interval, and by evaluating the specific damping capacity at various interval locations along the decay curve.
7. Determine the effect of material strain hardening and the amplification factor curve if the system or equipment is being evaluated for the first time
8. Reference or experimentally evaluate the environmental effects such as air drag resulting from changes in atmospheric pressure and the dependence of the specific damping capacity on temperature fluctuation for different alloy systems.
9. Determine experimentally the maximum obtainable frequency of vibration and calculate the corresponding minimum associated grain size from equation 2.2. If the peak frequency associated with the specimen grain size is greater than the maximum frequency that can

be experimentally obtained, then variations in specific damping should be considered only for the peak associated with the specimen thickness.

10. Obtain internal damping curves for both the virgin and immersed specimens. Frequency increases are accomplished by shortening the specimen length.
11. Test the proneness of exposed specimens for susceptibility to stress corrosion cracking by noting the amplitude of the internal friction curves in vicinity of the thermal diffusion peaks for both the virgin and exposed specimens. Susceptible materials experience decreasing internal friction curves. The decrease in the amplitude of the curves is proportional to the exposure time or to the severity of attack. This decrease results across either the thermal diffusion peak associated with the specimen thickness or the thermal diffusion peak associated with the grain size.

#### G. MECHANISM OF FAILURE

Since the advent of stress corrosion cracking, it was widely believed that there must be a common mechanism for all the corrosion produced cracking processes that generate the characteristic brittle cracks in so many families of alloys. Most of these alloys have been previously proven ductile in purely mechanical tests. This belief has persisted and resulted in the fact that the macrophenomenological definition of stress corrosion cracking appears well on its way to general usage rather than being restricted to a single mechanism.

The detailed mechanism which have been proposed for various stress corrosion systems can be grouped into the following categories:

1. Electrochemical-mechanical. This model proposes that there exist paths which are intrinsically susceptible to anodic electro-chemical dissolution, and the applied stress was suppose to open the cracks wide enough to prevent any stifling of the reaction by corrosion products. (43) Subsequent experience has shown that this early model does not agree very well with the observed results. Disagreement is found in the fact that the roles of the applied stress cannot be reverse of the electrode potential. Measured current densities are sufficient to stifle the reaction by polarizing the anodic area. However, Hoar and West (44) have shown that under conditions of continuous yielding, the effective polarization is minute and results from an increase in the dislocation density.

2. Embrittlement. These models are postulated as a periodic electro-chemical mechanical cycle in which the electrochemical corrosion process was pictured as embrittling the metal directly behind the corroding metal surface. (45) The embrittlement layer would ultimately fracture mechanically and expose fresh metal surfaces. A modified version of this model is considered reasonable for high strength steels in aqueous environments.

3. Adsorption and Film Rupture. The adsorption model pictures the reduction of the energy required to for a new surface by reducing the surface energy through the adsorption of a chemical species. (46) In the film rupture model, a brittle film of corrosion by product is envisioned to form and fractures after becoming sufficiently thick, exposing bare metal. The bare metal reacts to form a brittle film again and the cycle repeats itself. Evidence produced from these models can best be explained from other models.

In pursuit of any detailed mechanism that could be developed into a general theory of stress corrosion cracking, the following two facts must prevail. Firstly, any devised model must be in harmony with the fact that the corrosive



near the crack tip is grossly different from the bulk environment outside the crack. (47) Moreover, it is now clear that susceptible alloys exhibit planar arrays of dislocations, whereas immune alloys have tangled dislocation substructures. (48) A dislocation is defined herein as a linear defect which develops in the interior of a crystal as the boundary of a displacement zone. The two principle types of dislocations considered in this discussion are edge and screw type dislocations. An edge dislocation arises if one of the atomic planes ends in the interior of a crystal. The edge of this plane creates a linear defect called an edge dislocation. Atomic planes can also form a single screw surface bent along a screw line. Such a defect is called a screw dislocation. During each circuit on the atomic surface and along the dislocation line, the surface rises or falls by one screw jump which equals the lattice spacing or a multiple thereof.

It is not the intent of this discussion to add another model to those already presented, but rather to postulate a general theory of stress corrosion cracking based on the incorporated data. This general theory is unique in the fact that its postulation has not been previously attempted. The incorporated data presented in this dissertation shows that materials which are susceptible to stress corrosion cracking exhibit decreases in their peak amplitudes and that materials which are immune to stress corrosion cracking experience no changes in their peak amplitudes. For susceptible systems, the decreases amplitudes are shown to be proportional to the exposure time or to the severity of environmental attack, and the decrease results across either the thermal diffusion peak associated with the specimen thickness or with the grain size. Internal friction as considered on the atomic scale occurs from the pinned motion of dislocations by impurity atoms. In Chapter II, Koehler's theory was presented which related the logarithmic decrement as

inversely proportional to the fourth power of the dislocation density. Moreover, it was noted that impurity atoms tie down only edge type dislocations. The incorporated data indicates that susceptible alloys exhibit decreased logarithmic decrements and associated specific damping capacity values. In view of this theory, the decrease in specific damping capacity of susceptible alloys implies increased dislocation density resulting from impurity atoms. Susceptibility to stress corrosion cracking prescribes that impurity atoms enter the matrix material. Thus the above statements produce a logical sequence. As stated above, any general theory of stress corrosion cracking must be harmonious with the fact that susceptible alloys display planar arrays of dislocations whereas immune alloys have tangled dislocation substructures. In discussing internal friction due to dislocations, it was cited that impurity atoms tie down only edge type dislocations, and that the splitting of a whole dislocation into partial dislocations occurs in such a way that it is impossible to obtain a screw type dislocation. The concentration of impurity atoms in the stress field of a dislocation produces changes in the mechanical properties of the material. These changes result from the fact that the impurities anchor the dislocations by decreasing the respective dislocation length and thus making dislocation movement more difficult. Dislocation concentration by impurity atoms in the interior of the crystal or on the crystal boundary produces strong local increases in internal strains leading to the formation of stable microcracks. (49) Thus, the presented data shows that susceptible alloys experience an increase in their dislocation density because impurity atoms enter the matrix material during environmental exposure. Impurity atoms tie down only edge type dislocations, which decrease the respective dislocation lengths. Reduced dislocation lengths cause embrittlement in the matrix material which produces stable microcracks in the presence of a stress field. It is the

phenomena of susceptible alloys being subject to impurity atoms which tie down only edge type dislocations and whose concentration produces stable microcracks that explains stress corrosion cracking failure resulting from planar arrays of dislocations.

Since impurity atoms are unable to pin down screw type dislocation movements, the evidence of such dislocation movement does not imply an absence of such impurity atoms. However, the evidence of failure by screw dislocation movement does indeed imply an absence of impurity atoms. In the presence of impurity atoms, screw dislocations are pinned. The movement of screw dislocations is not hindered by impurity atoms. However material failure resulting from screw dislocations implies absence of impurity atoms. If the impurity atoms were present the material would not fail in screw dislocation but in planar array due to embrittlement resulting from the pinning of the edge dislocations. Thus non-susceptible systems fail by tangled substructures because of an absence of impurity atoms in the material's matrix.

Any general theory of stress corrosion cracking must also be in harmony with the fact that the corrodent near the crack tip is grossly different from the bulk environment outside the crack. Recognition of this fact was first obtained by measuring the pH of the corrodent in the crack tip region. (51) By this technique it was found that although the bulk corrodent was neutral, the solution at the tip of the crack was acidic with an approximate pH 4. If a neutral bulk solution is made alkaline (pH 10) by the addition of sodium hydroxide or is made acidic (pH 2) by the addition of hydrochloric acid, the pH at the crack tip remains approximately 4. Therefore, the solution chemistry inside the crack is fixed by the metal reactions. Moreover, recent polarization measurements made on steels at various potentials indicate that conditions at the crack tip are always favorable for hydrogen reduction. Thus there

is an excess of hydrogen ions at the crack tip which is true even when the steel is anodically polarized. This has been substantiated by direct measurements of hydrogen permeation.(52) The kinetics of stress corrosion cracking must consider the specimen potential in addition to the hydrogen ions at the crack tip. The conclusion reached is that stress corrosion cracking resulting in high strength steels that have been exposed to aqueous environments occurs by hydrogen assisted cracking. This observation is consistent with the general theory as presented above. The impurity atom in this specific case is hydrogen. Based upon these investigations, the general theory of stress corrosion cracking assumes that failure resulting from chemical and ionic diffusion is hydrogen assisted. Thus the chemical species at the crack tip remains acidic in respect to the environmental corrodent outside the crack. Mass diffusion, such as liquid metal, represents an amalgum of atom diffusion where the concept of pH does not exist. Mass diffusion must be discussed from an acid-base concept wherein an acid is defined as an electron acceptor and a base is an electron donor. Specifically in this respect aluminum is more acidic than mercury, because the aluminum atom is electron deficient and it accepts an electron to obtain a stable structure, whereas the mercury atom is an electron donor and thus basic. It therefore follows that the corrodent at the crack tip is different than the surrounding media, because of the depletion of the alloy elements dissolving in the mercury corrodent. The impurity atom, in this case mercury, enters the atomic structure either by filling the atomic cavity or by dissolving an alloy element in aluminum specimen and then filling such openings.

The proposed general theory relates to the different mechanisms of diffusion and includes the two paramount pillars of stress corrosion cracking. Within the realm of available information the theory is correct as approached from the concept of increased dislocation density and measurements in the

materials specific damping capacity. Internal damping measurements represent a sophisticated approach in achieving predictability regarding those combinations of alloys and environments which cause stress corrosion cracking.

Understanding the phenomenon of employing internal damping measurements for determining susceptibility to stress corrosion cracking necessitated several assumptions which are implicitly and explicitly made in this dissertation. Although these assumptions seem to be physically realistic, further investigations are required to verify them.

1. The experimental procedure assumes that the materials mechanical behavior is independent of the amplitude of deformation within the range of stress employed in the experiment. Thus, internal damping curves are obtained from a series of measurements made over a range of frequencies. It is imperative that further investigations be conducted on other metal corroderent systems in order to validate the amplitude independence.

2. The experimental support for the fact that the logarithmic decrement varies inversely with the concentration of impurities along the dislocation line is emperical. Thus, dependable experimental techniques must be developed to determine the dislocation line density and the pinning point density for virgin and exposed materials. Moreover, once the extent of the contribution from a given free length of dislocation to internal friction has been established, precise measurements can then be made regarding the concept of dislocation density in the general theory to an estimated time for crack initiation. Only in this fashion can scaling laws be developed and understood as related to the inception time for crack propagation.

3. Within the range of experimental data currently available for analysis, it appears irrelevant for the measurements to be made across both the specimen thickness and the grain size. However, if it is necessary to

determine the internal damping curve across very fine grain structures, it will be necessary to alter the present experimental procedure.

4. The contribution of specific damping measurements in determining susceptibility to stress corrosion cracking has immediate value as a laboratory tool for both material research and material evaluation. The long range goal of this technique should be a non-destructive test for environmental structures already completed and in operation. A non-destructive test which acts as a prediction device is one of the apparatus innovations that should be forthcoming.

5. The role of internal damping measurements and associated relaxation times on metallurgical phenomenon akin to stress corrosion cracking has not been investigated. Recently obtained experimental evidence (53) indicates that the internal damping curves show a shift in their peak frequencies (and associated relaxation times) as a function of corrosion fatigue. Additional investigations are needed to explore the implications of relaxation times on other metallurgical phenomenon.

6. A lack of published experimental evidence regarding the fact that stress corrosion cracking is assisted by hydrogen embrittlement is a limitation on the general theory. Such information has been established for certain steel alloys (54) but the testing has not been extended to other families of alloys.

7. The primary objective of this current effort is the establishment of internal damping to stress corrosion cracking susceptibility. With the experimental data currently available for analysis, a general theory of stress corrosion cracking has been postulated. However, the extensiveness of this theory will be determined by additional evidence as previously discussed.

8. It is recognized that what is presented in this paper is the beginning step towards an important goal of establishing relationships between changes in a materials damping properties and the materials reaction to its environment. The techniques and resulting data must be of importance to the designer and the engineer.



To ascertain susceptibility to stress corrosion cracking, a design procedure has been established wherein internal damping measurements are performed on materials subjected to environmental exposure. Based on the experimental data, the material's susceptibility to stress corrosion cracking was successfully related to its associated internal damping curves. Moreover, a general theory was postulated which included the two pillars of stress corrosion cracking as related to the different diffusion processes.

The investigative evidence in this dissertation finds that it is not the specific change in the material's damping properties that is indicative of the susceptibility to stress corrosion cracking, but rather the decreased amplitudes of the internal friction peaks. For susceptible systems, the decreased amplitudes are related to the exposure time or to the severity of environmental attack, and the decrease results across either the thermal diffusion peak associated with the specimen thickness or with the grain size. For non-susceptible systems, the peak amplitudes remain unchanged after environmental exposure and when compared to the same datum curve for the virgin specimen.

Stress corrosion cracking is caused by an increase in the dislocation density within the materials substructure. This increase in dislocation density is due to impurity atoms resulting from environmental exposure. In the presence of a stress field, dislocation concentration by impurity atoms in the interior of the crystal or on the crystal boundary produces strong local increases in internal strains leading to the formation of stable microcracks.

The experimental results of this investigation are especially intended for the use of the design engineer. The existence of internal damping measurements relating to stress corrosion cracking has great practical consequences on the design of environmental structures.

The scope of this investigation constitutes a major contribution to the field of stress corrosion cracking. It is recommended that future experiments establish the decrease in the internal damping curves to failure time. Furthermore, quantitative measurements are needed for the basic ocean engineering systems of titanium and high yield strength steels in sea water.

This study is to be viewed as the initial step in an overall project relating the dynamic response of materials to environmental cracking. In pursuing this goal it is anticipated that Project GIDTEC (Generalized Internal Damping Theory of Environmental Cracking) will develop. The authors believe that this study is the first investigation on the dynamic response of materials which is used to explain a static metallurgical phenomenon.

The future investigations that are directly related to this study should be pursued along the following three avenues.

1. Thickness Effect

The experimental procedure and apparatus must be designed so it will accommodate the larger thicknesses of materials. It is imperative that the dynamic response of larger section materials be obtained so the laboratory procedure can validate material thicknesses which are required for ocean engineering structures.

2. Engineering Applications

A necessary requirement for the technique is that it have application for evaluating engineering structures. The value of this technique will be derived from its use as a tool for evaluating such structures as airplane wings and models of ocean structures.

3. Previous Stress History

In the course of this investigation, slight evidence was obtained which indicated that the materials susceptibility to stress corrosion cracking in a corroding environment was dependent on the stress history of the material. Obtaining static fatigue data points for the aluminum-mercury system indicated much shorter times for cracking if the material had been previously stressed in air. This information would be extremely important to the design engineer.

#### ACKNOWLEDGEMENTS

This study has been supported by the Office of Naval Research and by the Maury Institute of Ocean Science under contract N00014-67-A-0377-0003. The authors wish to express their appreciation to the Monitor, Mr. John Gregory, for the opportunity of dealing with this problem. The manuscript was typed by Mrs. Margaret Patterson.

## REFERENCES

1. Brown, B.F., "Stress Corrosion Cracking; A Perspective Review of the Problem," NRL Report 7130, U.S. Naval Research Laboratory, Washington D.C., June 1970.
2. Horn, K., "Composite Materials for Pressure Hull Structures," Ocean Engineering Journal, Vol.1, (1969), pg. 315.
3. Gregory, J., Private Communique (1972).
4. Lindberg, R.I., "Aluminaut - Three Years Later," in "Materials Performance and the Deep Sea," American Society for Testing and Materials, Special Technical Publication 445 (1969).
5. Fontana, Mars G., "General Theory of Stress Corrosion," Advisory Group for Aerospace Research and Development, Conference Proceedings No.18, North Atlantic Treaty Organization (1967).
6. Symposium on "Stress Corrosion Cracking of Metals," American Society for Testing and Materials, Philadelphia, Pa., (December, 1944).
7. Brown, B.F., "A New Stress Corrosion Cracking Test for High Strength Alloys," Materials Research and Standards, American Society for Testing and Materials, Vol.6 (March, 1966), ppg.129-133.
8. Thiruvengadam, A., "Use of Internal Damping Measurements in the Study of Environmental Cracking," Corrosion, Vol.25 (June, 1969), pp.243-250.
9. Kalsky, H., "Stress Waves in Solids," Dover Publications, New York, New York, 1963.
10. Zener, C., "Internal Friction in Solids, Theory of Internal Friction in Reeds," Physical Review, Vol.52, pg.230, 1937.
11. Zener, C., "Internal Friction in Solids, General Theory of Thermoelastic Internal Friction," Physical Review, Vol.53, pg.90, 1938.
12. Randall, R.H., Rose, F.C., Zener, C., "Intercrystalline Thermal Currents as a Source of Internal Friction," Physical Review, Vol.56, pg.343, 1939.
13. Van Winkle, D., Nielson, H. and Zener, C., "High Temperature Internal Friction in Alpha Brass," Transactions American Institute Mining and Metallurgical Engineers, Vol.147, pg.98, 1942.
14. Ke, T.S., "Experimental Evidence of the Viscous Behavior of Grain Boundaries in Metals," Physical Review, Vol. 71, pg.533, 1947.

15. Orowan, I.E., "Mechanism of Viscous Flow in Solids," Proceedings West of Scotland Iron and Steel Institute, (February, 1947).
16. King, R., Cahn, R.W., and Chalmers, B., "Mechanical Behavior of Crystal Boundaries in Metals," Nature, Vol.161, pg.682, 1948.
17. Ke, T.S., "Stress Relaxation across Grain Boundaries in Metals," Physical Review, Vol.72, pg.41, 1947.
18. Seitz, F., Physics of Metals, Chapter X, McGraw-Hill Book Co., New York, New York, (1943).
19. Koehler, J.S., "The Influence of Dislocations and Impurities on the Damping and the Elastic Constants of Metal Crystals," Imperfections in Nearly Perfect Crystals, Edited by W. Shockley, John Wiley & Sons, Inc., New York, New York, (1962), page 191.
20. Heidenreich, R.D., and Shockley, W., "Dislocation Geometry," Conference on the Strength of Solids, University of Bristol, England Physical Society, London (1948).
21. Thompson, D.O. and Holmes, D.K., "Dependence of Young's Modulus and Internal Friction of Copper upon Neutron Bombardment," Journal of Applied Physics, Vol.27, pt.191, (1956).
22. Jensen, J.W., "Damping Capacity - Its Measurement and Significance," U.S. Bureau of Mines Report of Investigation 5441, U.S. Department of the Interior, (1959).
23. Bailey, G.L., "Specific Damping Capacity from the Measurement of Experimental Decay Curves," Journal of the Institute of Metals, Vol.74, (1948), pg.417.
24. Plunkett, R., "Measurement of Damping," Structural Damping, edited by J.E. Ruzicka, American Society for Testing and Materials, (December 1959), pg 117.
25. "Total Immersion Corrosion Test of Non-Ferrous Metals," American Society for Testing and Materials Designation B185-43T, Vol.3, (1963) pg.266.
26. Timoshenko, S.P., Vibration Problems in Engineering, D.Van Nostrand Co., Inc., New York, New York, (November, 1954), pg.338.
27. Crafton, Paul A., Shock and Vibration in Linear Systems, Harper & Brothers Inc., New York, New York, (1961), pg.315.
28. Mason, W.P., "Internal Friction and Fatigue in Metals at Large Strain Amplitudes," The Journal of the Acoustical Society of America, Vol.28 (November, 1956), pg 1207.

29. Jacobsen, L.S., "Measurement of Damping," American Society for Testing and Materials, Vol 52, (1930), pg. 169.
30. Crandall, S.H., "The Role of Damping in Vibration Theory," Journal Sound Vibration, Vol 11, (1976), pg 3.
31. Dorn, J.E., Editor, "Mechanical Behavior of Metals at Elevated Temperatures." The University of California Engineering Extension Series, McGraw Hill, Inc , New York, New York, (1961), pg.225.
32. Kimball, A.L., "Vibration Damping Including the Case of Solid Friction," American Society for Testing and Materials, Vol.51, (1929),pg.227.
33. Ormondroyd, J., "Vibration Problems - Part III," American Society for Testing and Materials, Vol.62, (1950), pg.34.
34. Lazan, B.J., Damping of Materials and Members in Structural Mechanics, Pergamon Press, New York, New York, (1968).
35. Baker, W.E., Woolam, W.E. and Young, D., "Air and Internal Damping of Thin Cantilever Beams," International Journal of Mechanical Science, Vol.9, (1967), pg 743
36. Bennewitz, K. and Rotger, H., "Über die Inner Reibungsfester Körper, Absorptions Frequency von Metallen in Akustischen Gebiet," Phys. Zietsehr, Vol.37, (1936), pg.578.
37. Boltzmann, L., "Zu Theorie der Elastische Nachwirkung," Ann. d. Phys., Vol 7, (1876), pg 624
38. Bastien, P.G. and Azou, P., "The Phenomena of Cracking and Fracture of Steel in the Presence of Hydrogen. Corrosion under Stress in the Presence of Moist Hydrogen Sulfide." Physical Metallurgy of Stress Corrosion Fracture, Editor T.N. Rhodin, Interscience Publishers, New York, New York, 1959
39. Mima, G. and Hori, S., "Study on the Stress Corrosion Cracking in Austenite Stainless Steels by Means of Internal Friction Measurements," Transaction Japanese Institute of Metals, Vol.5, (1967), pg.202.
40. See before in Introduction
41. Sprowis, D.O. and Brown, R.H., "Stress Corrosion Mechanisms for Aluminum Alloys," Proceedings of Conference, Fundamental Aspects of Stress Corrosion Cracking, National Association of Corrosion Engineers, Houston, Texas, 1969
42. Helfreich, W., "Stress Corrosion Performance of Aluminum Alloys in Potassium Dichromate Solution," Kaiser Aluminum Report No. MS-PR-6875, Kaiser Aluminum Company, 1968

43. Dix, E.H., "Acceleration of the Rate of Corrosion by High Constant Stress," Transactions, American Institute of Mining and Metallurgical Engineers, Vol. 137, pg.11, (1940).
44. Hoar, T.P., and West, J.M., "Mechano-chemical Anodic Dissolution of Austenitic Stainless Steel in Hot Chloride Solution," Proceedings, Royal Society, Vol.268, pg.304, (1962).
45. Keating, F.H., "Chemical Manifestations of Internal Stress," Symposium on Internal Stress in Metals and Alloys, Institute of Metals, London, pg.311, (1948).
46. Coleman, E.G., "On a Surface Energy Mechanism for Stress Corrosion Cracking," Acta Metallurgica, Vol.9, pg.491, (1961).
47. Fujii, C.T., and Dahlberg, E.P., "Methods for Studying the Solution Chemistry within Stress Corrosion Cracks," Journal Electrochemical Society, Vol.116, pg.218, (1969).
48. Swann, P.R. and Nutting, J., "Stacking Faults and the Failure of Alloys in Corrosive Media," Journal Institute of Metals, Vol.88, pg.478, (1960).
49. Auleytner, J., X-Ray Methods in the Study of Defect in Single Crystals, Pergamon Press, pg.13, (1967).
50. Smith, Charles D., The Science of Engineering Materials, Prentice-Hall, Inc., Englewood Cliffs, New Jersey, pg.83, (1959).
51. Brown, B.F., "Methods for Studying Solution Chemistry Within Stress Corrosion Cracks," Journal of the Electrochemical Society, Vol.116, pg.218, (1969).
52. Barth, C.F., Steigerwald, E.A. and Troiano, A.R., "Hydrogen Permeability and Delayed Failure of Polarized Martensitic Steels," Corrosion, Vol.25, pg.353, (1969).
53. Thiruvengadam, A., "On Cavitation Fatigue at High Frequencies," American Society for Testing and Materials, STP 503, pg.171, (1970).
54. Brown, B.F., "Stress Corrosion Cracking of High Strength Steels," Metallurgical Reviews, Vol 13, pg.170, (1968).